

# The Modeling of Human Sensation in Virtual Environments

Ka Keung Caramon LEE



A Thesis Submitted in Partial Fulfilment  
of the Requirements for the Degree of  
Master of Philosophy  
In  
Mechanical and Automation Engineering

© The Chinese University of Hong Kong

31 August 2000

The Chinese University of Hong Kong holds the copyright of this thesis. Any persons(s) intending to use a part or whole of the materials in the thesis in a proposed publication must seek copyright release from the Dean of the Graduate School.



---

# Abstract

In this thesis, we apply artificial intelligence learning techniques and statistical analysis towards the modeling of human sensation in virtual environments. This work has potential impact in a number of areas such as human-machine interaction, virtual reality and robotics. We specifically focus on the following important questions: (1) how to efficiently and effectively model the relationship between human sensations and the physical stimuli presented to humans, (2) how to validate the human sensation models, (3) when the sensory data size gets large, how to reduce the input data size and how to select the information which is most important to human sensation modeling, and (4) how to adjust the stimuli presented to individuals based on human sensation such that detrimental effects, both psychological and physiological, can be reduced and prevented.

In order to provide an experimental testbed for the implementation of the proposed learning and analysis techniques, we develop a full-body motion virtual reality interface, 'The Motion-Based Movie System'. The system is capable of recording human sensation while the human subjects are participating in the virtual reality journey. We propose using Cascade Neural Networks with Node-Decoupled Extended Kalman Filter Training for modeling human sensation in virtual environments. For the purpose of sensation model validation, we propose using a stochastic similarity measure based on Hidden Markov Models to calculate the relative similarity between model-generated sensations and actual human sensations. Next, we investigate a number of feature extraction and input selection techniques for reducing the input data size in human sensation modeling. We propose and develop a new input selection method based on Independent Component Analysis, which is capable of reducing the data size and selecting the stimuli information that is most important to human sensation. Further, we propose and develop a motion trajectory modification scheme which is able to modify the stimuli presented to the human subjects based on human sensation. The trajectory of the virtual reality motion system is adjusted such that the sensation intensities of the human subjects can be prevented from exceeding certain specified appropriate levels.



## 摘要

在這論文中，我們應用了人工智能學習技術及統計分析的方法來制作人類在虛擬環境中的感覺模型，此項研究對一些領域例如人機互動，虛擬真實及機械人研究等帶來潛在影響。我們特別專注在下列重要的問題：

- (1) 如何能有效實際地模擬人類感覺和在人類身上的物理刺激的關係。
- (2) 如何能驗證人類感覺模型的有效性。
- (3) 當感覺資料增多時，如何能減少輸入資料的數量及如何選擇對人類感覺模型最重要的資料。
- (4) 如何跟據人類感覺去調整在人類身上的物理刺激，以致能減少並防止在人類心理及生理上所產生的損害性影響。

爲了對我們提出的學習及分析技巧進行實驗，我們開發了一個名爲「動感電影系統」的全人體運動虛擬真實介面，此系統能夠在研究對象參與虛擬真實旅程時記錄他們的感覺。

我們提出使用級聯人工神經網絡及結點解耦延伸卡爾曼過濾訓練法來模擬人類在虛擬環境中的感覺。對於人類感覺模型驗證方面，我們提出使用基於隱含馬爾卡夫模型的隨機相似性量度指數來計算實際人類和模型所產生出來的感覺的相對相似度。

接著，我們研究數個特徵抽取及輸入選擇方法，目的是用作減少人類感覺模型輸入資料的數量。我們提出及開發了一種新的基於獨立成份分析的輸入選擇方法，它能夠減少資料數量並能選出對人類感覺最重要的刺激資料。

進一步，我們提出及開發了一種改變運動軌跡的方法，它能根據人類感覺而改變虛擬真實系統在人類身上的刺激，虛擬真實運動系統的軌跡被改變後，人類感覺的強烈程度可以不超越一個指定的合適水平。



# Acknowledgments

My sincere and heartfelt thanks go to my supervisor, Prof. YangSheng Xu. He has given me much research freedom and intellectual guidance throughout my two years of study. I also thank YangSheng for giving me the unique opportunity to visit the Robots and Automation Research Institute in Beijing.

The many scientists and engineers in the 811 factory of the China Academy of Launch Vehicle Technology in Beijing deserve thanks for their support. Their technical wizardry was crucial to the setup of the research equipments.

Thanks to the people who gave of their time to sit through the VR system for testing and data collection. Special thanks to Gary Lai and my undergraduate assistants, Alex Wu, Bill Wong and Kenneth Wong.

I thank Michael Nechyba whose work on Human Control Strategy has inspired mine. Thanks to my colleagues in the Advanced Robotics Lab, especially Samuel Au and Wilson Yu, for the many constructive discussions and suggestions.

Finally, with love and respect, I acknowledge the love and encouragement of my parents, without whom I surely would not have reached this stage in my life.



# Contents

<b>Contents</b>	<b>iii</b>
<b>List of Figures</b>	<b>vi</b>
<b>List of Tables</b>	<b>ix</b>
<b>1 Introduction</b>	<b>1</b>
1.1 Motivation . . . . .	1
1.2 Related Work . . . . .	3
1.2.1 Empirical Psychophysical Equations . . . . .	3
1.2.2 Industry Standards . . . . .	4
1.2.3 Fuzzy Logic . . . . .	4
1.2.4 Neural Networks . . . . .	5
1.3 Organization of Thesis . . . . .	7
<b>2 Experimental Design</b>	<b>9</b>
2.1 Human Motion Sense . . . . .	9
2.2 Full-Body Motion Virtual Reality System . . . . .	12
2.3 Human Sensation Measure . . . . .	15
2.4 Trajectory Segmentation . . . . .	16
<b>3 Learning and Validation of Human Sensation Models</b>	<b>22</b>
3.1 Cascade Neural Networks . . . . .	23
3.1.1 Dynamic Mapping . . . . .	26
3.2 Experimental Trajectory Data . . . . .	26
3.3 Effect of Trajectory Segmentation . . . . .	31
3.4 Model Validation . . . . .	32
3.5 Similarity Measure . . . . .	33

---

3.6	Similarity Measure Results . . . . .	38
<b>4</b>	<b>Input Reduction for Human Sensation Modeling</b>	<b>40</b>
4.1	Introduction . . . . .	40
4.2	Input Reduction . . . . .	41
4.3	Feature Extraction and Input Selection . . . . .	42
4.4	Feature Extraction Using Principal Component Analysis . . . . .	44
4.5	Independent Component Analysis . . . . .	48
4.5.1	Measure of Gaussianity . . . . .	50
4.5.2	The Fixed Point ICA Algorithm . . . . .	51
4.6	Input Reduction Using Independent Component Analysis . . . . .	52
4.6.1	ICA Without Dimension Reduction . . . . .	52
4.6.2	Feature Extraction Using ICA . . . . .	55
4.6.3	Input Selection Using ICA . . . . .	57
4.6.4	Applying Input Selection by ICA on the Furnace Data . . . . .	58
4.6.5	Applying Input Selection by ICA to Sensation Modeling . . . . .	65
4.6.6	Cross Verification of Selected Inputs . . . . .	70
4.7	Summary on Input Reduction for Human Sensation Modeling . . . . .	72
<b>5</b>	<b>Stimulus Modification Based on Human Sensation</b>	<b>74</b>
5.1	Need for Stimulus Modification . . . . .	74
5.2	Sensation Grades . . . . .	75
5.3	Trajectory Modification Scheme . . . . .	77
5.4	Experiments . . . . .	80
<b>6</b>	<b>Conclusion</b>	<b>86</b>
6.1	Contributions . . . . .	86
6.2	Future Work . . . . .	87
<b>A</b>	<b>Platform Model</b>	<b>88</b>
A.1	Inverse Kinematics . . . . .	90
A.2	Forward Kinematics . . . . .	93



A.3 Platform Dynamics . . . . . 99

**Bibliography** . . . . . **100**

# List of Figures

2.1	Motion-Based Movie System . . . . .	13
2.2	Experimental Setup . . . . .	14
2.3	Teach Pendant . . . . .	15
2.4	Level of Excitement Input Device. . . . .	17
2.5	Types of Segment in the 2-DOF case. . . . .	18
2.6	Types of Segment in the 3-DOF case (1). . . . .	20
2.7	Types of Segment in the 3-DOF case (2). . . . .	21
3.1	Cascade Neural Network . . . . .	24
3.2	Platform Trajectory for the Movie . . . . .	27
3.3	Sensation Trajectory of Subject 1 . . . . .	29
3.4	Sensation Trajectory of Model 1 of Subject 1 . . . . .	29
3.5	Sensation Trajectory of Model 2 of Subject 1 . . . . .	29
3.6	Sensation Trajectory of Subject 2 . . . . .	30
3.7	Sensation Trajectory of Model 1 of Subject 2 . . . . .	30
3.8	Sensation Trajectory of Model 2 of Subject 2 . . . . .	30
3.9	Original Sensation Trajectory of Subject 1 . . . . .	31
3.10	Trajectory of Model Trained by Unsegmented Motion Data . . . . .	31
3.11	Hidden Markov Model . . . . .	32
3.12	Conversion of Human Sensation Trajectory to a Sequence of Discrete Symbols	37
3.13	Discontinuity Causes Similar Motion Inputs to be Mapped to Different Sensa- tion Outputs . . . . .	39
4.1	Input Selection . . . . .	43
4.2	Feature Extraction . . . . .	43
4.3	Sensation Model 1, Motion Data Processed by PCA Feature Extraction . . .	47
4.4	Sensation Model 2, Motion Data Processed by PCA Feature Extraction . . .	47
4.5	Sensation Model 3, Motion Data Processed by PCA Feature Extraction . . .	47

4.6	Sensation Model 1, Motion Data Processed by ICA, No Input Reduction . . .	54
4.7	Sensation Model 2, Motion Data Processed by ICA, No Input Reduction . . .	54
4.8	Sensation Model 3, Motion Data Processed by ICA, No Input Reduction . . .	54
4.9	Sensation Model 1, Motion Data Reduced by ICA Feature Extraction . . . . .	56
4.10	Sensation Model 2, Motion Data Reduced by ICA Feature Extraction . . . . .	56
4.11	Sensation Model 3, Motion Data Reduced by ICA Feature Extraction . . . . .	56
4.12	Original Input of Furnace . . . . .	59
4.13	Original Output of Furnace . . . . .	59
4.14	Furnace Model 1, Trained Using Full Set of Candidate Inputs . . . . .	60
4.15	Furnace Model 2, Trained Using Full Set of Candidate Inputs . . . . .	60
4.16	Furnace Model 3, Trained Using Full Set of Candidate Inputs . . . . .	60
4.17	Output of Furnace Model 1 Trained Using ICA-Selected Input Set 1 . . . . .	62
4.18	Output of Furnace Model 2 Trained Using ICA-Selected Input Set 1 . . . . .	62
4.19	Output of Furnace Model 3 Trained Using ICA-Selected Input Set 1 . . . . .	62
4.20	Output of Furnace Model 1 Trained Using ICA-Selected Input Set 2 . . . . .	63
4.21	Output of Furnace Model 2 Trained Using ICA-Selected Input Set 2 . . . . .	63
4.22	Output of Furnace Model 3 Trained Using ICA-Selected Input Set 2 . . . . .	63
4.23	Output of Furnace Model 1 Trained Using ICA-Selected Input Set 3 . . . . .	64
4.24	Output of Furnace Model 2 Trained Using ICA-Selected Input Set 3 . . . . .	64
4.25	Output of Furnace Model 3 Trained Using ICA-Selected Input Set 3 . . . . .	64
4.26	Sensation Model 1 of Subject 1, Input Selected by ICA . . . . .	66
4.27	Sensation Model 2 of Subject 1, Input Selected by ICA . . . . .	67
4.28	Sensation Model 3 of Subject 1, Input Selected by ICA . . . . .	67
4.29	Sensation Model 1 of Subject 2, Input Selected by ICA . . . . .	69
4.30	Sensation Model 2 of Subject 2, Input Selected by ICA . . . . .	69
4.31	Sensation Model 3 of Subject 2, Input Selected by ICA . . . . .	70
5.1	Modified Pitch Trajectory for Sensation Grade 2 of Subject 1 . . . . .	81
5.2	Modified Roll Trajectory for Sensation Grade 2 of Subject 1 . . . . .	81
5.3	Modified Pitch Trajectory for Sensation Grade 4 of Subject 1 . . . . .	81
5.4	Modified Roll Trajectory for Sensation Grade 4 of Subject 1 . . . . .	82
5.5	Modified Pitch Trajectory for Sensation Grade 2 of Subject 2 . . . . .	82



---

5.6	Modified Roll Trajectory for Sensation Grade 2 of Subject 2 . . . . .	82
5.7	Modified Pitch Trajectory for Sensation Grade 4 of Subject 2 . . . . .	83
5.8	Modified Roll Trajectory for Sensation Grade 4 of Subject 2 . . . . .	83
5.9	Sensation of Subject 1 on Motion Trajectory Modified to Sensation Grade 2 .	84
5.10	Sensation of Subject 1 on Motion Trajectory Modified to Sensation Grade 4 .	85
5.11	Sensation of Subject 2 on Motion Trajectory Modified to Sensation Grade 2 .	85
5.12	Sensation of Subject 2 on Motion Trajectory Modified to Sensation Grade 4 .	85
A.1	Diagram of Motion Platform . . . . .	88
A.2	Motion Platform . . . . .	89

# List of Tables

2.1	Types of Human Motion Sense . . . . .	11
3.1	Similarity Measure Result . . . . .	38
4.1	Model Similarity Measure Result for Motion Data Reduced by PCA Feature Extraction . . . . .	46
4.2	Model Similarity Measure Result for Motion Data Processed by ICA Without Input Reduction . . . . .	53
4.3	Model Similarity Measure Result for Motion Data Reduced by ICA Feature Extraction . . . . .	55
4.4	Furnace Similarity Measure Result for Model Trained Using Full Set of Can- didate Inputs . . . . .	59
4.5	Inputs Selected for the Furnace Model Using ICA . . . . .	61
4.6	Furnace Model Similarity Measure Result for Inputs Selected by ICA . . . . .	61
4.7	Mixing Matrix of the First ICA Model for Subject 1 . . . . .	66
4.8	Mixing Matrix of the Second ICA Model for Subject 1 . . . . .	66
4.9	Similarity Measure Result for Models Trained Using ICA-Selected Inputs for Subject 1 . . . . .	67
4.10	Mixing Matrix of the First ICA Model for Subject 2 . . . . .	68
4.11	Mixing Matrix of the Second ICA Model for Subject 2 . . . . .	69
4.12	Similarity Measure Result for Models Trained Using ICA-Selected Inputs for Subject 2 . . . . .	70
4.13	Model Similarity Measure Result, All Models Trained Using Inputs : $\alpha, \theta, \dot{\theta}, \ddot{\theta}$ .	71
4.14	Model Similarity Measure Result, All Models Trained Using Inputs : $\alpha, \theta$ . . .	71
4.15	Model Similarity Measure Result, Models of Subject 1 Trained Using Inputs : $\alpha, \theta, \dot{\theta}, \ddot{\theta}$ . Models of Subject 2 Trained Using Inputs : $\alpha, \theta$ . . . . .	72
4.16	Summary of Results of Data Processing Methods on Subject 1 . . . . .	72
5.1	Sensation Grade and the Range of Level of Excitement Represented . . . . .	76

---

5.2	Average Values of Motion Attributes (and Standard Deviations) at Various Sensation Grades for Subject 1 . . . . .	76
5.3	Average Values of Motion Attributes (and Standard Deviations) at Various Sensation Grades for Subject 2 . . . . .	77
A.1	Motion Range of Platform . . . . .	89
A.2	Physical Dimension of Motion Platform . . . . .	90



# Chapter 1

## Introduction

Nowadays, increased processing power has allowed complex real-world applications to be handled by computers and robots. Since humans and machines have different performances in various areas, the co-operations between humans and machines have become more and more essential in resolving sophisticated engineering problems. In the development of human-machine interaction, virtual reality (VR) plays an important role as it actualizes a high level of integration between humans and computer generated environments. However, one major difference between machines and humans is that human beings have complicated feelings, sensations and emotions, while machines do not. Our everyday experience tells us that the internal sensations of our body and mind have great impact on our behaviors and intelligent skills. If we want to expand the capability of human-machine systems and the extent to which humans and machines can interact efficiently and safely together, the incorporation of computational models of human sensations into the human-computer systems is inevitable.

### 1.1 Motivation

The study of human sensation examines the relationship between input from the world and the manner in which people react to it [61]. It is the conscious experience resulting from the stimulation of sense organs and sensory areas in the brain. No meaning and interpretation is given to the sensory messages, otherwise we'll call it perception.

One important point we want to make is that we need to distinguish between a physical stimulus and the stimulus that is experienced by an observer. For example, the temperature in an ambient environment is related to the level of background radiation energy, which can be measured using a thermometer. The feeling of warmth is the level of radiation that is subjectively experienced by the human. However, temperature may sometimes be deceptive

related to level of warmth. The relationship between the physical attributes of a stimulus and the subjective experience of those attributes is what we are interested in.

Although bodily sensations often fail to correspond to physical reality, many human reactions are characteristically evoked by these subjective bodily experience. It is natural for us to talk about what feels to us to be the case, whether or not it is actually the case in physical reality. The understanding of human sensation models would give us more insights on how humans interact with the physical environment, as well as with robots and computers.

Virtual reality describes a computer-based generation of an intuitive perceivable and experiencible scene of a natural or abstract environment [36]. Hopefully, the synthetic sensory experience created by a computer system may one day be indistinguishable from the real world. But at present time the Virtual Environments (VE) generated by the state-of-the-art systems can only approximate several attributes of the real world.

Since virtual environment systems are highly configurable, it has found applications in various areas. The success of a system depends heavily on its compatibility with humans. Virtual reality is intimately bound to both engineering requirements and human factors, which certainly include human sensation.

Human sensation is extremely complex and everyone has different sensations under different situations, so it is difficult to model sensation analytically. Once we have developed the human sensation model, it can be transferred to machines. Machines such as robots will have the ability to understand how humans feel. The application of models of human sensation can also lead to the improvement of human-machine interface, because the models can act as a tool for the assessment of the quality and effectiveness of different human-machine systems.

In the case of virtual reality, involvement of human sensation models can improve the level of presence in the virtual world. By providing sensation inputs and interaction signals which the users are already familiar or feeling comfortable with, the participants will be able to adapt to the virtual immersion more easily.

Cyber-sickness is an important issue of concern in the development of virtual reality systems and human sensory conflicts are generally viewed as a major cause [37]. Humans may suffer from nausea, sweat palms and dizziness if the sensory signals received from the virtual world are not coordinated in the appropriate fashion. Modeling of human sensation may offer a solution to this problem. Incorporation of human sensation model will also allow



us to develop personalized VR systems, based on individual sensation limits and personal preferences. Sensation models of human can also provide the realism required in virtual human modeling. Simulated agents can become more vivid and life-like.

## 1.2 Related Work

A number of approaches have been proposed and implemented in order to model simple human sensation. They include *empirical formulae*, *industry standards*, *fuzzy systems* and *neural networks*.

### 1.2.1 Empirical Psychophysical Equations

In the past few decades, many empirical formulae had been proposed by psycho-physicists in order to capture the relationships between physical stimuli and human sensations. The famous ones include Weber's Law, Fechner's Law and Steven's Law [39]. Steven's Law has the form :  $S = aX^b$ , where  $S$  is the mean magnitude estimate of the stimulus by the human observer,  $X$  is the physical measurement of the stimulus,  $a$  is a scale factor and  $b$  is the exponent characteristic of the attribute.

In psychophysics, we distinguish between two kinds of sensations.

1. Prothetic Continua : principles of superposition applies at the physical level of description, generating an additive scale with respect to a natural measure of the stimulus magnitude.
2. Methathetic Continua : it involves the substitution of one stimulus in an ordered series for another.

Empirical Laws only applies to Prothetic Continua sensations but not Methathetic Continua sensations.



### 1.2.2 Industry Standards

The transportation industry has a history of studying the bodily sensation of passengers and drivers. Various standards have been published [30] [20]. The British Standard guide BS6841 [12] gives methods for quantifying vibrations and repeated shocks in relation to human health interference with activities, discomfort, the probability of vibration perception and the incidence of motion sickness.

It is believed by the developers of the standards that the complex distribution of oscillatory motion and the force within the body during whole body vibration produce complex sensations. The character of the sensation vary greatly mainly according to the vibration frequency and axis. In the standard the term *discomfort* is applied to the sensation arising directly from the vibration.

The manner in which vibration affects human sensation is dependent on vibration frequency. Different frequency weightings are required for the different axes of vibration and for the different effects on the body. To characterize the discomfort of the vibrating environment by a single quantity, the r.m.s. value is determined by a linear integration of each of the frequency-weighted acceleration signals.

Comfort contours, which relate vibration magnitude to frequency for equal sensation are determined for various situations by researchers [19] [11]. The major drawback of this approach is that the vibration signals have to be very well behaved, that means the frequency and magnitude of vibrations have to be kept constant for a period of time. The assumption that human sensation intensity is always proportional to the linear weighted sum of the individual acceleration components is highly questionable. Also, the weights assigned to each axis are determined regardless of the difference between individual persons.

### 1.2.3 Fuzzy Logic

Recently, Fuzzy Logic has become more and more popular in control and human modeling applications. In a fuzzy scheme, human can use common linguistic terms (for example, "better", "slower") as control inputs to interact with the system. A series of "If-Then" rules have to be specified such that the relationship between the input and output variables can

be established.

Berretti, et al. [5] developed a painting database system utilizing fuzzy logic. The qualities and spatial arrangements of colors on a painting convey different sensations to observers, such as warmth, harmony and excitement. The system uses fuzzy sets to represent low-level region properties such as hue, saturation and size. Based on this representation of region properties, a formal language and a set of model checking rules are implemented to manipulate (such as retrieval and groupings) the paintings in the database based on human's sensation about the paintings.

A fuzzy-controlled residential Heating, Ventilating and Air Conditioning (HVAC) system is developed by Hamdi and Lachiver [23]. The system controls the temperature based on the human sensation of thermal comfort. The control scheme based on fuzzy criteria regulates the thermal comfort-influencing factors to provide thermal comfort in the indoor space. A Thermal Comfort Level (TCL) is calculated from factors including humidity, air velocity and activity level of humans, etc. Once the TCL is calculated, it is compared to the user's actual thermal sensation in order to improve the fuzzy approximation of the specific user's thermal comfort level on-line.

Fuzzy schemes generally perform well in systems with small input dimensions. Since the control functions are actualized through a set of fuzzy "If-Then" rules, the understanding of the system model is essential. The "If-Then" rules cannot be developed if the relationship between the inputs and outputs are not known. If the input dimension of the system is large and the relative importance of the inputs are not certain, fuzzy systems may not be suitable.

#### 1.2.4 Neural Networks

Neural Networks are famous for their promising performance as function approximators. They consist of a large number of interconnected processing elements in an architecture inspired by the structure of the cerebral cortex of the brain. They have been applied successfully in many areas, including those involve human sensation.

Jagielski [31] uses neural networks to replicate human aesthetic judgment of binary images. The design is based on the belief that the intrinsic value of visual art, though difficult to define, can be learnt by neural networks, which consequently become capable to emulate



human aesthetic judgment by learning from examples.

Rosenblem, et al. [57] developed a radial basis function network architecture that learns the correlation of facial feature motion patterns and human emotion. There are three levels in the architecture which determine motion directions, motions of facial features and emotions, respectively. Example pictures of human emotions, such as ‘happiness’ and ‘fear’, are input to the network for training. The system processes short motion segments and incorporates experts rules for analysis of motion sequences.

Neural networks have also been applied to analyze the response of human under whole body vibration. Study has been done by Shiliang, et al. [59] to model the relationship between the resonant frequency of the whole human body, human body weight, height and vibration level. A feed-forward 3-level network is used for training and response prediction.

The previous research work discussed above suffers from a number of limitations. First of all, human sensation is simply too complex to be modeled by analytical methods, we will explain more about this in chapter 2. In the experiments above, only a very small number of input stimuli are presented to the humans at one time. The dimension of input stimuli tends to be low. Most of the inputs presented to the humans belong to the same kind of sensory stimulus. Multi-modal stimuli are in general poorly handle using the linear weighted sum approach. Also, sensory signals presented are simple and usually well-behaved. For example, in the case of full-body vibration, constant vibrations of fixed magnitude and frequency are presented. In the case of fuzzy room environment control, a constant temperature is maintained. The sensory signals supplied in the experiments are not dynamic enough. Furthermore, a strong assumption is made about the structure of the sensation model. It is assumed that every person reacts to the same stimulus in a similar way. This assumption is reflected in the fixed “If-Then” rules used in fuzzy systems and the fixed structures in neural networks. The inter-personal differences are only encoded in the coefficients of the models. However, we believe that both the model parameters and model structure are important in modeling



complex human sensation.

## 1.3 Organization of Thesis

The research in modeling human sensation from human data has thus far not addressed a number of important issues. Much of the previous work models only sensation caused by simple stimuli. In general, the work has not focussed on abstracting models of dynamic human sensations. Therefore, this thesis applies machine learning techniques and statistical analysis towards abstracting models of human sensation. It is our contention that such individual-based models can be learned efficiently under the situation where the stimuli presented to the human subjects are complex, dynamic and multi-dimensional.

The thesis is organized as follows. In chapter 2, we discuss the design of our experiments. The human sensation involved in full-body motion is chosen for study and the nature of this sensation in VR is explored. We then describe a full-body motion virtual reality system which we have developed - ‘the motion-based movie system’. We argue that such a VR simulation environment is well suited for our experimentation purpose. The VR system is capable of recording the sensation trajectories of the human subjects as they are participating in the VR journey. The sensation models aim to capture the relationship between their sensation and the stimuli presented to them. We will focus on the sensation of *excitement* experienced by the subjects caused by the motion of the VR platform. In order to reduce the size of the motion stimulus data and to retrieve meaningful information, we present a method to segment the trajectories of the motion platform.

In chapter 3, we propose using an efficient continuous learning framework for modeling human sensation that combines cascade neural networks with node-decoupled extended Kalman filtering. In order to compare the model-generated human sensation trajectories with their respective human sensation, we propose using a stochastic similarity measure, based on Hidden Markov Model analysis. Sensation models are trained using sensation data recorded from human subjects and motion trajectories of the VR system. The sensation models are validated through the use of the HMM-based measure.

In chapter 4, we study the problem of input reduction in human sensation modeling. Since the dimension of the stimuli presented to the human subjects can get quite high, it is

desirable to reduce the size of the data used for sensation model training. We investigate the performance of a number of feature extraction and input selection techniques, which involve the employment of principal component analysis and independent component analysis. We propose and develop a new input selection method based on independent component analysis, which is capable of reducing the data size and selecting the stimuli information that is most important to human sensation.

After we select the motion attributes that are related to the sensation of individuals, in chapter 5 we set out to modify the stimuli such that the maximum sensation intensity of the subjects can be controlled. For reasons of safety and enjoyment, we want to modify the trajectories of the VR motion system so that the sensation of the participants do not exceed a specified appropriate limit. We propose a motion trajectory modification scheme based on human sensation. The proposed scheme is shown to be able to modify the motion of the VR system and lead to the adjustment of sensation of the subjects involved.

A summary of the contributions of the thesis is given in chapter 6. Possible directions that can be taken to increase the sophistication of human sensation modeling are listed in this chapter as well.



# Chapter 2

## Experimental Design

The principle approach to further understanding of the relation between stimulation from the virtual environments and human sensations has been the systematic laboratory study of the extent to which variations in virtual stimuli produce changes in subjects' judgment of sensations. The sensation invoked by full-body motion in an virtual environment is to be investigated in this thesis.

In this chapter, we firstly discuss the nature of human senses and sensations, especially those related to full-body motion. We have developed a full-body motion virtual reality interface - 'The Motion-Based Movie System'. We introduce the architecture of the system and argue that the system provides a good experimental testbed for the development of human sensation models. Since we want to explore the relationship between human sensation and the stimuli presented to human subjects, the motion trajectory of the VR platform and the level of human sensation are to be recorded. The sensation of excitement experienced by the human subjects is to be analyzed in the thesis. In order to reduce the data size of the trajectories and retrieve meaningful information from the trajectories, we develop a motion trajectory segmentation method for data modeling.

### 2.1 Human Motion Sense

In our study, we will concentrate on the sensation caused by full-body motion. There are a number of sensory systems inside the human body which are responsible for motion sensing and body posture control (orientation and balance). The types of sense, related organs and the names of the systems are listed in table 2.1. In the context of full-body movement, visual and vestibular systems play the most important role in providing information about self-motion to the central nervous system [63].



In order to illustrate the complexity of full-body human motion sense, we will discuss the functions of the visual and vestibular systems in some details. The visual system is both a sensory system and a motor system. As a sensory system, the eyes can detect the position and movement of the head in relation to the surrounding environment and provides information about the vertical axis. In its role as a motor system, the visual receptors that sense slipping of the retinal image supplement compensatory eye movements through a tracking mechanism called the optokinetic reflex.

The vestibular system can also act as both a sensor system and a motor system [44]. As a sensory system, it provides information about the movement of the head and the position of the head with respect to gravity and any other acting inertial forces. There are two types of sensory organs inside the inner ears. The first of these are the semi-circular canals which can detect the angular velocity of the head. These canals are filled with fluids and hair cells. As the head moves, the inertia of the fluid will cause the hair cells to fire neural signals to excite the vestibular nerves. The firing rate is proportional to the head velocity over the range of frequencies in which the head normally moves, that is 0.5 to 7 Hz. There are three canals on each side of the ear which are aligned mutually perpendicular to each other. The two sets of canals work complementarily together in a push-pull relationship. This arrangement allows the system to detect both forward and backward head rotation in 3-D space. The second type of vestibular sensory organ is the otolith organ. There are two otolith organs associated with each set of semi-circular canals. They provide information about linear acceleration and head tilt with respect to the gravitational axis. The saccular otolith provides information about vertical linear acceleration and the utricular otolith responds to horizontal acceleration.

Ambiguity can occur in body motion sensing. For example, head rotation detected by the semi-circular canals can be caused by a head movement on the neck or a body movement on the waist. Information from other sensory systems, such as the visual or proprioceptive systems, will be required to resolve these ambiguities when they occur. In general, the semi-circular canals are most sensitive to fast head movements and the otoliths responds best to slow movements.

If a free seat is used to move in the  $x$  or  $y$  body axis, the threshold for detection of tilt from the vertical is on the order of 2 degrees. The perception of angular motion varies with frequencies, falling at around 0.2 log unit/decade between 0.1 and 1.0 Hz, and falling at -1

log unit/decade below 0.1 Hz. The common peak angular velocity for passive nodding of the head, such as the motions that occur during running or walking, is about  $\pm 10 \text{deg/sec}$ . Transient movements lasting less than 10 seconds with a change in angular velocity below roughly  $2 \text{deg/sec}$ , or peak acceleration below roughly  $0.05 \text{m/sec}^2$ , may be undetected.

Physiological System	Sensor	Parameters
Visual	Eyes	Position
Vestibular	Inner Ear •Semi-Circular Canals •Otoliths	Tilt Angle Angular Velocity Linear Acceleration
Somatosensory	Skin	Pressure
Proprioceptive	•Tendons •Muscles •Joints	Muscle Tension Muscle Length Joint Angle
Auditory	Ear	Sound

Table 2.1: Types of Human Motion Sense

Early studies carried out by the researchers in the transportation industry were mainly concerned with the effects of varying the vibration frequency presented to the subjects. Recent studies have investigated more complex conditions, including multiple-frequency vibration, multiple-axis vibration and shock [20]. These investigations involve systematic study of the effect caused by individual vibration variables. However, they have generally been limited to only a few conditions. The range and complexity of the motion variables (eg. frequency, axis, duration), together with other inter-dependence in the virtual environments, make it difficult to establish a model of human sensation, especially when individual variability is taken into account.

The difference in judgment of sensation that occurs between individuals should be expected to be of great importance. For example, the relative sensation caused by two motions can be very different in two different subjects. However, there have been very few studies in inter-subject variability. One consequence of the large variability is that the judgment of any one subject cannot be relied upon to optimize the virtual environment system to be used by



others.

In the investigation of human sensation in virtual environments, there are a number of factors we may need to consider in terms of inter-subject variability :

1. **Body Size** : For both male and female it has been reported that larger subjects tend to be relatively less sensitive to motions with low frequencies less than 6 Hz, and more sensitive to high frequencies of vertical motions [21]. There is also a lower sensitivity in larger subjects for roll, pitch and yaw motions [52].
2. **Body Dynamics** : The greater the transmission of motion to the head, the greater the subject's sensation to motion [21]. Human bodies have resonant frequencies range between 4Hz to 7Hz, depending on the mass distribution of the bodies [59].
3. **Age and Gender** : It has been reported that there is no significant difference in sensation of motion for subjects with different age [22] and gender [52].
4. **Personality** : Healey[25] reported a study of motion sensation in which personality was found to have no effect on judgment. However. Bennett [4] found that personality had an effect on physiological reactions during exposure to full-body motion. Subjects with an internal locus of control have higher heart rates than subjects with an external locus of control.

## 2.2 Full-Body Motion Virtual Reality System

Based on the discussions in the previous section, it is clear that modeling the human sensation of full-body motion is not an easy task. Also, full-body motion system is commonly regarded as one of the most challenging VR interface technologies to be developed. One example of a full-body motion interface is motion-based movie in which the participants are moved through a VE in a vehicle (figure 2.1).

In such an application, the participants watch a movie while sitting on a motion platform. The motion in the movie and the movements generated by the motion platform are coordinated to provide a sense of excitement to the audience [6].

Such a passive VR application is chosen for study because of the following reasons :



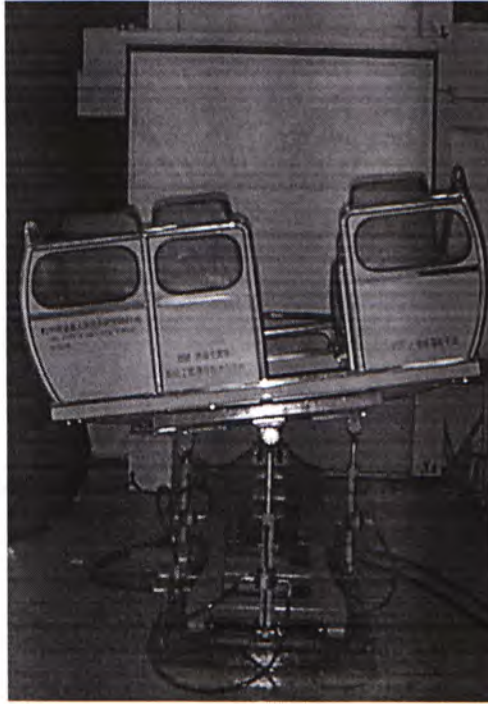


Figure 2.1: Motion-Based Movie System

1. A motion platform can generate various kinds of full-body movements, which lead to different kinds of internal bodily sensation at various intensities.
2. Since we are interested in modeling human sensation, which is not a skill, but a reflection of bodily feeling over a period of time, complex control and manipulation operations will distract the humans' attention away from their internal feelings.
3. Passive motion interfaces will continue to play an important role in training simulations and entertainment applications. The techniques involved in dealing with passive VR systems will allow the more general purposed and complex VR systems to be developed.

Our motion-based movie system consists of two main parts :

- the motion platform system
- the movie system

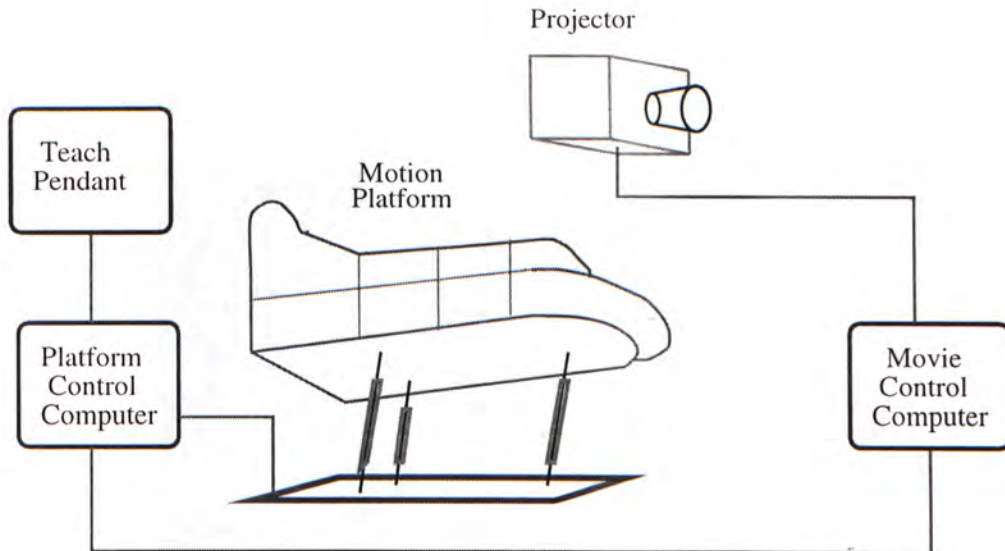


Figure 2.2: Experimental Setup

1. The motion platform system is capable of generating body movements to the audience. The motion platform is a parallel mechanism with 3 degrees of freedom : roll, pitch and heave. The motion platform is actuated by hydraulic pumps. The motion ranges of the platform are  $\pm 22$  degrees in roll,  $\pm 18$  degrees in pitch and 0 – 420mm in heave. The motion of the platform is controlled by a 486 100MHz PC. Sensors are installed on the platform, enabling the system to record the joint positions, tilt angles, angular velocities and linear accelerations of the platform. The kinematic model of the motion platform is described in Appendix A.
2. The movie system is composed of a multi-media Pentium III PC and a digital projector. It can play digital media such as VCD, DVD and other media files which are readable by a PC. The movie is projected on the screen in front of the motion platform. The synchronization between the platform motion and the movie is achieved through the communication channel between the movie control PC and the motion control PC. The communication ensures that the movie and the platform motion start at the same time. For any movie, we can use a teach pendant (figure 2.3) to record the platform motion such that the platform motion is synchronized with the movie motion. The mechanical



structure of the teach pendant is built to be a scaled down version of the original motion platform. The trajectory can be saved to a file and allowed for replay.

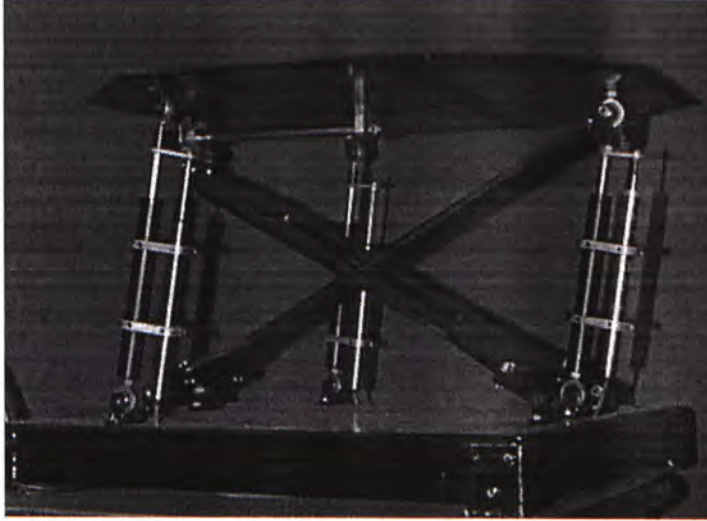


Figure 2.3: Teach Pendant

## 2.3 Human Sensation Measure

The experience generated by the VR system can evoke different kinds of bodily feelings at various intensities. In such an entertainment application, we would like to concentrate on the feeling of *excitement* experienced by the users.

Our main objective is to study the various motion-related factors affecting the sensation of excitement and to quantify human sensation such that platform motion can be controlled to :

1. provide suitable levels of excitement and enjoyment
2. prevent human health from being affected
3. maintain human task performance in some other interactive VR systems

It is preferable to ask subjects to judge the sensation they actually experience. Therefore we phrase the judgment as to emphasize the subjective sensations and to avoid words that may relate only to the physical magnitude of the stimulus. Method of Scaling can be used to determine the extent to which sensation changes when the physical magnitude of the stimulus is altered.

There are two approaches in the method of scaling : the ‘absolute’ method and the ‘relative’ method [39]. In the ‘absolute’ method, subjects use a rating scale to describe their sensations (eg. ‘slightly uncomfortable’, ‘uncomfortable’, ‘very uncomfortable’, etc.). The ‘relative’ technique is most usually restricted to the laboratory with a single subject judging each stimulus separately and pairs of stimuli are compared.

For our application, the absolute method is more suitable because of a number of reasons. Firstly, the stimulus of the motion platform will be presented to the subjects in a continuous manner for a long period of time, instead of in short separate segments. Secondly, we would like to record the sensation of the subjects as the stimulus are presented to them in real-time. Thirdly, the ‘absolute’ method is easy to use in both the real and virtual environments, and many subjects can make their response at the same time.

Input devices are developed to record the level of excitement experienced by the users as they are participating in the motion-based movie journey (figure 2.4). The device is a hand-held box with a simple linear variable resistor mounted on it. The participants are instructed to push the knob along the track to indicate the current level of excitement experienced. The level of excitement marked on the device include : *Not Exciting*, *A Bit Exciting*, *Exciting*, *Very Exciting* and *Too Exciting*.

The level of excitement will be recorded by the motion control PC as the participants are watching the motion-based movie. The discrete scale is shown in linguistic terms for easy comprehension for humans. However, for the purpose of sensation modeling, the actual data will be recorded in a continuous scale and normalized to be within  $[-1,1]$ .

## 2.4 Trajectory Segmentation

The servo loop of the motion platform is running at 100Hz. For a normal 5 minute movie, we will get around 90000 points of position data for the three DOFs. If velocity and acceleration





Figure 2.4: Level of Excitement Input Device.

are also considered, the data size will be three times of that size. In order to reduce the size of the data to be processed and to retrieve meaningful information from the signal, we want to segment the trajectory data.

One characteristic we observe from this motion-based movie application is that at the point in time when there is a distinct motion event occurring on the screen, the roll, pitch or heave trajectory will change direction. For example, when there is a sudden turning in the path of the vehicle or the vehicle crashes onto some obstacles, the motion platform will always change its direction of motion. In order to consider the inter-axis relation, we segment the trajectory data at the position turning point of either roll, pitch or height. A segment begins at a turning point of a DOF curve (velocity=0) and ends at the next point in time when one of the DOFs' velocity reaches 0.

In general, for  $d$  DOFs, the number of types of segment  $s$  is

$$s = 2d \times 2^{d-1} + 2d \times (2d - 2) \times 2^{d-2} \quad (2.1)$$

The first term,  $2d \times 2^{d-1}$ , shows the number of possible segments formed by the change in the same degree of freedom, while the second term,  $2d \times (2d - 2) \times 2^{d-2}$ , represents the segments formed by the change of motion in two different degrees of freedom.

Figure 2.5 shows the 16 types of segment in the 2-DOF case. The first kind of segment starts from a local minima in roll and ends with a local maxima in roll. It is a segment in which the platform is rolling to the left and pitching down. In segment 7, the segment starts at a local minima in pitch and ends with a local maxima in pitch. The platform is pitching up and rolling right. For Segment 11, it starts with a maxima in roll and ends with a maxima in pitch. During this segment, the platform is rolling to the left and pitching down at the same time.







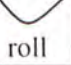





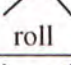
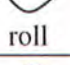
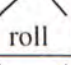
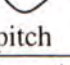
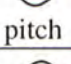
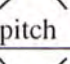
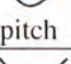
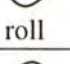
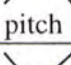

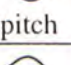
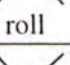
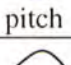

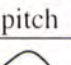
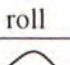
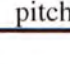


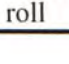
	Start	End	Motion		Start	End	Motion
1			roll right (pitch down)	9			roll right pitch down
2			roll left (pitch down)	10			roll right pitch up
3			roll right (pitch up)	11			roll left pitch down
4			roll left (pitch up)	12			roll left pitch up
5			pitch down (roll left)	13			pitch down roll left
6			pitch up (roll left)	14			pitch down roll right
7			pitch down (roll right)	15			pitch up roll left
8			pitch up (roll right)	16			pitch up roll right

Figure 2.5: Types of Segment in the 2-DOF case.

For each segment, the following data are recorded for modeling:

- Segment type
- Segment length (in time)
- Maximum roll angle, velocity and acceleration
- Maximum pitch angle, velocity and acceleration



- Maximum vertical velocity and acceleration

In our body, we do not have sensory organ for the measurement of absolute height. Without any reference with the ambient environment, the participants on the platform generally do not know how high the platform actually is. Therefore, we assume that the absolute height does not contribute to the level of excitement.

For our 3-DOF motion platform, there are a total of 60 different kinds of trajectory segment (figures 2.6 and 2.7). For each segment, there are 10 different data elements. These data elements will be used as inputs to the computational model of human sensation.

In this chapter, we have reviewed the complexity of human sense related to full-body motion. Our full-body motion VR interface is designed to act as an experimental testbed for the ideas we propose in the coming chapters. The sensation experienced by the participants during the VR journey can be recorded by the system. The segmented platform motion trajectories and the sensation data are used for the development of human sensation models. In the next chapter, we will discuss the design and validation of such models.









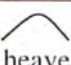

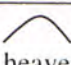
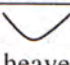
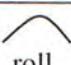
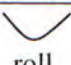
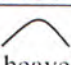
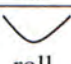
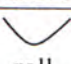
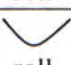
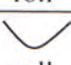
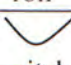
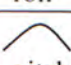
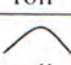
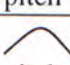
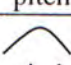

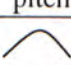



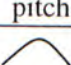
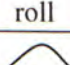

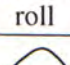

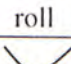
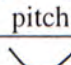

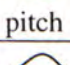
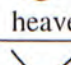
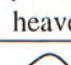
	Start	End	Motion		Start	End	Motion
1			roll right (pitch down) (move up)	19			move up (pitch up) (roll left)
2			roll right (pitch down) (move down)	20			move up (pitch up) (roll right)
3			roll right (pitch up) (move up)	21			move down (pitch down) (roll left)
4			roll right (pitch up) (move down)	22			move down (pitch down) (roll right)
5			roll left (pitch down) (move up)	23			move down (pitch up) (roll left)
6			roll left (pitch down) (move down)	24			move down (pitch up) (roll right)
7			roll left (pitch up) (move up)	25			roll right pitch down (move up)
8			roll left (pitch up) (move down)	26			roll right pitch up (move up)
9			pitch down (roll right) (move up)	27			roll left pitch down (move up)
10			pitch down (roll right) (move down)	28			roll left pitch up (move up)
11			pitch down (roll left) (move up)	29			pitch down roll left (move up)
12			pitch down (roll left) (move down)	30			pitch down roll right (move up)
13			pitch up (roll right) (move up)	31			pitch up roll left (move up)
14			pitch up (roll right) (move down)	32			pitch up roll right (move up)
15			pitch up (roll left) (move up)	33			roll right pitch down (move down)
16			pitch up (roll left) (move down)	34			roll right pitch up (move down)
17			move up (pitch down) (roll left)	35			roll left pitch down (move down)
18			move up (pitch down) (roll right)	36			roll left pitch up (move down)

Figure 2.6: Types of Segment in the 3-DOF case (1).






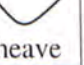

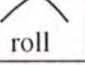

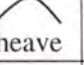
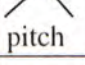
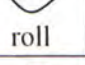
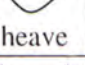
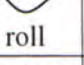
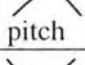
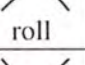
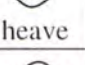
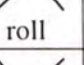
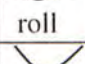
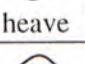
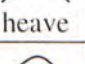
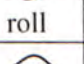
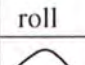
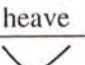
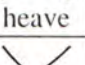
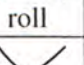

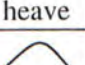
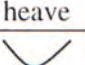







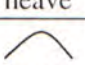
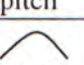
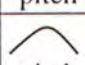
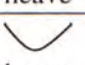
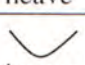
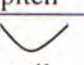
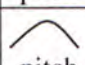
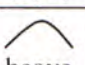

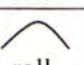
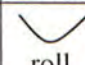
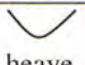
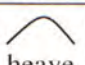














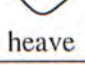


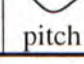
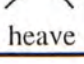
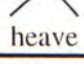
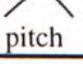




	Start	End	Motion		Start	End	Motion
37			pitch down roll left (move up)	55			pitch up move down (roll left)
38			pitch down roll right (move up)	56			pitch up move up (roll left)
39			pitch up roll left (move up)	57			move up roll left (pitch up)
40			pitch up roll right (move up)	58			move up roll right (pitch up)
41			roll right move down (pitch up)	59			move down roll left (pitch up)
42			roll right move up (pitch up)	60			move down roll right (pitch up)
43			roll left move down (pitch up)	61			move up pitch up (roll right)
44			roll left move up (pitch up)	62			move up pitch down (roll right)
45			pitch down move down (roll right)	63			move down pitch up (roll right)
46			pitch down move up (roll right)	64			move down pitch down (roll right)
47			pitch up move down (roll right)	65			move up roll left (pitch down)
48			pitch up move up (roll right)	66			move up roll right (pitch down)
49			roll right move down (pitch down)	67			move down roll left (pitch down)
50			roll right move up (pitch down)	68			move down roll right (pitch down)
51			roll left move down (pitch down)	69			move up pitch up (roll left)
52			roll left move up (pitch down)	70			move up pitch down (roll left)
53			pitch down move down (roll left)	71			move down pitch up (roll left)
54			pitch down move up (roll left)	72			move down pitch down (roll left)

Figure 2.7: Types of Segment in the 3-DOF case (2).

# Chapter 3

## Learning and Validation of Human Sensation Models

We propose using Cascade Neural Network (CNN) with Node-Decoupled Extended Kalman Filter (NDEKF) training for modeling human sensation in virtual environments. This type of neural network outperforms other traditional networks in our application because the cascade neural network is flexible in its architecture and NDEKF training has the property of fast convergence.

In order to establish the degree to which the sensation model is able to capture the characteristics of human sensation, it is important that we measure the relative similarity between the original human sensation data and the sensation outputs of the models. For model validation, we propose using a stochastic similarity measure based on Hidden Markov Model (HMM) analysis for comparing the sensation trajectories of humans and trained sensation models.

In this chapter, we explain the architecture and training process of the cascade neural network. The dynamic nature of human sensation can be modeled using the network by including historic inputs in the training. Two subjects participate in the activity of our virtual environment system and their sensations are recorded and modeled. The effect of trajectory segmentation in the modeling process is then demonstrated. Finally, we discuss the HMM-based similarity measure scheme for comparing stochastic and dynamic trajectories of human sensation. This similarity measure is used to compare the sensation data of human and trained models.



## 3.1 Cascade Neural Networks

It is well known that artificial neural networks are capable of capturing the complex non-linear mappings between input and output data of unknown systems [56] [24]. There are two main drawbacks associated with the traditional fixed-structured neural networks. First, the structure of the network, including the number of hidden neurons and the nature of the activation functions, is very difficult to determine. Second, traditional training schemes, such as back-propagation and other gradient descent algorithms, converge slowly.

In order to capture the characteristics of human sensation into a computational model, we need to specify two things. The first is the structure of the model. The second is the parameters of the model. However, all of the previous sensation modeling techniques only addressed the parameter issue. Here we want to point out that both the model structure and parameters are equally important in modeling human sensation.

Based on the above belief, we propose using Cascade Neural Network (CNN) [13] [14] as a modeling tool for human sensation. Cascade neural networks have been successfully applied in modeling human control strategies in simulated vehicle driving [50] and in controlling a single wheel robot [66]. It differs from the rest of the network models in a number of aspects. The network structure and size are not fixed, but dynamically adjusting during the training process. The final network size is minimized, because the network starts from the minimal size and gradually increases in size as the training continues. Training stops when the network size has reached a given level or the desired performance is achieved. It also allows the existence of different kinds of activation functions.

In the network training aspect, Node-Decoupled Extended Kalman Filtering (NDEKF) is applied.

The cascade neural network is trained by following the steps below (figure 3.1):

1. No hidden unit is installed in the network in the beginning. The weights of the input and output nodes are trained first, thereby capturing the linear relationship between the input and output nodes.
2. If there is no further decrease in the RMS error, one hidden unit will be added to the network from a pool of candidate units.

3. Quickprop [15] algorithm will be used to train the candidate units, using different random initial weights. The candidate units are trained independently and in parallel.
4. If there is no further decrease in the RMS error, the best candidate unit will be installed in the network.
5. Freeze the input weights to the new hidden unit and train the weights to the output unit. Freezing the input weights of all previous hidden units in the training is equivalent to training a 3-layered feedforward network with only one hidden unit. It allows for faster convergence.
6. The above steps are repeated until the RMS error is low enough or the number of hidden units has reached a specified value.

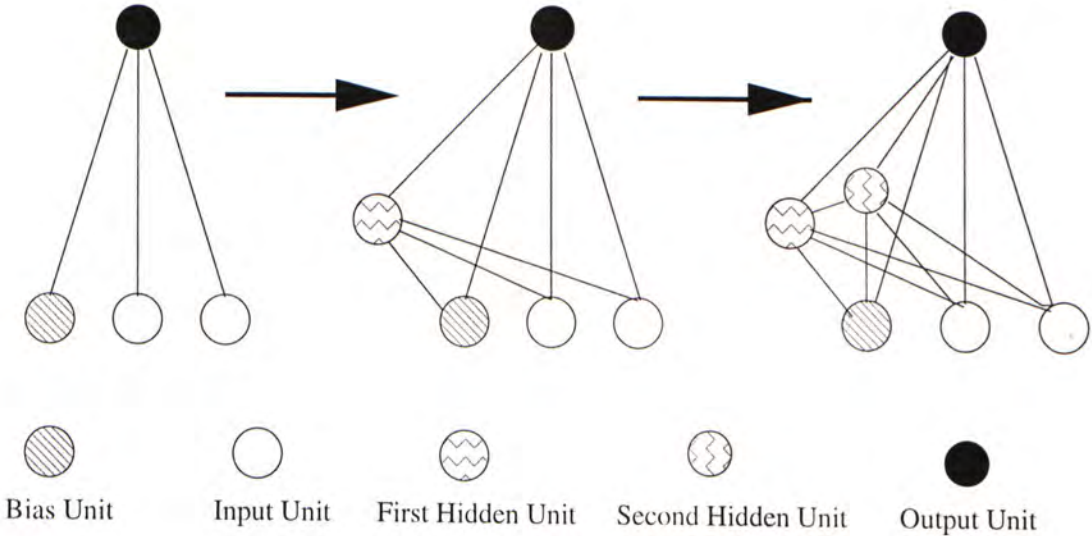


Figure 3.1: Cascade Neural Network

New hidden units receive connections from all input units as well as all previous hidden units, that is why the network is named as cascade neural network.

Assume that a cascade network has  $n_{in}$  input units (including bias unit),  $n_h$  hidden units and  $n_o$  output units, the total number of connection in the network  $n_w$  is :

$$n_w = n_{in}n_o + n_h(n_{in} + n_o) + (n_h + 1)n_h/2 \quad (3.1)$$



For a given network node, the kind of activation function which gives the best performance will be installed. During the training process, the kind of activation function which reduces the RMS error the most is selected. The available types of activation functions include Sigmoid, Gaussian, Bessel, and sinusoids of various frequencies [48].

In general extended Kalman filtering, there is a conditional error covariance matrix which stores the interdependence of each pair of weights in the network. NDEKF simplifies the algorithm by considering only the interdependence of weights that feed into the same node. By iteratively training one hidden unit at a time and then freezing that unit's weights, the detrimental effect of node-decoupling is minimized.

The NDEKF weight-update recursion is given by :

$$\omega_{k+1}^i = \omega_k^i + \{(\psi_k^i)^T (A_k \xi_k)\} \phi_k^i \quad (3.2)$$

where  $\xi_k$  is the  $n_o$ -dimensional error vector for the current training pattern,  $\psi_k^i$  is the  $n_o$ -dimensional vector of partial-derivatives of the network's output unit signal with respect to the  $i^{th}$  unit's net input, and  $\omega_k^i$  is the input-side weight vector of length  $n_w^i$  at iteration  $k$  for unit  $i \in \{0, 1, \dots, n_o\}$ .  $i = 0$  corresponds to the current hidden unit being trained, and  $i \in \{1, \dots, n_o\}$  corresponds to the  $i^{th}$  output unit, and,

$$\phi_k^i = P_k^i \xi_k^i \quad (3.3)$$

$$A_k = \left[ I + \sum_{i=0}^{n_o} \{(\xi_k^i)^T \phi_k^i\} \left[ \psi_k^i (\psi_k^i)^T \right] \right]^{-1} \quad (3.4)$$

$$P_{k+1}^i = P_k^i - \{(\psi_k^i)^T (A_k \psi_k^i)\} \left[ \phi_k^i (\phi_k^i)^T \right] + \eta_Q I \quad (3.5)$$

$$P_0^i = (1/\eta_P) I \quad (3.6)$$

where  $\xi_k^i$  is the  $n_w^i$ -dimensional input vector for the  $i^{th}$  unit, and  $P_k^i$  is the  $n_w^i \times n_w^i$  approximate conditional error covariance matrix for the  $i^{th}$  unit. Parameter  $\eta_Q$  (0.0001) is included in equation (3.5) to alleviate singularity problems for error covariance matrices [54].

The cascade neural network has a number of advantages. Since the network gradually organizes its structure to optimize the performance, no a priori model assumption about human sensation is required. Network size is minimized as it grows from a simple two layer network. It possesses good sensation function approximation properties. In NDEKF training,

only part of the network is trained at any one time, so it converges within fewer number of training epochs compared to the traditional quick-prop algorithm. The final RMS error is better than quick-prop training in an order of magnitude difference.

### 3.1.1 Dynamic Mapping

The cascade architecture only approximates a static mapping between the motion input and sensation output. However, the human sensation function is dynamic. The current level of sensation is dependent on the level of sensation experienced a short period ago. In general, any unknown dynamic system can be approximated by providing a set of time history data [46]. Therefore, we approximate this dynamic system by a difference equation :

$$\begin{aligned} \bar{u}(k+1) = & \Gamma[\bar{u}(k), \bar{u}(k-1), \dots, \bar{u}(k-n_u), \\ & \bar{x}(k), \bar{x}(k-1), \dots, \bar{x}(k-n_x)] \end{aligned} \quad (3.7)$$

where  $\Gamma()$  is some non-linear map,  $\bar{u}(k)$  is the sensation level at time  $k$ ,  $\bar{x}(k)$  is the sensory stimulus at time  $k$ .  $n_u$  and  $n_x$  are the orders of the dynamic system.

At any given time, the sensation output is a function of the current motion input and sensation level, as well as some previous motion inputs and sensation levels. In our experiments, 3 sets of previous segment data are included in the modeling. which gives a total input dimension of 40.

## 3.2 Experimental Trajectory Data

In our experiments, we adopt a sample movie and produce the corresponding platform motion trajectory using the teach pendant. We ask two persons to participate in the VR journey and let them record the level of excitement.



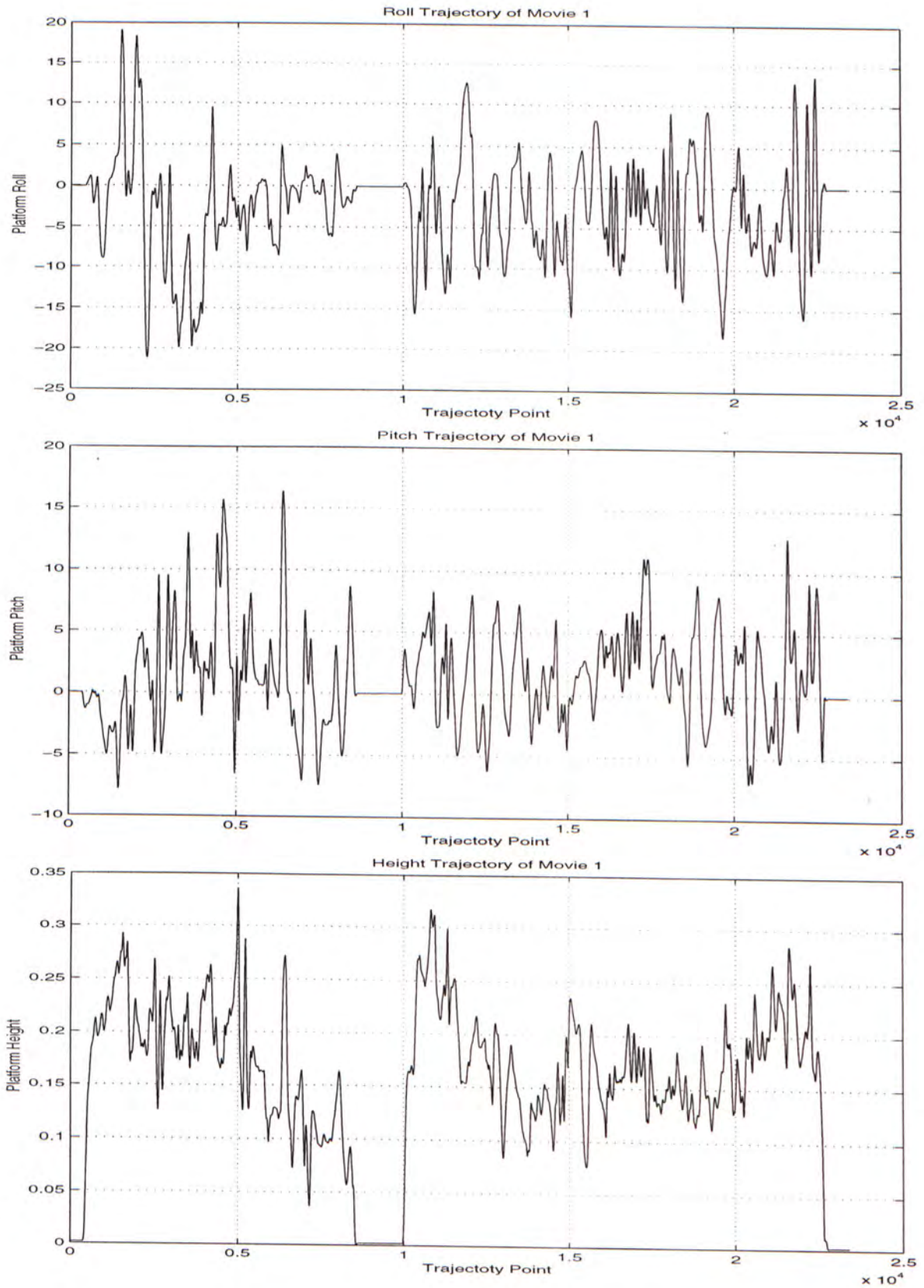


Figure 3.2: Platform Trajectory for the Movie

Figures 3.2 shows the roll, pitch and height trajectories of the motion platform during the movie journey. The movie is about 4 minutes long and each DOF contains about 24000 data points. The straight horizontal segments at both ends and in the middle of the trajectories represent the time during when the motion platform is placed at rest without any motion.

Figure 3.3 shows the sensation record of subject 1 during the VR movie journey. The sensation data is normalized between -1 and 1. When the knob of the sensation input device is pushed to the top, the sensation level is 1. And when the knob of the sensation input device is pushed to the bottom, the sensation level is -1. At the beginning of the movie, subject 1 feels very excited. When the platform stops, the subject does not have any sensation of excitement.

Figures 3.4 and 3.5 are generated from two different sensation models trained from the data of subject 1.

All of the activation functions selected during the training are sine functions. There are a total of 15 hidden units in the network.

The model outputs do not diverge and can follow the trajectory of the original human sensation data. When the human sensation input is constant, there are some fluctuations above and below the curve. The cascade neural network model is able to capture the stochastic properties of the human response and reveal it in the output. When the human data is changing fast, the model output matches it quite closely.

Figure 3.6 shows the human excitement response for subject 2 in the movie. For the same platform trajectory, it is apparent that different people have very different sensation responses. Two separate models are also trained to capture the sensation. The models perform quite well as long as the platform keeps moving and the sensation keeps changing (figures 3.7 and 3.8).



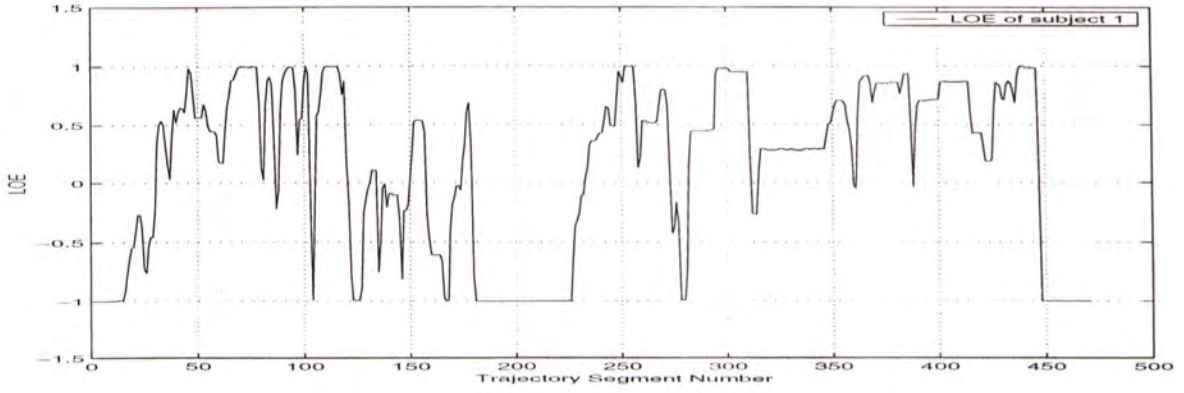


Figure 3.3: Sensation Trajectory of Subject 1

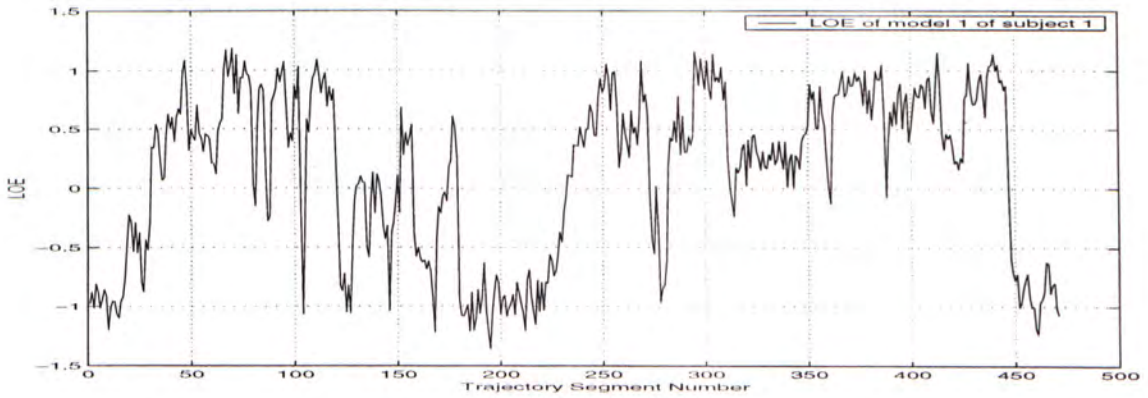


Figure 3.4: Sensation Trajectory of Model 1 of Subject 1

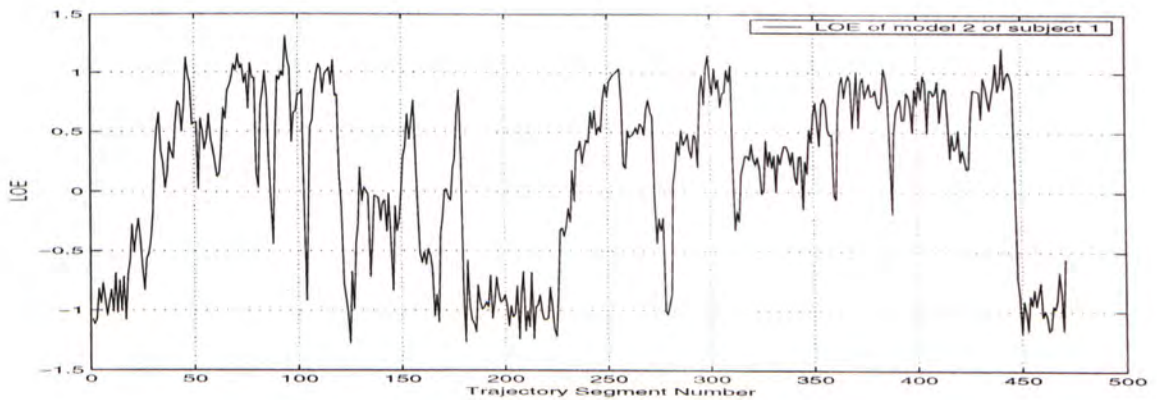


Figure 3.5: Sensation Trajectory of Model 2 of Subject 1

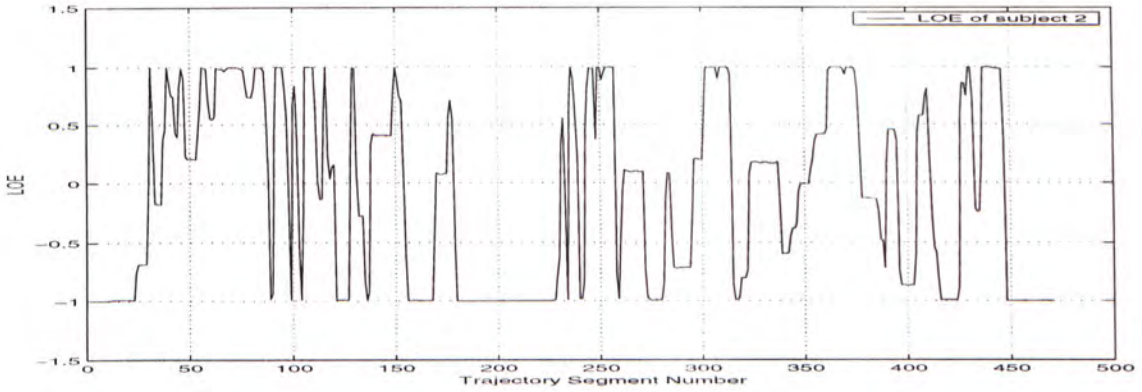


Figure 3.6: Sensation Trajectory of Subject 2

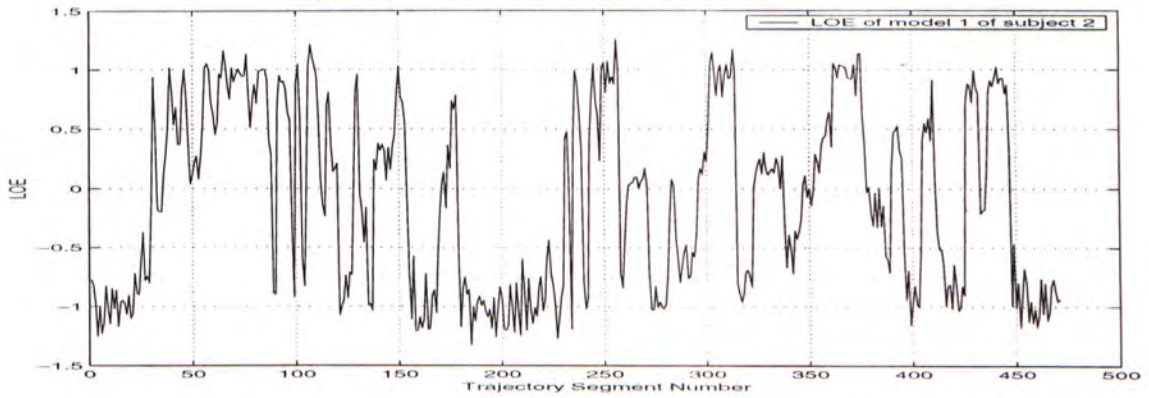


Figure 3.7: Sensation Trajectory of Model 1 of Subject 2

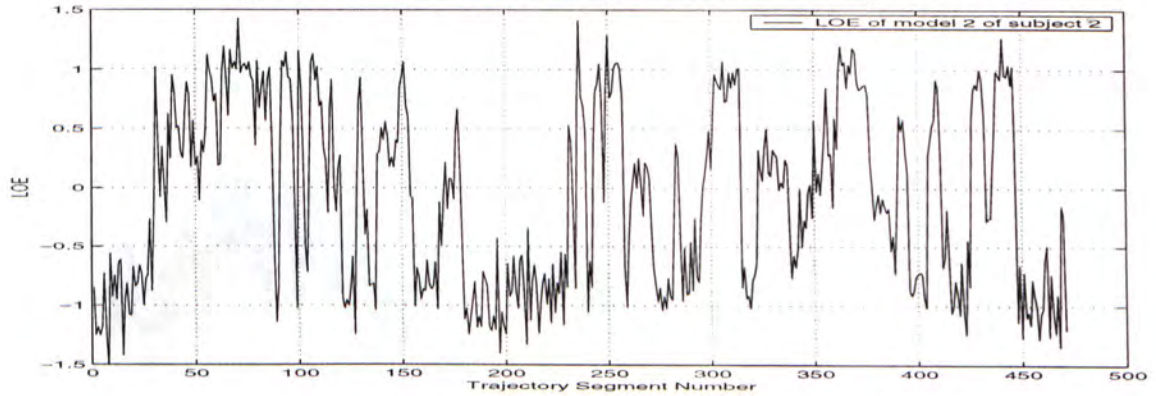


Figure 3.8: Sensation Trajectory of Model 2 of Subject 2



### 3.3 Effect of Trajectory Segmentation

The movie is about 4 minutes long and the original motion trajectory has a length of about 24000 groups of data. After segmentation, the trajectory length is reduced to 471. Figure 3.10 shows the sensation output of a model trained using the original unsegmented trajectory of subject 1. Compared to the original sensation of subject 1 and the outputs of the models trained using the segmented data, the modeling capability of the system trained using the original raw data is very weak. Based on the result of the model, it is clear that the data segmentation technique not only can reduce the input data size, but it also improves the modeling capability.

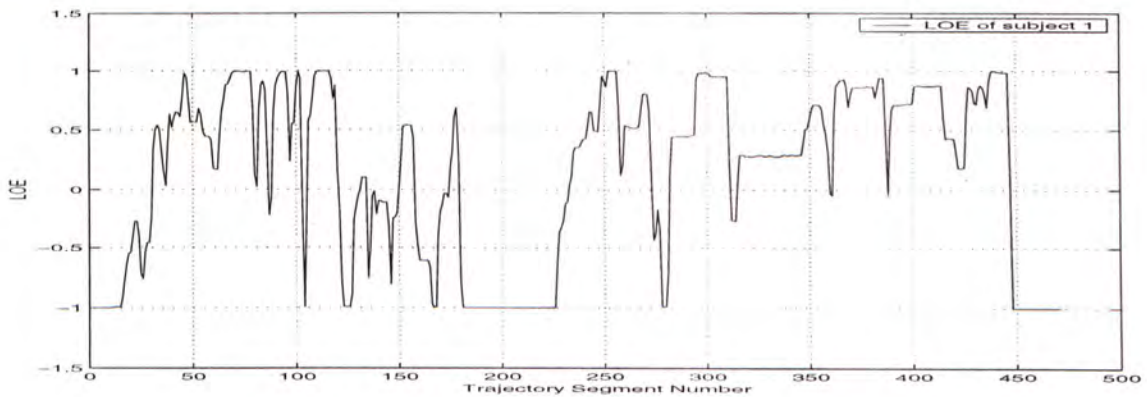


Figure 3.9: Original Sensation Trajectory of Subject 1

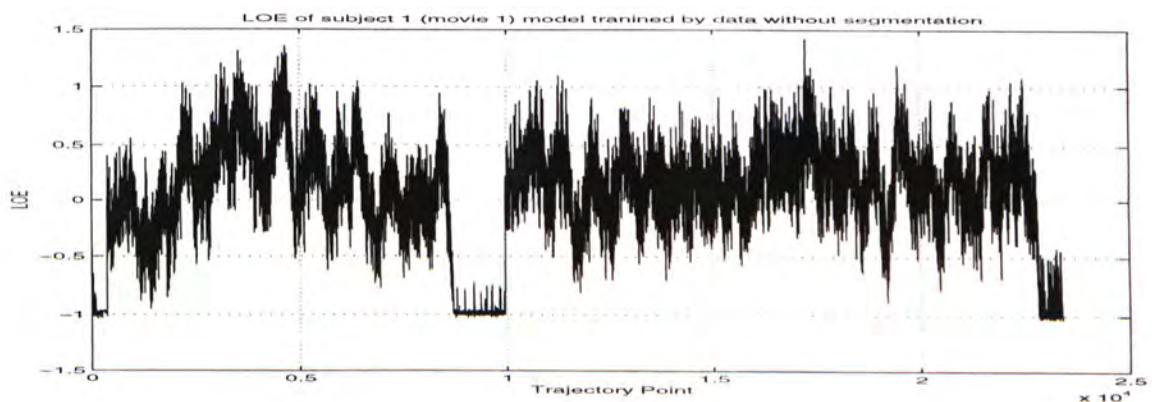


Figure 3.10: Trajectory of Model Trained by Unsegmented Motion Data

## 3.4 Model Validation

The main strength of modeling human sensation by learning is that no explicit physical human model is needed. That means we can model the reaction of human even though we have not yet had enough psychological and biological understanding about the process. However, the lack of scientific justification of the learnt models may detract from the confidence we can show in the outputs. In order to measure the level to which human and model-generated trajectories are similar, we need to perform model validation. Since the human sensation models are learnt from experimental data, we must independently verify and validate the computed models' fidelity to the source human data. It is desirable to compare the similarity between the overall system trajectories, not just the similarity between individual training patterns. Validations have to be done across human and human, model and model, and human and model.

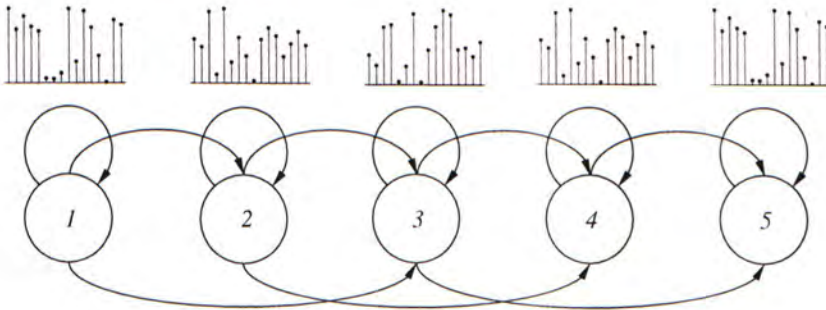


Figure 3.11: Hidden Markov Model

The human sensation trajectories are dynamic, nonlinear, stochastic and long. The Hidden-Markov-Model-based similarity measure scheme developed in [49] is employed to compare the similarity between different sensation trajectories. HMMs are doubly stochastic trainable statistical models [55]. No a priori assumption is made about the statistical distribution of the data, and a high degree of sequential structure can be encoded within the HMM model. HMMs have been widely used in the areas of signal processing [38] and speech recognition [26]. Yang and Xu applied HMMs to open-loop skill learning [64] and gesture recognition [65]. The HMM-based similarity measure scheme performs better than the Bayes



optimal classifier and the fast Fourier transform based spectral classifier [50].

Figure 3.11 shows the structure of a HMM. A Hidden Markov Model consists of  $n$  different states and can move between different states according to probabilistic transitions. At each state, an output symbol will be randomly produced. The HMM  $\lambda$  can be specified by 3 matrices.

$$\lambda = \{A, B, \pi\} \quad (3.8)$$

$A$  is the  $n \times n$  state transition matrix which shows the probability of transition between different states at any given state.  $B$  is the  $L \times n$  output probability matrix which shows the probability of producing  $L$  different output symbols at any given state.  $\pi$  is the  $n$ -length initial state probability distribution vector. For a given  $\lambda$ , it is capable of producing a series of output symbols which we call observation sequence  $O$ .

There are two operations we can do using HMM in our model validation.

- Train a HMM  $\lambda$  given an observation sequence - that is to maximize  $P(\lambda|O)$  using the Baum-Welch Expectation Maximization Algorithm.
- Calculate the probability that a given observation sequence  $O$  is generated from a HMM model  $\lambda$  - that is to calculate  $P(O|\lambda)$  using the Forward-Backward Algorithm.

## 3.5 Similarity Measure

The similarity measure  $\sigma$  between two observation sequences  $O_1, O_2$  are calculated using equations (3.9) and (3.10). Equation (3.10) shows the probability of the observation sequence  $O_i$  given model  $\lambda_j$ , normalized with respect to the sequence length  $T$ . The power and  $\log$  operations are applied to prevent the data underflow problem.

$$\sigma(O_1, O_2) = \sqrt{\frac{P_{21}P_{12}}{P_{11}P_{22}}} \quad (3.9)$$

$$P_{ij} = 10^{\log P(O_i|\lambda_j)/T_j} \quad (3.10)$$

Equations (3.11) to (3.13) show the properties of this similarity measure.

$$\sigma(O_1, O_2) = \sigma(O_2, O_1) \quad (3.11)$$

$$0 \leq \sigma(O_1, O_2) \leq 1 \quad (3.12)$$

$$\sigma(O_1, O_2) = 1 \quad \text{if and only if} \quad \lambda_1 = \lambda_2 \quad (3.13)$$

The human sensation data and the model-generated data are both real-valued. The real-valued data are converted into sequence of discrete symbols by data preprocessing. The preprocessing include a number of steps : 1) normalization, 2) spectral conversion, 3) power spectral density (PSD) estimation and 4) vector quantization.

### 1. Normalization

In the normalization step, the data is scaled such that it is ranged between -1 and 1. The scale factor for a given dimension has to be the same.

### 2. Spectral Conversion

After normalization, spectral conversion is performed on the data. The data is segmented into possibly overlapping window frames. Hamming window is applied to each frame to minimize spectral leakage caused by data windowing [53]. We then use Discrete Fourier Transform to convert the real vector to complex vector.

The Hamming window transform  $T_H^v(\cdot)$  maps a  $k$ -length real vector  $\bar{y} = [y_1 y_2 \dots y_k]^T$  to a  $k$ -length real vector  $\bar{h}$ .

$$\bar{h} = T_H^v(\bar{y}) = [H_1 y_1 \quad H_2 y_2 \quad \dots \quad H_k y_k], \text{ where} \quad (3.14)$$

$$H_p = 0.54 - 0.46 \cos \left[ \frac{2\pi(p-1)}{k-1} \right], p \in \{1, 2, \dots, k\} \quad (3.15)$$

The Discrete Fourier Transform  $T_F^v(\cdot)$  maps a  $k$ -length real vector  $\bar{y} = [y_1 y_2 \dots y_k]^T$  to a  $k$ -length complex vector  $\bar{z}$ .

$$\bar{z} = T_F^v(\bar{y}) = [F_0(\bar{y}) \quad F_1(\bar{y}) \quad \dots \quad F_{k-1}(\bar{y})], \text{ where} \quad (3.16)$$

$$F_p(\bar{y}) = \sum_{q=0}^{k-1} y_{q+1} e^{2\pi i p q / k}, p \in \{0, 1, \dots, k-1\}. \quad (3.17)$$

### 3. Power Spectral Density

The Power Spectral Density estimate produces a feature matrix for the Hamming-Fourier transform and is defined as :

$$P_{HF}^v(\bar{f}) = [P_{HF0}(\bar{f}) \quad P_{HF1}(\bar{f}) \quad \dots \quad P_{HF(k/2)}(\bar{f})], \text{ where} \quad (3.18)$$



$$P_{HF0}(\bar{f}) = \frac{|f_0|^2}{H_{ss}} \quad (3.19)$$

$$P_{HFp}(\bar{f}) = \frac{1}{H_{ss}}(|f_p|^2 + |f_{k-p}|^2), p \in \{1, 2, \dots, k/2 - 1\} \quad (3.20)$$

$$P_{HF(k/2)}(\bar{f}) = \frac{|f_{(k/2)}|^2}{H_{ss}}, \text{ and} \quad (3.21)$$

$$H_{ss} = k \sum_{q=1}^k H_k^2 \quad (3.22)$$

We define two unity transforms

$$P_G^v(\bar{y}) = T_G^v(\bar{y}) = \bar{y}, \quad \text{and let} \quad (3.23)$$

$$\bar{y}_{[\tau, k]} = [y_\tau \quad y_{\tau+1} \quad \dots \quad y_{\tau+k-1}^i]^T \quad (3.24)$$

be the  $k$ -length segment, beginning at element  $\tau$ , for the  $t$ -length vector  $\bar{y}$ . Define the vector-to-matrix transform :

$$T_{(\varphi, [k_1, k_2])}^{vm}(\bar{y}) = \begin{bmatrix} P_\varphi^v\{T_\varphi^v(\bar{y}_{[1, k_1]})\} \\ P_\varphi^v\{T_\varphi^v(\bar{y}_{[k_2+1, k_1]})\} \\ P_\varphi^v\{T_\varphi^v(\bar{y}_{[2k_2+1, k_1]})\} \\ \vdots \end{bmatrix}, \varphi \in \{F, HF, G\}. \quad (3.25)$$

Given a matrix  $U = [\bar{u}_1 \quad \bar{u}_2 \quad \dots \quad \bar{u}_d]$ , let's define the matrix-to-matrix transform  $T_{(\bar{\varphi}, [k_1, k_2])}^{mm}(\cdot)$ .

$$T_{(\bar{\varphi}, [k_1, k_2])}^{mm}(U) = [T_{(\varphi_1, [k_1, k_2])}^{vm}(\bar{u}_1) \quad T_{(\varphi_2, [k_1, k_2])}^{vm}(\bar{u}_2) \quad \dots \quad T_{(\varphi_D, [k_1, k_2])}^{vm}(\bar{u}_D)], \quad (3.26)$$

$$\bar{\varphi} = [\varphi_1 \quad \varphi_2 \quad \dots \quad \varphi_D], \quad \varphi_d \in \{F, HF, G\}, \quad d \in \{1, 2, \dots, D\} \quad (3.27)$$

The spectral conversion and PSD estimation can be expressed as,

$$V^n = T_{(\bar{\varphi}, [\kappa_1, \kappa_2])}^{mm}(U^n), \quad (3.28)$$

where the input is a  $t_n \times D$  matrix  $U^n$  and the output is a  $T_n \times K$  matrix  $V^n$ .

$$T_n = \text{floor} \left( \frac{t_n - \kappa_1}{\kappa_2} + 1 \right), \quad K = \sum_{\varphi_d \in \{F, HF\}} (\kappa_1/2 + 1) + \sum_{\varphi_d = G} \kappa_1. \quad (3.29)$$

The integer constants  $\kappa_1 \geq \kappa_2 > 0$  define the length of each window frame as  $\kappa_1$  and the window overlap as  $\kappa_2 - \kappa_1$ .

## 4. Vector Quantization

In this step, we convert the feature vector  $V$  into  $L$  discrete symbols, where  $L$  is the number of output observable symbols in the Hidden Markov Model. Let  $V = \{\bar{v}_t^n\}$ ,  $t \in \{1, 2, \dots, T_n\}$ ,  $n \in \{1, 2, \dots, N\}$  denote the set of feature vectors, where  $\bar{v}_t^n$  is the  $j^{\text{th}}$  row of the  $i^{\text{th}}$  feature matrix. In vector quantization, the many  $\bar{v}_t^n$  are replaced with  $L$  prototype vectors  $Q_L = \{\bar{q}_l\}$ ,  $l \in \{1, 2, \dots, L\}$ , known as the codebook, such that the total distortion  $D(V, Q_L)$  is minimized over all feature vectors, where

$$D(V, Q_L) = \sum_{n,t} \min_l d(\bar{v}_t^n, \bar{q}_l), \quad \text{and} \quad d(\bar{v}_t^n, \bar{q}_l) = (\bar{q}_l - \bar{v}_t^n) \cdot (\bar{q}_l - \bar{v}_t^n) \quad (3.30)$$

The quantization is performed by using the LBG vector quantization algorithm [42]. Given a codebook size of  $L = 2^m$ ,  $m \in \{0, 1, 2, \dots\}$ , the algorithm can be stopped at an appropriate level of discretization for the available data.

Given a trained VQ codebook  $Q_L$ , the feature vectors  $V^n$  can be converted into a sequence of discrete symbols  $O_n = \{o_1^n, o_2^n, \dots, o_{T_n}^n\}$ .

$$O_n = T_{VQ}^m(V^n, Q_L) = \{T_{VQ}^v(\bar{v}_1^n, Q_L), T_{VQ}^v(\bar{v}_2^n, Q_L), \dots, T_{VQ}^v(\bar{v}_{T_n}^n, Q_L)\} \quad (3.31)$$

$$\text{where} \quad o_t^n = T_{VQ}^v(\bar{v}_t^n, Q_L) = \text{index}[\min_l d(\bar{v}_t^n, \bar{q}_l)] \quad (3.32)$$

The quantized sequences of human sensation data will be used to train HMMs for similarity measure.



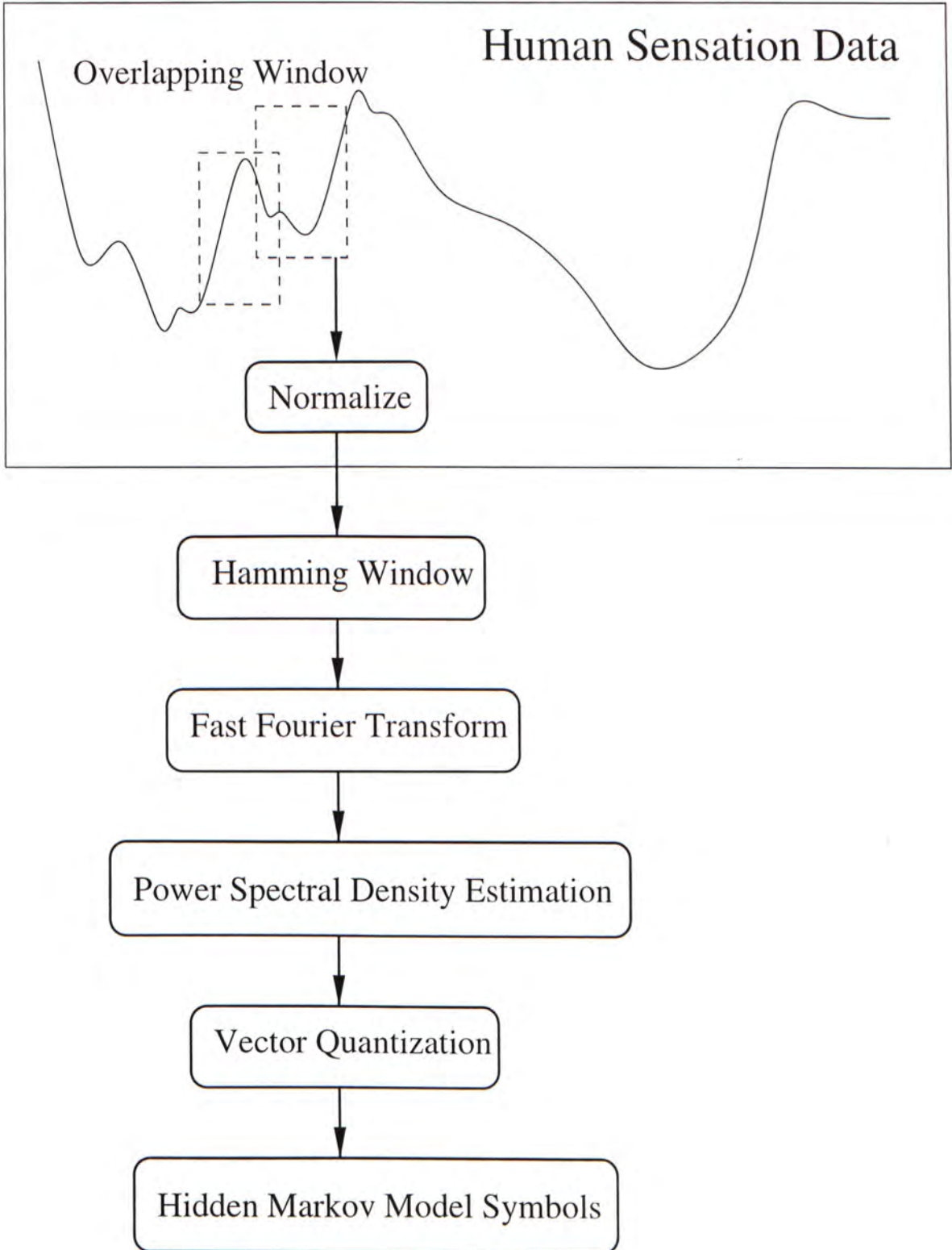


Figure 3.12: Conversion of Human Sensation Trajectory to a Sequence of Discrete Symbols

## 3.6 Similarity Measure Results

Using the HMM-based similarity measure scheme, we are able to calculate the relative similarity between the human sensation data and the machine-generated sensation data. Table 3.1 shows the results for the similarity measure between the model outputs and the human outputs.

	Subject 1	Subject 2	Subject 1 Model 1	Subject 1 Model 2	Subject 2 Model 1	Subject 2 Model 2
Subject 1	1	0.183	<i>0.320</i>	<i>0.388</i>	0.183	0.098
Subject 2	0.183	1	0.140	0.107	<i>0.286</i>	<i>0.266</i>
Sub 1 Model 1	<i>0.320</i>	0.140	1	<i>0.659</i>	0.264	0.181
Sub 1 Model 2	<i>0.388</i>	0.107	<i>0.659</i>	1	0.180	0.220
Sub 2 Model 1	0.183	<i>0.286</i>	0.264	0.180	1	<i>0.417</i>
Sub 2 Model 2	0.098	<i>0.266</i>	0.181	0.220	<i>0.417</i>	1

Table 3.1: Similarity Measure Result

Here we have 6 sensation trajectories (figures 3.3 to 3.8) : the sensation trajectory of subject 1, the sensation trajectory of subject 2, the output of first model of subject 1, the output of second model of subject 1, the output of first model of subject 2 and the output of the second model of subject 2. The diagonal elements are 1 because the similarity measure between the same trajectory is always 1.

From the table, we can see that the sensation data of the human subjects have the highest similarity values with the outputs of the corresponding trained models. It is exactly what we expect. For example, in column one, the human data of subject 1 closely matches with the output of its two models. We can see that model 2 performs a bit better than model 1. For the second model of subject 2 (final column), it has the highest similarity measure with the sensation trajectory of subject 2 and the output of the first model of subject 2. A particular individual's models not only match the sensation data of that individual, but also exhibit a



lesser degree of similarity with another individual's sensation data. We can conclude that the HMM-based similarity measure has successfully indicated the relative similarity between the human sensation data and the modeled sensation data.

The models of subject 1 capture the characteristics of the original human sensation better than the models of subjects 2 do. This difference is due to the modeling capability of the cascade neural network. The cascade neural network tends to model continuous data better than data with switching and discontinuity. As we can see from figures 3.3 to 3.8, there is more discontinuity in the sensation trajectory of subject 2 than subject 1. Therefore, in the case of subject 2, discontinuity in the data causes similar inputs to be mapped to radically different outputs. This problem not only appears in cascade neural network, but in all continuous function approximators (figure 3.13). However, in the application of human sensation recording, the detrimental effect introduced is still acceptable.

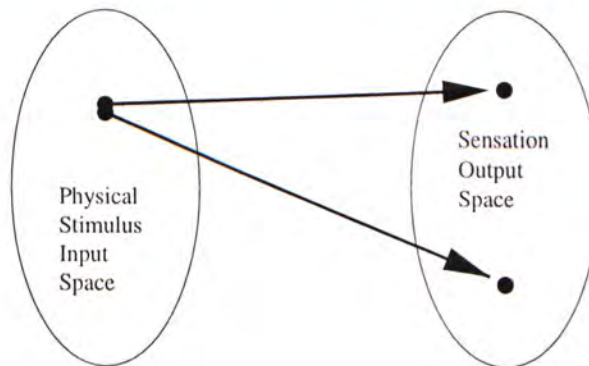


Figure 3.13: Discontinuity Causes Similar Motion Inputs to be Mapped to Different Sensation Outputs

In summary, we have developed a framework for the learning and validation of human sensation models. Cascade neural networks are able to capture the essence of human sensation in virtual environments and the similarity measure based on Hidden Markov Models are capable of revealing the relative similarities between the sensation trajectories of humans and trained models. In the next chapter, we will study the problem of data reduction for human sensation modeling. The performance of the sensation models trained by the reduced set of data will be evaluated by the similarity measure discussed.

# Chapter 4

## Input Reduction for Human Sensation Modeling

In the previous chapter, we investigated a method for modeling the relationship between virtual motion inputs and human sensation outputs. The performance of the models can be validated using a similarity measure based on Hidden Markov Models. In modeling human sensation, it is possible that the dimension of inputs presented to the human be very high. In this chapter, we will consider a number of input selection and feature extraction methods which can reduce the size of the stimulus inputs for modeling human sensation.

We firstly apply Principal Component Analysis (PCA) as an input extraction technique for sensation modeling, then Independent Component Analysis (ICA) is introduced. Independent component analysis is to be used both for input selection and feature extraction. A novel technique of input selection using ICA is verified on a classic set of statistical sample, the furnace data. All the input reduction methods are applied on the human sensation data obtained on the full-body motion VR system and the performance of the techniques are compared using the HMM-based similarity measure.

Experimental results show that the ICA-based input selection scheme is capable of improving the modeling performance of the computational sensation systems and reducing the input dimension by 60%.

### 4.1 Introduction

Although the physical stimuli presented to the participants in the virtual environments can be well under control, the amount of perceptual data received by the humans are still very large. In terms of human sensation modeling, that means the dimension of inputs of the



sensation model can be very high. Therefore it is desirable to reduce the dimension of the sensation inputs in the modeling process in order to reduce the computational complexity and memory requirements.

It is suggested that the goal of biological sensory coding in the brain is to transform the input signals such that the redundancy between the inputs can be reduced [2]. Motivated by the results in neurosciences, Independent Component Analysis is shown to be a possible tool for extracting features from sensory data. The effect produced by Independent Component Analysis can be interpreted as dimension reduction in the sense that the mutual information in the transformed components are minimized [41].

In the following sections, we will propose using a fixed point algorithm for Independent Component Analysis to reduce the dimension of the inputs to the sensation modeling process. The sensation output of a human participant and those of the sensation models will be compared using the HMM-based similarity measure scheme.

## 4.2 Input Reduction

Input Reduction (or Data Reduction) refers to the process which reduces the amount of data input to a system such that most of the intrinsic information content of data can be retained. In the context of human sensation modeling, that means we want to reduce the size of the virtual environmental stimulus input to the model while keeping the model output similar to the actual human sensation levels.

The subject of input reduction is concerned with the mathematical tool for reducing the dimensionality of pattern representation. Pattern descriptors constituting the lower-dimensional representation are referred to as features because of their fundamental role in characterizing the distinguishing properties of pattern classes.

There are two different ways to categorize methods of data reduction. The first one is model-based vs model-free [7] and the second way is feature extraction vs input selection [32]. Model-based methods usually involve selecting a model, choosing the inputs to use, optimizing the parameters and measure the performance. A test procedure is designed to choose the subsets of inputs to use based on the performance results. Model-free methods are based on performing a statistical test between the subsets of input variables and the

desired outputs from the model. In this chapter, we will focus on input reduction by feature extraction and input selection.

In modeling human sensation, it is important to form an appropriate set of inputs which are required by the models, so that the performance of the models can be optimized in some sense. If too much inputs are used in the modeling process, many problems may occur. The purpose of input selection and feature extraction in human sensation modeling is multifold. Firstly, as the input size gets large, the sensation models become more complex and the resources requirements, such as memory, will increase significantly. Secondly, if large amount of unrequired inputs are present, learning and model training will become more difficult. Unrequired inputs may cause the models to misconverge to inappropriate positions and reduce the accuracy of the models. Thirdly, large input sets tend to create larger models. If two models of different sizes are giving comparable results, the structure and nature of the more complex model is more difficult to analyze and understand. Fourthly, as the complexity of a sensation model and the complexity of the virtual reality system implementation grow rapidly with the number of dimensions of the stimuli input space, it is important to base decision only on the most essential discriminatory information conveyed by the features. Fifthly, compressing the modeling information may facilitate a considerable reduction in the required communication-channel capacity. Sixthly, identification of stimuli measurement which are redundant or irrelevant with regard to a particular sensation modeling task is important for reducing the overall cost of measurement extraction. Finally, a useful by-product of feature evaluation is that it provides the means for assessing the potential of a given stimulus representation space for discriminating between elements of different sensation levels. If the sensation overlap is too high even in the stimulus representation space, then new sources of stimulus information will need to be sought to enhance sensation level separability.

### 4.3 Feature Extraction and Input Selection

Data reduction methods can be classified into two different approaches : *feature extraction* and *input selection*.

Input selection, also known as variable selection, selects a subset of variables from an original set of available variables. A number of methods have been proposed to tackle the



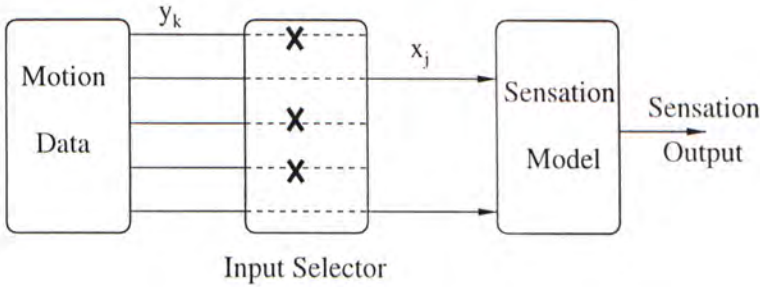


Figure 4.1: Input Selection

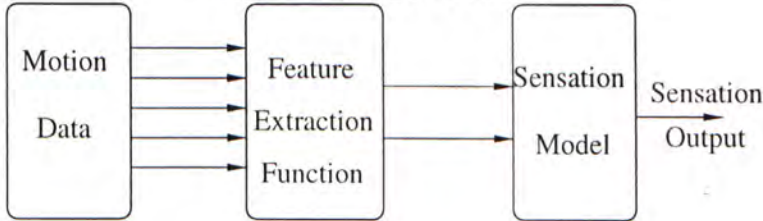


Figure 4.2: Feature Extraction

problem of input selection, mainly contributed by the statisticians in the pattern recognition area. Floating search method [45] finds a sub-optimal set that is near to the optimal solution. Some variable selection methods utilizing neural networks have also been developed recently [9]. To the input selection problem, there is no optimal and generally applicable solution exists. Depending on the understanding of the problem, some methods may be more suitable for an application under certain conditions than other methods. The problem of input selection is one of selecting a small subset of  $d$  inputs  $x_j, j = 1, 2, \dots, d$ , out of the available  $D$  measurements  $y_k, k = 1, 2, \dots, D$ . The redundant and irrelevant stimulus measurements are simply ignored (figure 4.1).

Feature extraction transforms a set of inputs into a lower-dimensional feature space. The compression is achieved by a mapping process the goal of which is to project useful information contained in the original observations onto a very few composite feature variables, while ignoring redundant and irrelevant information. The transformation can be either linear or non-linear (figure 4.2). The computational load of the modeling would be shifted from the classification stage to the feature extraction stage. One of the most famous schemes of feature extraction is Principal Component Analysis [33].

## 4.4 Feature Extraction Using Principal Component Analysis

Principal Component Analysis (PCA) is a popular feature extraction technique for creating new variables which are linear combination of the original variables [33]. The new variables are uncorrelated among themselves.

Geometrically, the objective of PCA is to identify a set of orthogonal axes called the principal components. The new variables (principal component scores) are formed by projecting the original variables on the principal components.

$$\begin{aligned}
 q_1 &= w_{11}x_1 + w_{12}x_2 + \dots + w_{1p}x_p \\
 q_2 &= w_{21}x_1 + w_{22}x_2 + \dots + w_{2p}x_p \\
 &\dots \\
 q_m &= w_{p1}x_1 + w_{p2}x_2 + \dots + w_{pp}x_p
 \end{aligned} \tag{4.1}$$

where  $x_1, x_2, \dots, x_m$  are the original variables,  $q_1, q_2, \dots, q_m$  are the  $m$  principal components and  $w_{ij}$  is the weight of the  $j^{\text{th}}$  variable for the  $i^{\text{th}}$  principal components.

The transformation is performed such that the first new variable accounts for the maximum variance in the data. The second new variable accounts for the maximum variance which has not been accounted for by the first variable. In general, the  $p^{\text{th}}$  new variable accounts for the maximum variance which has not been accounted for by the  $p - 1$  variables.

When PCA is used as a tool for feature extraction, we determine how many new variables are retained for analysis. The sum of the variances of the new variables not used to represent the data can be considered as a measure of the loss of information in the dimension reduction process.

Let  $X$  denote an  $m$ -dimensional random vector representing the original data having a mean of zero. If  $X$  has a non-zero mean, its mean is subtracted from it before proceeding with the analysis. Let  $q$  denote a unit vector of dimension  $m$ .  $X$  is to be projected on  $q$  and this projection can be defined by the inner product between these two vectors.

$$A = X^T q = q^T X \tag{4.2}$$



The norm of  $q$  is assumed to be 1.

$$|q| = (q^T q)^{\frac{1}{2}} = 1 \quad (4.3)$$

The projection  $A$  is also a random variable with a mean of zero. Its mean and variance are related to the statistics of  $X$ .

$$E[A] = E[X] = q^T E[X] = 0 \quad (4.4)$$

The variance of  $A$  is the same as its mean-square value.

$$\begin{aligned} \sigma^2 &= E[A^2] \\ &= E[(q^T X)(X^T q)] \\ &= q^T E[XX^T]q \\ &= q^T Rq \end{aligned} \quad (4.5)$$

The  $m$ -by- $m$  matrix  $R$  is the correlation matrix of the random vector  $X$ . The next step is to find out those vectors  $q$  along which the variance of  $A$  has extremal or stationary values. The question can be transformed into an eigenvalue problem.

$$Rq = \lambda q \quad (4.6)$$

The correlation matrix  $R$  is symmetric and the eigenvalues are real and non-negative. Let the eigenvalues of the  $m$ -by- $m$  matrix  $R$  be denoted by  $\lambda_1, \lambda_2, \dots, \lambda_m$  and the associated eigenvectors be denoted by  $q_1, q_2, \dots, q_m$ .

$$Rq_j = \lambda_j q_j \quad j = 1, 2, \dots, m \quad (4.7)$$

To compute the dimensionality reduction of some input data, the eigenvalues and eigenvectors of the correlation matrix of the input data vector are first calculated. The original data are then projected onto the subspace spanned by the eigenvectors belonging to the dominant eigenvalues.

In general, the weights  $w_{ij}$  assigned to the original variables  $x_i$  are affected by the relative variance of the variables. The original data is standardized before PCA because we do not

want the relative variance to affect the weight. The variance of each variable is made to one because there is no compelling reason to believe that any one motion factor is more important than others in forming the principal components. And a motion factor should not receive an artificially higher weight due to the variance in its intensity.

There are originally 40 motion variables in our motion data. They are transformed into 40 principal components. The first 17 PCs are selected. They cover 81% of the total variance of the data set. The 17 transformed vectors and the human sensation data of subject 1 are used as training data for the sensation models. Three models are trained (figures 4.3 to 4.5) and the similarity values against the original human data (table 4.1) are as follows :

Model Number	Similarity
1	0.0033
2	0.0130
3	0.0132

Table 4.1: Model Similarity Measure Result for Motion Data Reduced by PCA Feature Extraction

The performance is worse than the models trained by the original unreduced data.



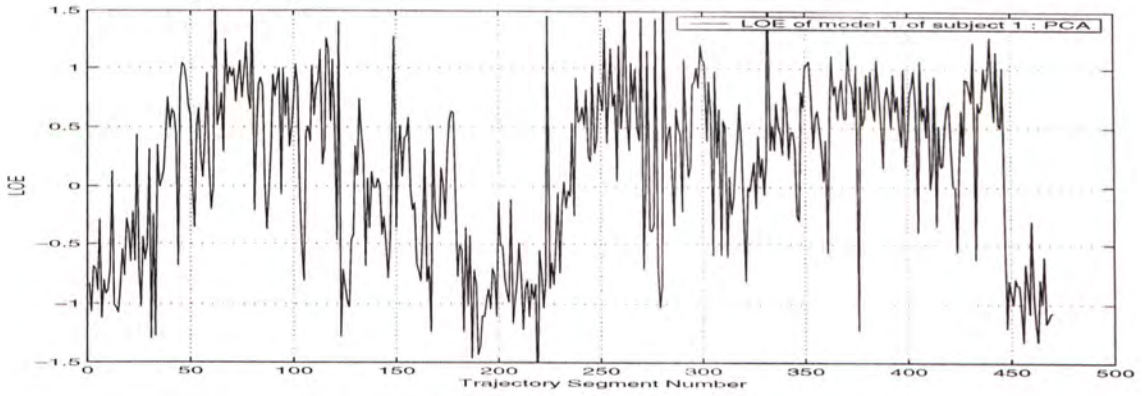


Figure 4.3: Sensation Model 1, Motion Data Processed by PCA Feature Extraction

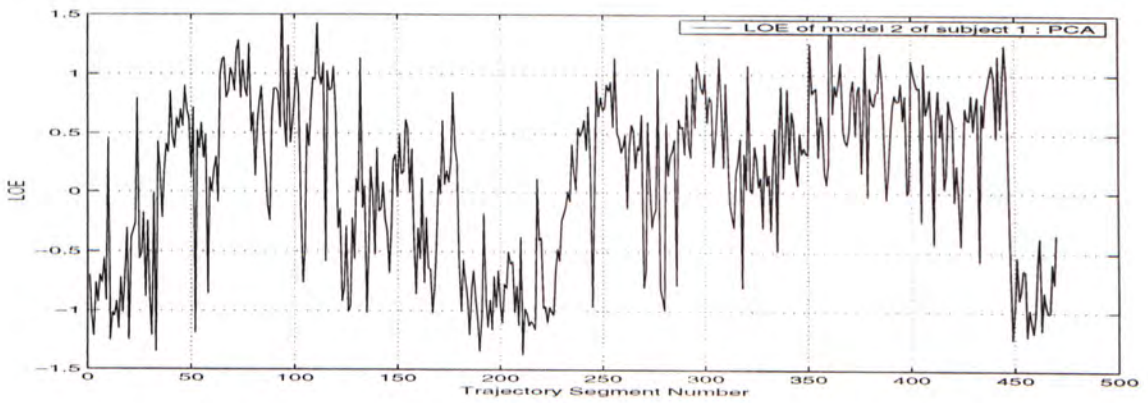


Figure 4.4: Sensation Model 2, Motion Data Processed by PCA Feature Extraction

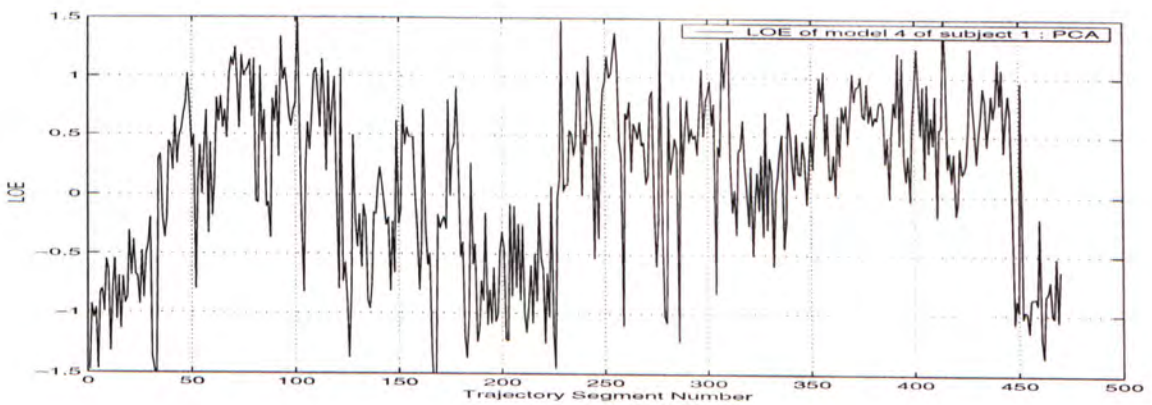


Figure 4.5: Sensation Model 3, Motion Data Processed by PCA Feature Extraction

## 4.5 Independent Component Analysis

We propose using Independent Component Analysis (ICA) to reduce the dimension of the motion trajectory inputs for human sensation modeling. Independent Component Analysis is a statistical method which transforms an observed multi-dimensional vector into components that are statistically as independent as possible.

ICA has been applied in a number of areas, including blind source separation, biomedical analysis and image processing. Blind source separation is the classical application of the ICA model [35]. One well known example of blind source separation is the cocktail party problem. Assume that several people are speaking simultaneously in the same room, as in a cocktail party. Then the problem is to separate the voices of the different speakers, using recordings of the microphones in the room [40]. Electroencephalographic (EEG) recordings are one example of using ICA for biomedical signal processing [62]. ICA algorithms have been extended to investigate task-related human brain activity in functional Magnetic Resonance Imaging (fMRI) data [43]. ICA is applied because this method can segregate overlapping neural activities into independent components. It is assumed that those biomedical data are summed approximately linearly and are temporally independent. In image processing, Bell and Sejnowski suggested that ICA can be used to extract features (filters) from natural scenes that are localized edge detectors [3]. Gray, et al. demonstrated the successful use of ICA filters as features in face recognition tasks and lipreading tasks [18].

The variables  $x_1$  and  $x_2$  are said to be independent if the value of  $x_1$  does not give any information of the value of  $x_2$ , and vice versa. Let's denote by  $p(x_1, x_2)$  the joint probability density function (pdf) of  $x_1$  and  $x_2$ , and by  $p_1(x_1)$  the marginal pdf of  $x_1$  :

$$p_1(x_1) = \int p(x_1, x_2) dx_2, \quad (4.8)$$

and similarly for  $x_2$ .  $x_1$  and  $x_2$  are independent if and only if the joint pdf is factorizable in the following way:

$$p(x_1, x_2) = p_1(x_1)p_2(x_2). \quad (4.9)$$

The definition extends for any number  $n$  of random variables and the joint density will be a product of  $n$  terms.

The underlying  $m$  time-varying factors are represented by  $s_i(t), i = 1, \dots, m$  (*the source*)



and the  $n$ -dimension trajectory of the motion platform is denoted by  $x_j(t), j = 1, \dots, n$  (*the observed data*).  $t$  is the discrete time and  $s_i(t)$ 's are thought to be independent sources of information. We suppose that both the independent sources and the observed data have zero mean. Since the relationship between the source and the observed data is assumed linear, the process can be represented by :

$$x_j(t) = \sum_i a_{ij} s_i(t) \quad (4.10)$$

where  $a_{ij}$  are the mixing coefficients which describe the influence of the independent components on the observed data.

Using vector-matrix notation, the above relation can be expressed as :

$$\mathbf{x}(t) = \mathbf{A}\mathbf{s}(t) \quad (4.11)$$

where  $\mathbf{x}(t)$  denotes the platform trajectory data vector with elements  $x_j(t)$ ,  $\mathbf{s}(t)$  denotes the underlying independent component vector with elements  $s_i(t)$  and  $\mathbf{A}$  is the mixing matrix with elements  $a_{ij}$ .

The independent components are latent variables, which means that they cannot be directly observed. The basic idea of ICA is to estimate  $\mathbf{s}$  and  $\mathbf{A}$  using the observed  $\mathbf{x}$ , based on the assumption that the elements of the vector  $\mathbf{s}$  are statistically independent. It is also assumed that the independent components have non-gaussian distributions.

A fixed-point algorithm is employed for independent component analysis [28]. In this algorithm, we do not need to know the number  $m$  of the underlying factors in advance. Firstly, the vector  $\mathbf{x}$  is centered, that is to subtract its mean so as to make  $\mathbf{x}$ 's mean equals to zero. Secondly, the centered  $\mathbf{x}$  is whitened.  $\mathbf{x}$  is transformed linearly to  $\mathbf{x}'$  so that its components are uncorrelated and their variances equal unity. This step is achieved by using Principal Component Analysis and the transformation is always possible. Elements with small variance can be removed from the original data and the dimension of the data can be reduced. After the whitening process, we get

$$\mathbf{s}(t) = \mathbf{B}^T \mathbf{x}'(t) \quad (4.12)$$

where  $\mathbf{B}$  is an orthogonal square matrix and the problem is simplified.

### 4.5.1 Measure of Gaussianity

Based on the concepts of information theory, the entropy of a random variable measures the level of information that the observation of the variable gives. For equal variances, the random variable which has the highest entropy is gaussian. Entropy  $H$  is defined for a discrete random variable  $Y$  whose density is  $P()$  as

$$H(Y) = - \sum_i P(Y = a_i) \log P(Y = a_i) \quad (4.13)$$

where  $a_i$  are the possible values of  $Y$ .

There are a number of method to measure the gaussianity of a random variable for ICA estimation. Here we will discuss three of them : Kurtosis, Negentropy and the approximation of Negentropy.

The traditional measure of non-gaussianity is kurtosis or the fourth-order cumulant. The kurtosis of  $y$  is defined by :

$$kurt(y) = E\{y^4\} - 3(E\{y^2\})^2 \quad (4.14)$$

Typically non-gaussianity is measured by the absolute value of kurtosis. It is zero for a gaussian variable and greater than zero for non-gaussian variables. Kurtosis has some drawbacks in practice, especially when its value has to be estimated from a measured sample. The main problem is that kurtosis can be very sensitive to outliers [27]. Its value may depend on only a few observations in the tails of its distribution, which may be erroneous or irrelevant observation. In other words, kurtosis is not a robust measure of gaussianity.

The second non-gaussianity measure is negentropy, which is defined as :

$$J(y) = H(y_{gauss}) - H(y) \quad (4.15)$$

where  $y_{gauss}$  is a gaussian random variable of the the same covariance matrix as  $y$ . Negentropy is always non-negative and is invariant for invertible linear transformation. It is in some sense the optimal estimator of gaussianity [10] but it is computationally very difficult. Estimation of negentropy using the definition will require the use of the pdf, therefore a more simple estimation of gaussianity is desirable.

The third non-gaussianity measure is the approximation of negentropy based on maximum-entropy principle [29]. A simple approximation of the negentropy  $J$  of random variable  $y$  is



of the form :

$$J(y) \propto [E\{g(y)\} - E\{g(\nu)\}]^2 \quad (4.16)$$

where  $g()$  is any non-quadratic function,  $\nu$  is a standardized gaussian variable of zero mean and unit variance and  $E\{\}$  is the expected value.

Equation (11) can now be used as a robust contrast function in the ICA algorithm with

$$g(u) = \tanh(au) \quad (4.17)$$

where  $1 \leq a \leq 2$ .

### 4.5.2 The Fixed Point ICA Algorithm

The goal of the ICA algorithm is to search for a linear combination of the prewhitened data  $x'_i(t)$ , where  $y = w^T x'(t)$ , such that the negentropy (non-gaussianity) is maximized.  $w$  is assumed to be bounded to have norm of 1 and  $g'$  is the derivative of  $g$ . The fixed point algorithm [28] is as follows :

1. Generate an initial random vector  $w_{k-1}$ ,  $k = 1$
2.  $w_k = E\{x'g(w_{k-1}^T x')\} - E\{g'(w_{k-1}^T x')\}w_{k-1}$
3.  $w_k = w_k / \|w_k\|$
4. Stop if converged ( $\|w_k - w_{k-1}\|$  is smaller than certain defined threshold). Otherwise, increment  $k$  by 1 and return to step 2.

If the process converges successfully, the vector  $w_k$  produced can be converted to one of the underlying independent components by  $w_k^T x'(t)$ ,  $t = 1, 2, \dots, m$ . Due to the whitening process, the columns of  $B$  are orthonormal. By projecting the current estimates on the subspace orthogonal to the columns of the matrix  $B$  which are found previously, we are able to retrieve the components one after the other. Using this approach, the knowledge about the sensation model is not required.

The algorithm of ICA adopted has a number of desirable properties. Firstly, under the assumption of the data model, the convergence is cubic, or least quadratic. This is in contrast to the ordinary gradient descent method [17], which has a slow convergence speed. Secondly,

the algorithm is easy to use because there is no step size parameter to choose. Thirdly, the algorithm can find independent components of any non-gaussian distribution using any non-linearity  $g$ . Fourthly, the performance of the algorithm can be optimized by choosing a suitable non-linearity  $g$ . Fifthly, The ICs can be estimated one-by-one. This method can reduce the computational load in the case where only a number of the ICs are needed to be estimated. Finally, this algorithm enjoys most of the benefits of the traditional neural approaches : it is parallel, distributed, computationally simple and requires little memory space.

## 4.6 Input Reduction Using Independent Component Analysis

Three different kinds of ICA processing methods are applied to the motion data. In the first experiment, the results of ICA are directly used as inputs of the modeling process. Independent variables are used for training and the total number of input variables are retained. In the second part, ICA is applied as a feature extraction technique. The data size is reduced and the ICs which cover the majority of the variances are used as model inputs. Finally, we propose using ICA for selecting a subset of inputs from the original set of inputs. The proposed input selection scheme is verified by applying it on a classic statistical data set, the furnace data. Then the method is performed on the motion data for reduction. Three models are produced using the data processed by each of the above approaches. The sensation outputs of the trained models are compared using the Hidden-Markov-Model-based similarity measure. The performance of the processing methods can be evaluated based on the relative similarity between the outputs of the sensation models and the original sensation data of the subject.

### 4.6.1 ICA Without Dimension Reduction

The fixed-point ICA algorithm is applied to the motion data to convert the original data into mutually independent vectors. The number of dimension of the motion data is not changed



after the process. The dimension of the data remains 40. 100% of the non-zero eigenvalues are retained. The information carried by each vector is independent of all the other vectors. In the ICA transformation, the values of the eigenvalues ranges from 0.510131 to 0.00540708.

Three sensation models are trained using the transformed vectors and the sensation data of subject 1. Figures 4.6 to 4.8 are generated from the sensation models trained from the data processed by ICA without dimension reduction.

Model Number	Similarity
1	0.0398
2	0.0256
3	0.0172

Table 4.2: Model Similarity Measure Result for Motion Data Processed by ICA Without Input Reduction

The similarity between the original human sensation and the outputs of the models trained using motion data processed by ICA without input reduction is shown in table 4.2.

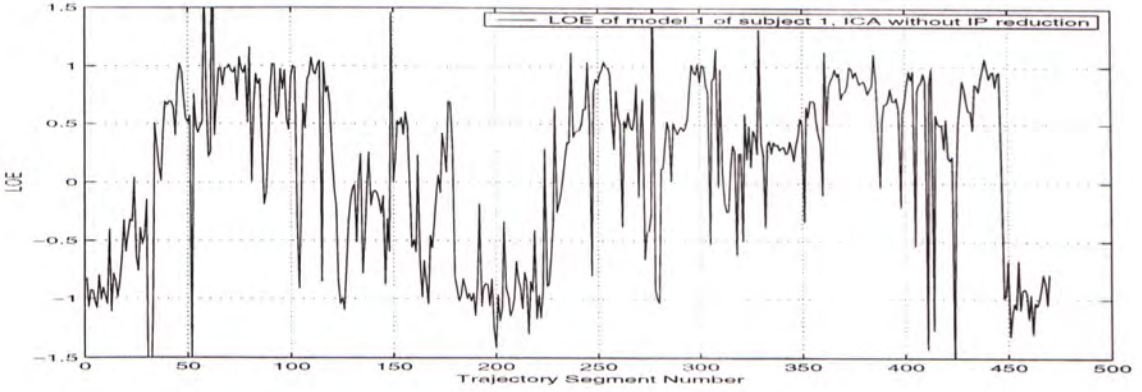


Figure 4.6: Sensation Model 1, Motion Data Processed by ICA, No Input Reduction

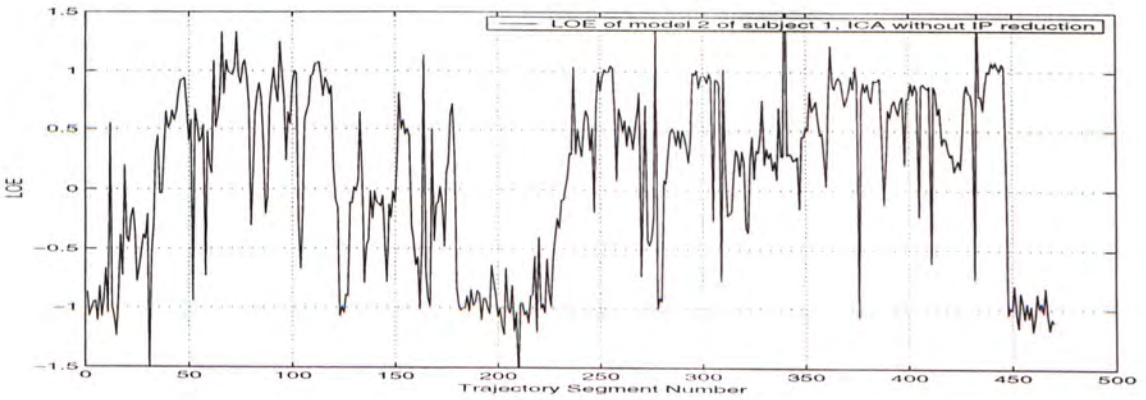


Figure 4.7: Sensation Model 2, Motion Data Processed by ICA, No Input Reduction

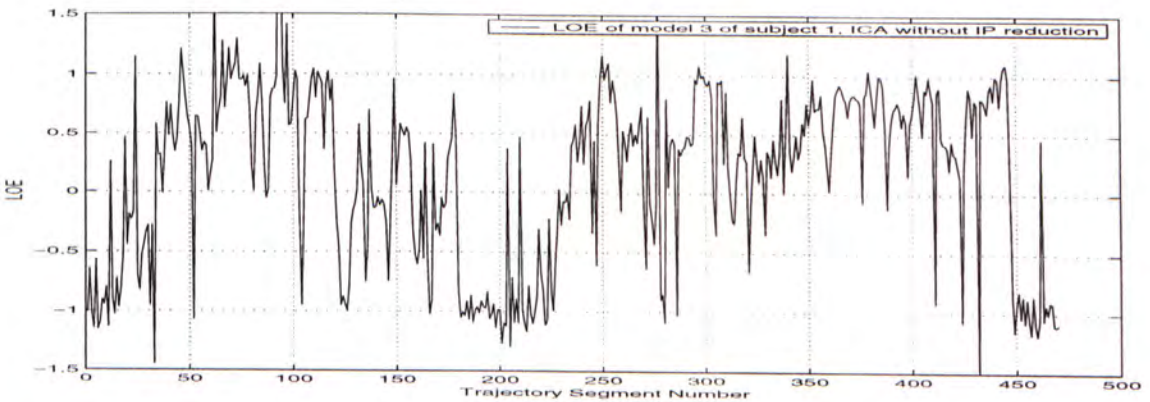


Figure 4.8: Sensation Model 3, Motion Data Processed by ICA, No Input Reduction



### 4.6.2 Feature Extraction Using ICA

The original 10 input components without time-shifting are reduced into 4 principal components in the whitening step. The trajectory data of the platform is then projected onto the subspace spanned by these 4 principal components. Less than 30% of the energy of the original data is removed in the process. 4 independent components are retrieved using the fixed-point ICA algorithm. These 4 independent components are then time-shifted to obtain 3 more groups of time history data for sensation modeling according to equation (3.7). The total sensory input dimension is reduced from 40 to 16. Figures 4.9 to 4.11 are generated from the sensation models trained from the features extracted using ICA. The similarity between the original human sensation and the outputs of the models trained using the feature extracted by ICA with input reduction is shown in table 4.3.

Model Number	Similarity
1	0.1316
2	0.1116
3	0.1126

Table 4.3: Model Similarity Measure Result for Motion Data Reduced by ICA Feature Extraction

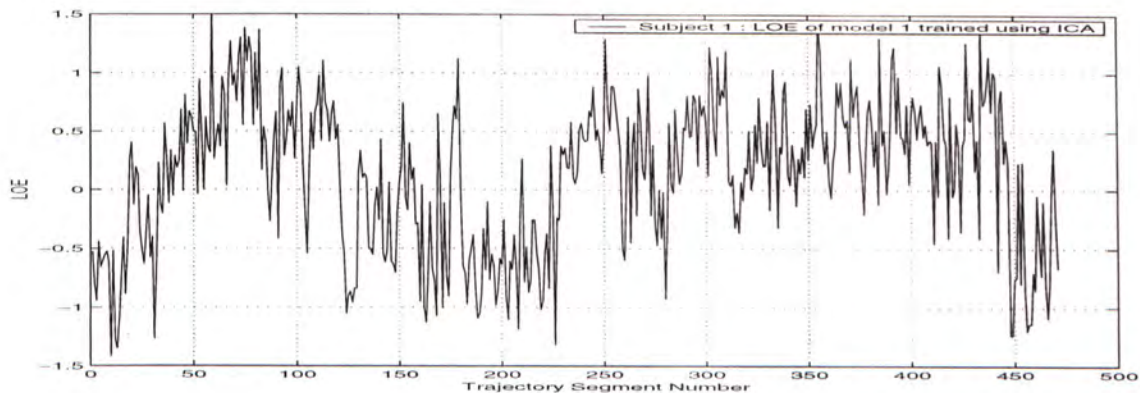


Figure 4.9: Sensation Model 1, Motion Data Reduced by ICA Feature Extraction

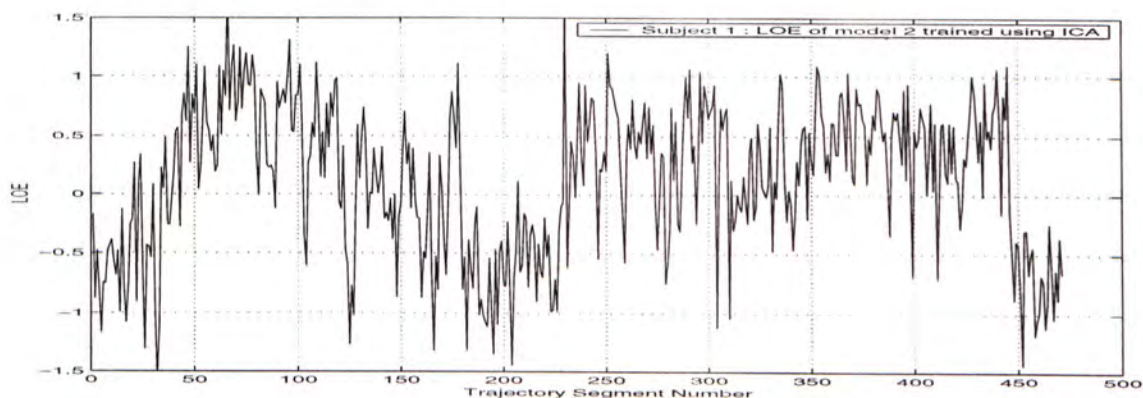


Figure 4.10: Sensation Model 2, Motion Data Reduced by ICA Feature Extraction

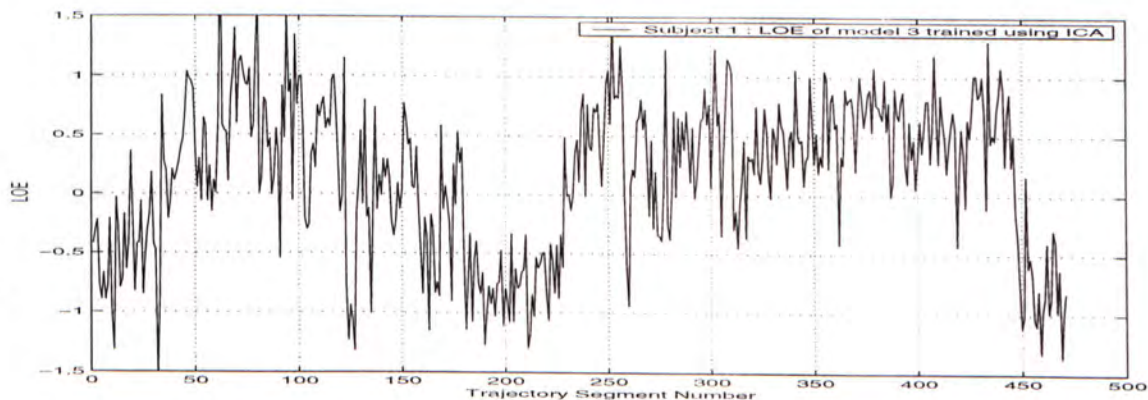


Figure 4.11: Sensation Model 3, Motion Data Reduced by ICA Feature Extraction



### 4.6.3 Input Selection Using ICA

In this part of the experiment, ICA is used as a technique for input selection. From the above discussions of ICA, we know that the independent components  $s_i$ 's can be linearly transformed to the original variables through the multiplication of the mixing matrix  $\mathbf{A}$  (equation (4.11)).

Columns of the matrix  $\mathbf{A}$  can be viewed as individual features, with each column representing one feature. Independent component  $s_i$  is the coefficient of the  $i^{\text{th}}$  feature in the original observed data  $x$ . Any one column of  $\mathbf{A}$  represents the contribution of a particular IC to all  $x_i$ 's. For example, the second column of matrix  $\mathbf{A}$  describes the influence of the second IC to the original variables.

Each original variable has a linear relationship with a number of independent components and in general certain ICs would have stronger influence on particular variables. Based on this property, we can classify the variables according to the weights in the mixing matrix.

The input selection process is as follows :

1. Perform ICA on the motion data and the sensation variable.
2. Determine the feature which has the highest influence on the sensation output variable.
3. Select the motion variables which are also heavily dependent on the IC of the selected feature.

A feature is selected if its weight which relates to the human sensation variable is larger than or equal to a certain feature selection threshold  $\epsilon$ . Among the variables in the selected feature, if the weights have values higher than or equal to an input selection threshold  $\eta$ , the corresponding inputs will be selected. The values of the thresholds are application dependent. The selected inputs variables have high correlation with the sensation output because they are all dependent on the same independent source of information.

Mathematically speaking,  $\mathbf{A}$  is the mixing matrix of the ICA model. The size of  $\mathbf{A}$  is  $(n + 1) \times (n + 1)$  where  $n$  is the number of motion inputs to the sensation model and the 1 represents the single output of the sensation model.  $a_{ij}$  denotes the element of matrix  $\mathbf{A}$  where  $i \in \{1, 2, \dots, n + 1\}$  and  $j \in \{1, 2, \dots, n + 1\}$ .

Let  $C \in \mathfrak{R}^{(n+1) \times 1}$  represents the set of column vectors of  $\mathbf{A}$ . Assume that  $K$  is the set of selected features and a feature column  $k_j$  is selected from  $C$  if its element related to sensation level is higher than or equal to the feature selection threshold  $\epsilon$ .

$$K = \{k_j \in \mathfrak{R}^{(n+1) \times 1} | k_j \in C \text{ and } |a_{(n+1)j}| \geq \epsilon\} \quad (4.18)$$

Let  $u_{pq}$  be the elements of the  $q^{\text{th}}$  selected column features, where  $p \in \{1, 2, \dots, n\}$ . And we further let  $L$  denote the set of selected inputs from the original set of inputs  $I$ . An input  $l_p$  is selected if the corresponding element in the selected feature column is higher than or equal to the input selection threshold  $\eta$ .

$$L = \{l_p \in I | |u_{pq}| \geq \eta\} \quad (4.19)$$

#### 4.6.4 Applying Input Selection by ICA on the Furnace Data

Our input selection method based on ICA is tested on a well-known problem of system identification given by Box and Jenkins [8]. The process to be modeled involves a gas furnace. The single input  $i(t)$  to the model is the input gas feedrate and the single output  $o(t)$  is the corresponding  $CO_2$  concentration(%) coming out from the furnace. The continuous data representing the dynamics of the system contains 296 pairs of data in the form  $[i(t); o(t)]$ . In order to extract the dynamic process model we arrange a candidate input set of 11 variables in the form  $[i(t), i(t-1), \dots, i(t-6), o(t-1), \dots, o(t-4)]$ , which include the current input, 4 elements in the output history and 6 elements from the input history. The original input and output of the furnace are shown in figures 4.12 and 4.13.

The furnace data is modeled using cascade neural networks. The original set of candidate inputs is modeled first. Three models are trained and they contained 15 hidden units. The outputs of the three trained models are shown in figures 4.14 to 4.16. The similarity between the original furnace output and the outputs of the three models is shown in table 4.4.



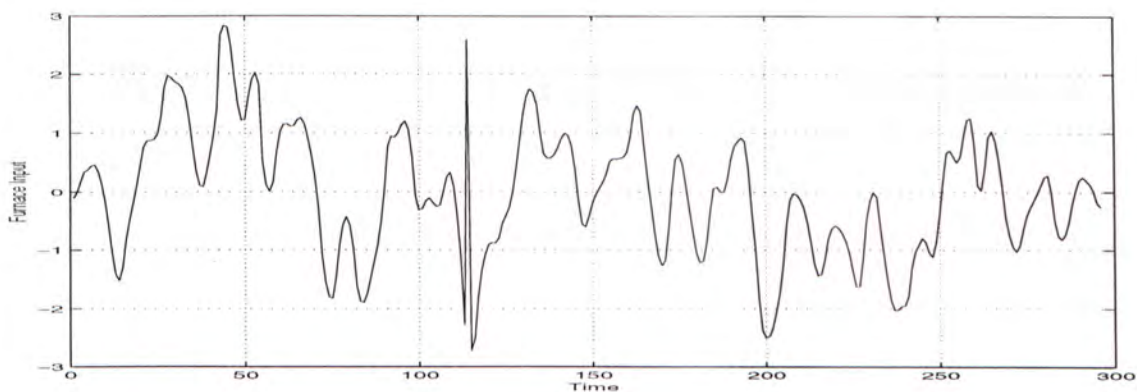


Figure 4.12: Original Input of Furnace

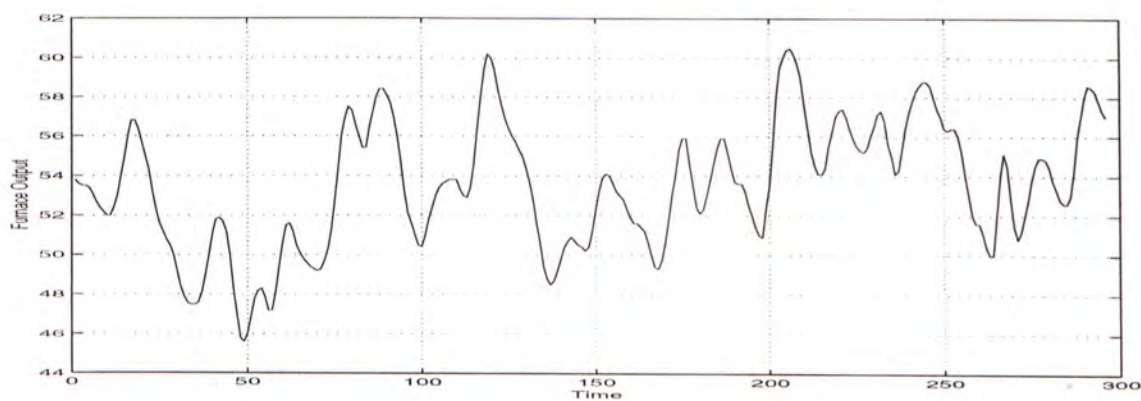


Figure 4.13: Original Output of Furnace

Model Number	Similarity
1	0.3655
2	0.5196
3	0.3244

Table 4.4: Furnace Similarity Measure Result for Model Trained Using Full Set of Candidate Inputs

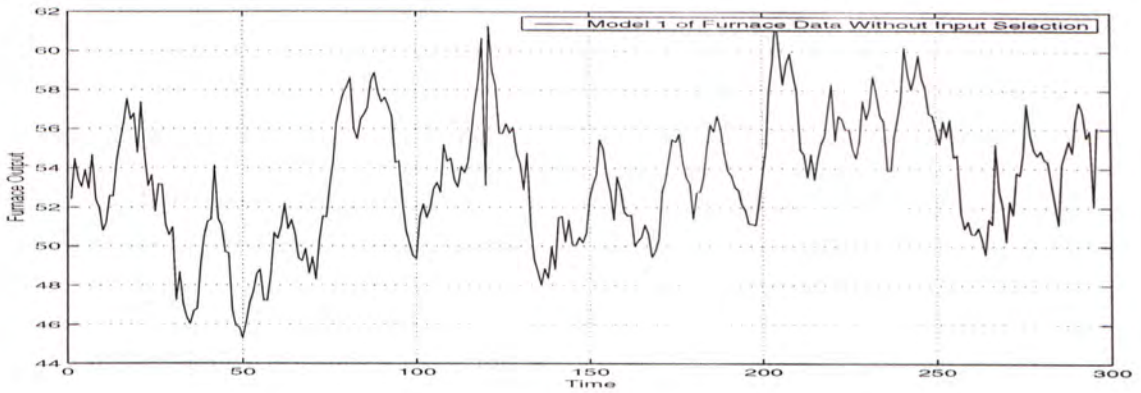


Figure 4.14: Furnace Model 1, Trained Using Full Set of Candidate Inputs

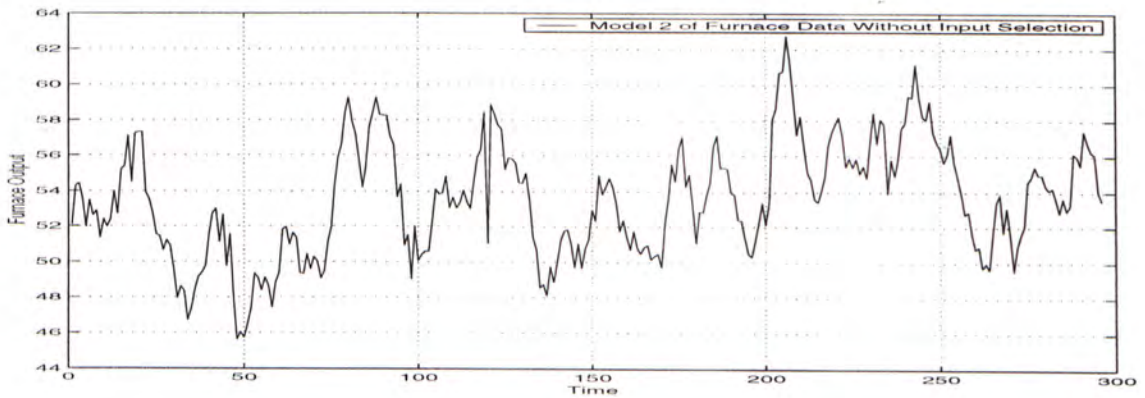


Figure 4.15: Furnace Model 2, Trained Using Full Set of Candidate Inputs

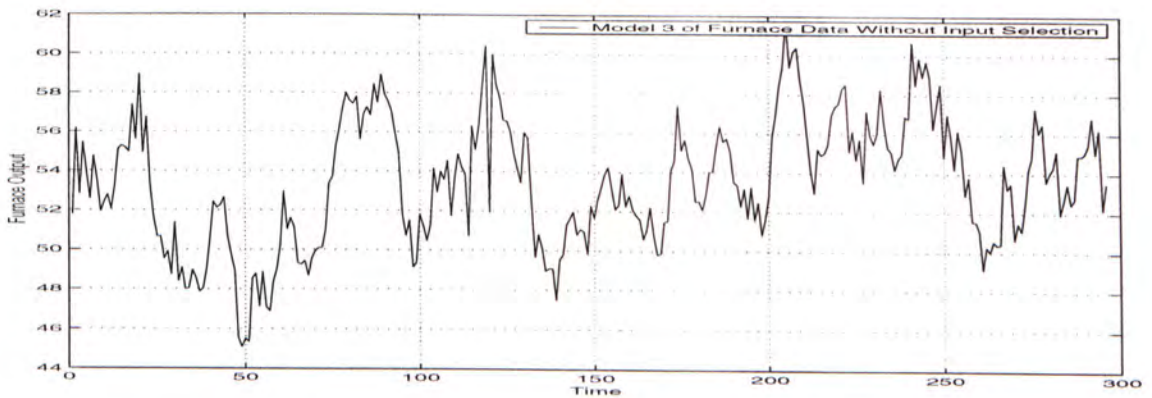


Figure 4.16: Furnace Model 3, Trained Using Full Set of Candidate Inputs



The proposed input selection scheme based on ICA is performed on the furnace data set. Three ICA models are produced from the candidate input set and the output data. The furnace data are converted into independent components and the procedure outlined in section 4.6.3 is applied to select the suitable inputs from the candidate input set. The selected inputs in the three different ICA models are shown in table 4.5. Three different cascade neural network models are trained using each of the three selected input sets. The outputs of the models are shown in figures 4.17 to 4.25. The trained cascade neural networks have 6 hidden units each. The similarity values between the original furnace output and the outputs of the models trained using the selected inputs are shown in table 4.6. It can be seen that the input selection method not only is able to reduce the level of inputs, but it also increases the similarity between the model outputs and the original output.

ICA Model Number	Selected Inputs
1	$i(t), i(t-4), o(t-3), o(t-2)$
2	$i(t-4), i(t-5), o(t-2), o(t-3), o(t-4)$
3	$i(t-2), i(t-6), o(t-3), o(t-4)$

Table 4.5: Inputs Selected for the Furnace Model Using ICA

	Model 1	Model 2	Model 3
Selected Input Set 1	0.4519	0.5422	0.5973
Selected Input Set 2	0.4892	0.6500	0.6692
Selected Input Set 3	0.5722	0.8892	0.4879

Table 4.6: Furnace Model Similarity Measure Result for Inputs Selected by ICA

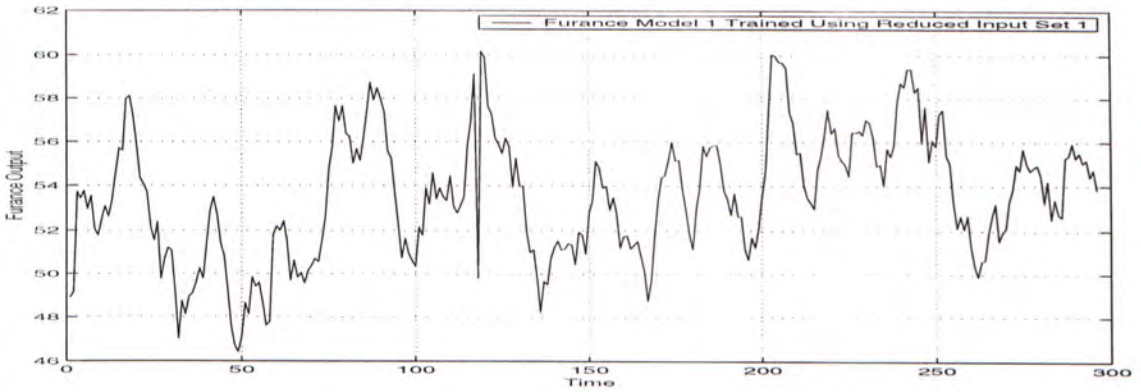


Figure 4.17: Output of Furnace Model 1 Trained Using ICA-Selected Input Set 1

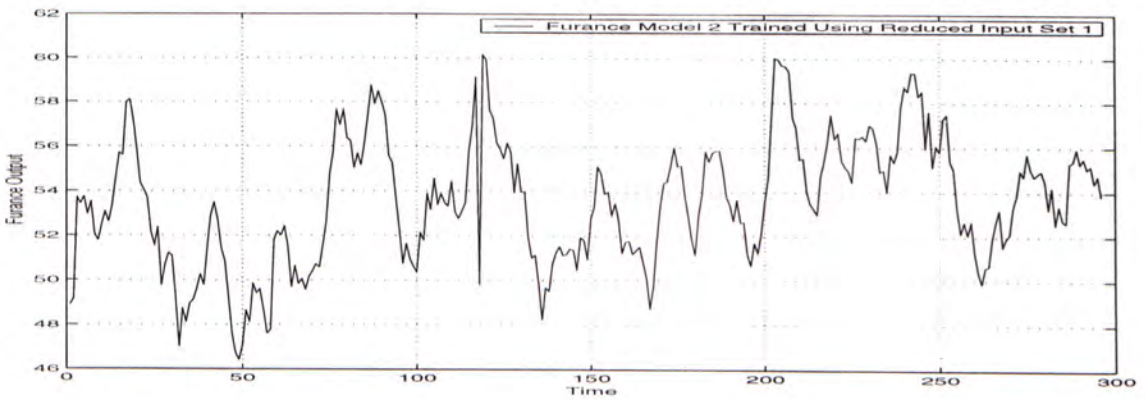


Figure 4.18: Output of Furnace Model 2 Trained Using ICA-Selected Input Set 1

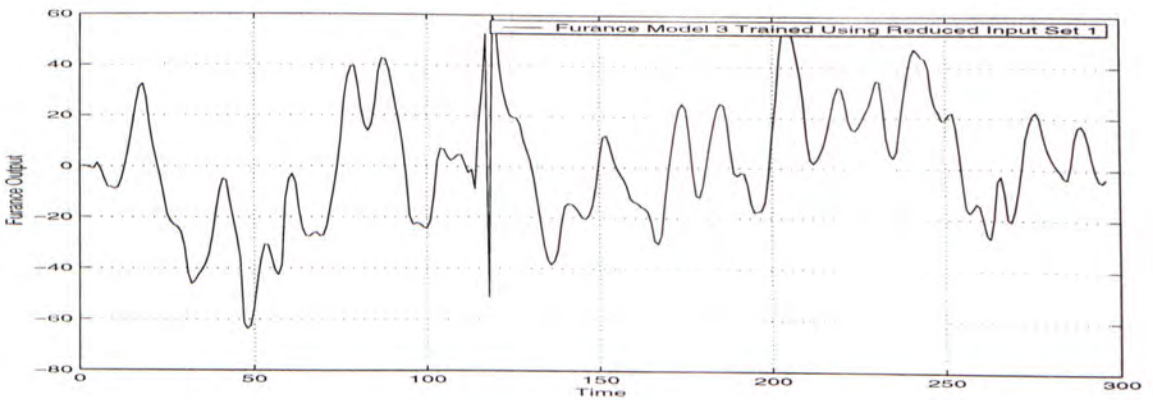


Figure 4.19: Output of Furnace Model 3 Trained Using ICA-Selected Input Set 1



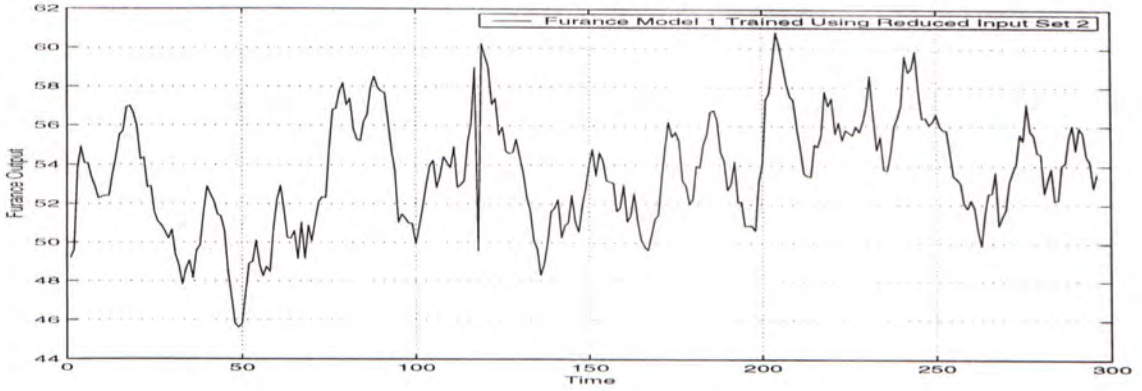


Figure 4.20: Output of Furnace Model 1 Trained Using ICA-Selected Input Set 2

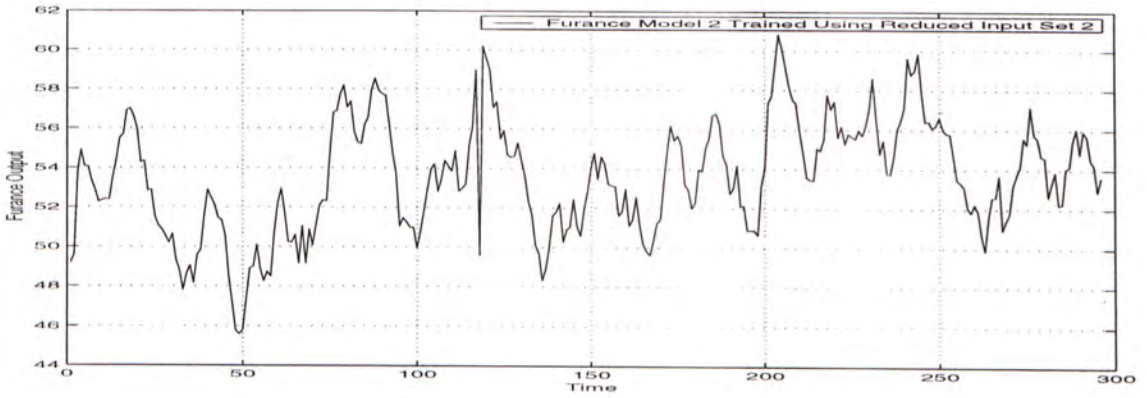


Figure 4.21: Output of Furnace Model 2 Trained Using ICA-Selected Input Set 2

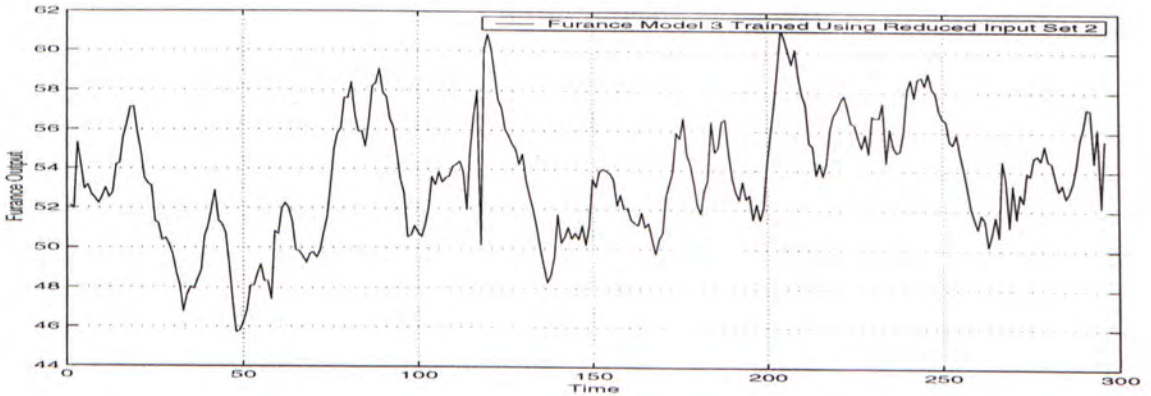


Figure 4.22: Output of Furnace Model 3 Trained Using ICA-Selected Input Set 2

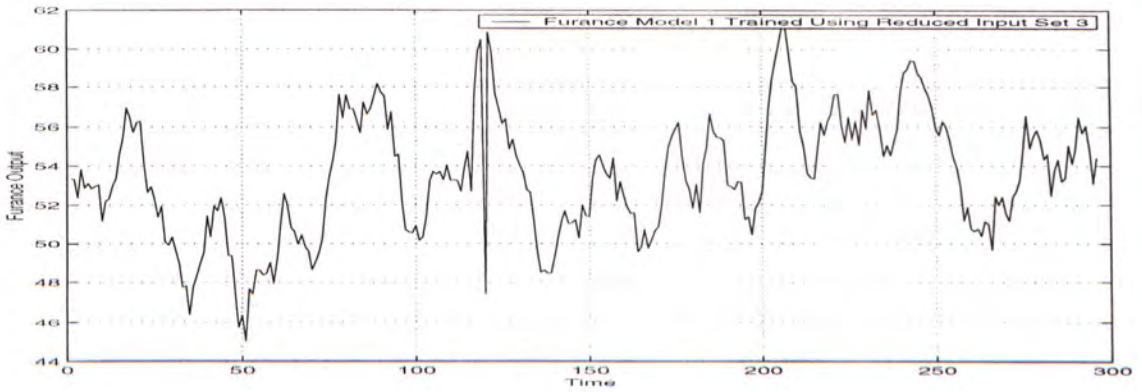


Figure 4.23: Output of Furnace Model 1 Trained Using ICA-Selected Input Set 3

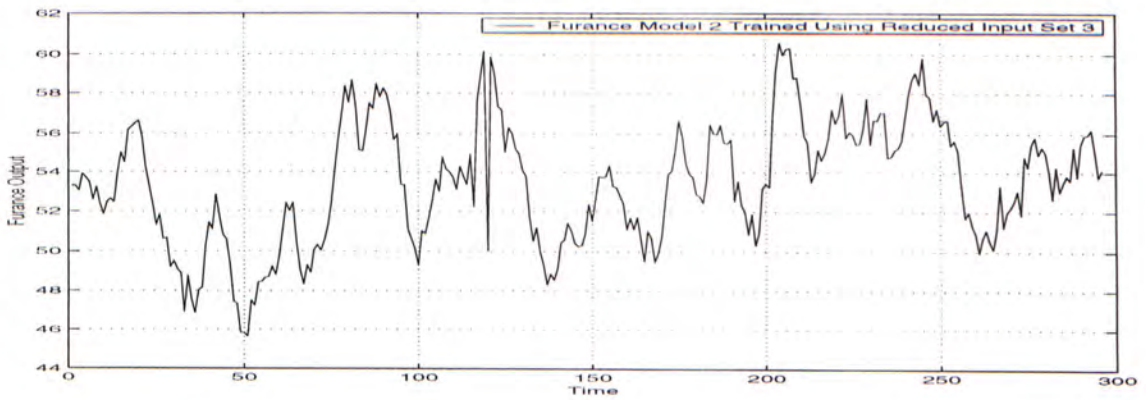


Figure 4.24: Output of Furnace Model 2 Trained Using ICA-Selected Input Set 3

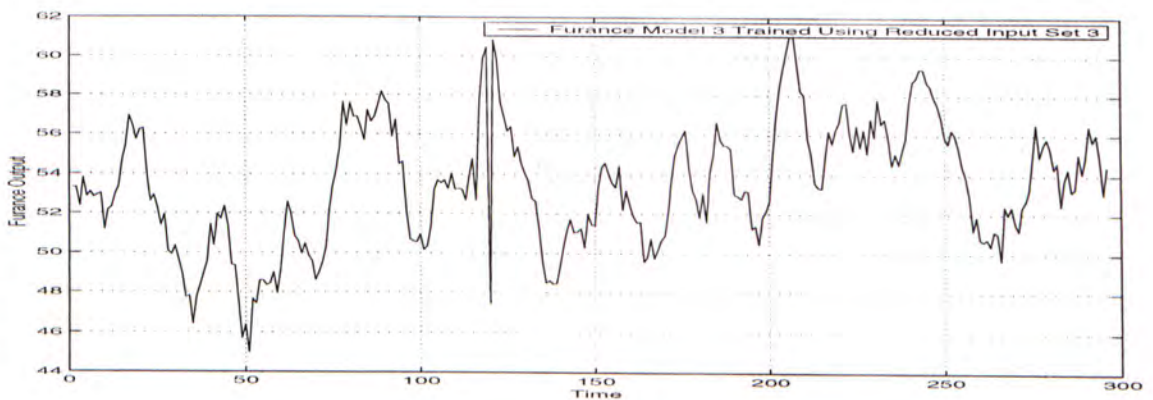


Figure 4.25: Output of Furnace Model 3 Trained Using ICA-Selected Input Set 3



### 4.6.5 Applying Input Selection by ICA to Sensation Modeling

The ICA-based input selection method is applied to the motion and sensation data. For each of our two subjects, two different ICA models are produced. ICA is applied on the sensation data and the 10 motion data without time-shifting. The data are then converted into 11 independent components and the size of the mixing matrix of the ICA model is  $11 \times 11$ .

Tables 4.7 and 4.8 show the mixing matrices  $\mathbf{A}$  of the two ICA models of subject 1. It can be seen that the values in the two matrices are very similar. This is different from the case of the furnace model in which different trained ICA models give different mixing matrices and hence lead to different selected inputs. ICA models tend to be more identifiable if the original data set is not time-shifted and be more independent among itself.

Using a feature selection threshold of 0.7, IC 7 in model 1 and IC 9 in model 2 are selected. Using an input selection threshold of 0.05, the inputs selected for subject 1 include roll angle  $\alpha$ , pitch angle  $\theta$ , pitch velocity  $\dot{\theta}$  and pitch acceleration  $\ddot{\theta}$ . These motion attributes are found to be most influential to the sensation of subject 1 based on this approach. Three sets of selected previous motion data and the current motion data are grouped together to form the reduced input variable set. The total dimension of inputs is reduced from 40 to 16.

Figures 4.26 to 4.27 are generated from the sensation models of subject 1 trained from the inputs selected using ICA. The similarity values between the original human sensation output of subject 1 and the outputs of the three representative trained human sensation models are shown in table 4.9.

	IC 1	IC 2	IC 3	IC 4	IC 5	IC 6	IC 7	IC 8	IC 9	IC 10	IC 11
Type	0.0154	-0.0027	0.0034	-0.0114	-0.0408	-0.4102	-0.0012	-0.0796	0.0139	-0.0511	-0.0120
Length	0.0587	0.0199	-0.0244	-0.0215	0.0089	0.0080	-0.0008	0.0017	0.0618	0.5825	-0.0641
$\ddot{\alpha}$	0.0242	0.2216	0.0138	-0.2256	-0.0535	0.0029	0.0015	0.0143	-0.0517	-0.0227	-0.0691
$\ddot{\theta}(selected)$	0.1106	0.0120	0.0534	0.0408	-0.0195	0.0236	<b>0.0636</b>	-0.0697	-0.1663	-0.0068	-0.1401
$\dot{z}_C$	-0.0799	-0.0105	0.2041	-0.0067	0.0023	0.0076	-0.0023	-0.0069	0.0045	-0.0009	-0.1973
$\dot{\alpha}$	-0.0230	0.1968	0.0204	0.1878	-0.0171	-0.0051	-0.0043	-0.0139	0.0078	-0.0232	-0.0130
$\dot{\theta}(selected)$	-0.1418	-0.0037	0.0922	0.0552	-0.0205	-0.0248	<b>0.0729</b>	0.0688	-0.1445	0.0142	0.1112
$z_C$	0.0539	0.0333	0.1884	-0.0003	0.0186	0.0034	0.0031	-0.0308	0.0120	0.0226	0.1556
$\alpha(selected)$	-0.0144	-0.1271	0.0136	0.1130	-0.2485	0.0314	<b>0.0830</b>	0.0311	0.0497	0.0159	0.0203
$\theta(selected)$	0.0655	-0.0354	-0.0002	0.0045	0.0423	-0.0636	<b>-0.0647</b>	0.2074	0.0645	0.0130	0.0439
Sensation	0.0217	-0.0209	-0.0412	0.0074	0.0090	0.0058	<b>-0.7142</b>	0.0049	-0.0379	0.0010	0.0063

Table 4.7: Mixing Matrix of the First ICA Model for Subject 1

	IC 1	IC 2	IC 3	IC 4	IC 5	IC 6	IC 7	IC 8	IC 9	IC 10	IC 11
Type	-0.4114	-0.0119	0.0518	0.0154	0.0125	-0.0129	0.0357	-0.0036	-0.0001	0.0760	0.0030
Length	0.0072	-0.0667	-0.5827	0.0544	0.0195	-0.0615	-0.0128	0.0167	-0.0013	0.0016	-0.0248
$\ddot{\alpha}$	0.0044	-0.0724	0.0207	0.0227	0.2232	0.0511	0.0573	0.2230	0.0013	-0.0048	0.0124
$\ddot{\theta}(selected)$	0.0231	-0.1421	0.0060	0.1008	-0.0415	0.1694	0.0163	0.0089	<b>0.0636</b>	0.0748	0.0521
$\dot{z}_C$	0.0079	-0.1941	0.0013	-0.0878	0.0063	-0.0049	-0.0029	-0.0103	-0.0025	0.0116	0.2037
$\dot{\alpha}$	-0.0072	-0.0124	0.0234	-0.0206	-0.1881	-0.0069	-0.0001	0.1972	-0.0037	0.0176	0.0202
$\dot{\theta}(selected)$	-0.0259	0.1144	-0.0134	-0.1365	-0.0553	0.1413	0.0203	0.0011	<b>0.0732</b>	-0.0788	0.0931
$z_C$	0.0027	0.1535	-0.0229	0.0602	0.0022	-0.0100	-0.0213	0.0328	0.0032	0.0291	0.1884
$\alpha(selected)$	0.0293	0.0214	-0.0169	-0.0151	-0.1253	-0.0521	0.2480	-0.1169	<b>0.0825</b>	-0.0238	0.0153
$\theta(selected)$	-0.0598	0.0348	-0.0120	0.0742	-0.0015	-0.0682	-0.0336	-0.0330	<b>-0.0648</b>	-0.2082	0.0011
Sensation	0.0041	0.0063	-0.0005	0.0209	-0.0080	0.0386	-0.0091	-0.0205	<b>-0.7141</b>	-0.0054	-0.0415

Table 4.8: Mixing Matrix of the Second ICA Model for Subject 1

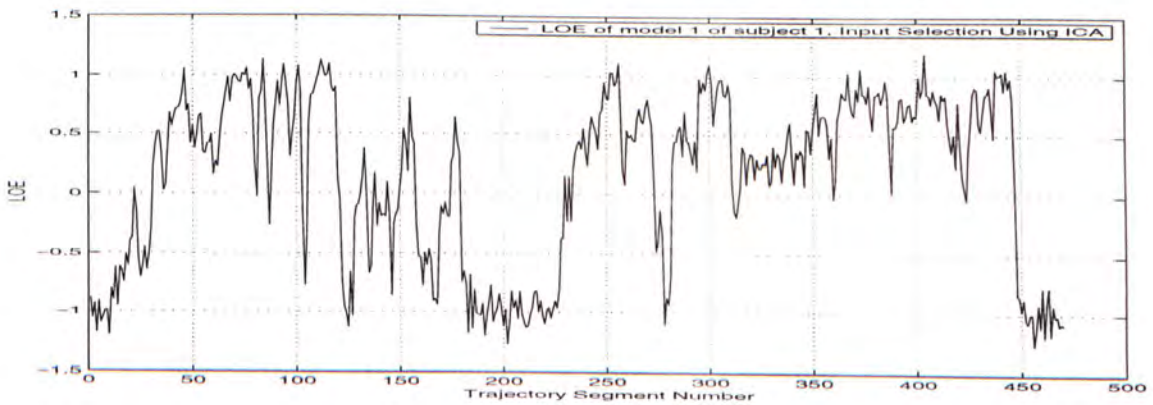


Figure 4.26: Sensation Model 1 of Subject 1, Input Selected by ICA



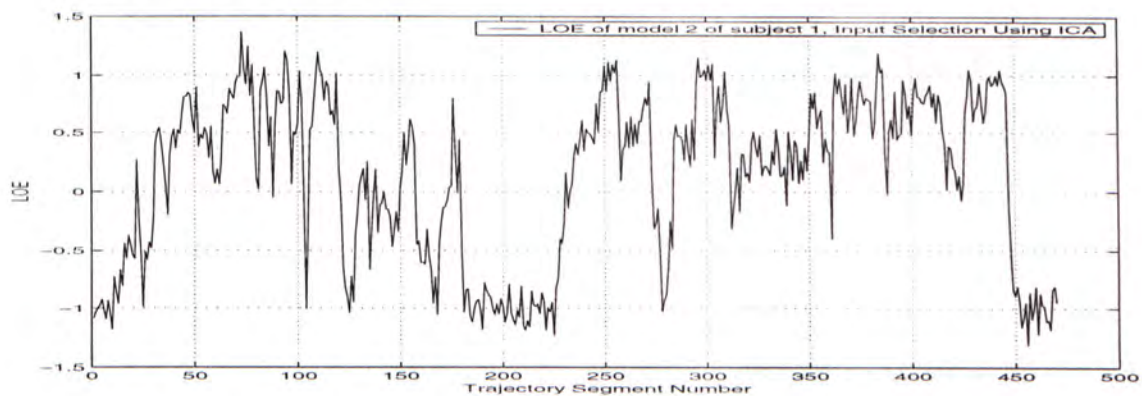


Figure 4.27: Sensation Model 2 of Subject 1, Input Selected by ICA

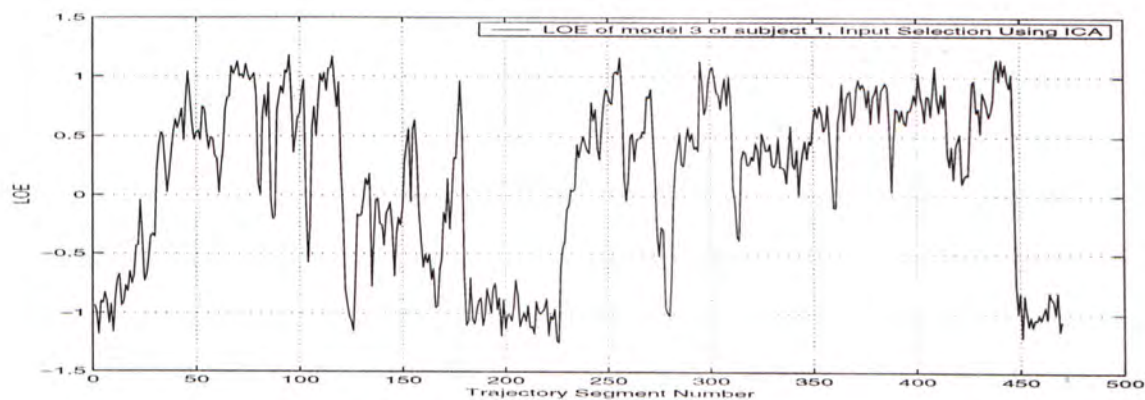


Figure 4.28: Sensation Model 3 of Subject 1, Input Selected by ICA

Model Number	Similarity
1	0.4786
2	0.4501
3	0.4589

Table 4.9: Similarity Measure Result for Models Trained Using ICA-Selected Inputs for Subject 1

	IC 1	IC 2	IC 3	IC 4	IC 5	IC 6	IC 7	IC 8	IC 9	IC 10	IC 11
Type	-0.0083	-0.0543	-0.0144	0.0078	-0.0726	0.0015	-0.0131	-0.0115	0.0010	0.4079	0.0441
Length	-0.0197	0.5819	-0.0561	0.0689	-0.0066	-0.0182	-0.0612	0.0205	0.0256	-0.0001	-0.0134
$\ddot{\alpha}$	-0.2579	-0.0250	-0.0255	0.0823	0.0162	-0.2538	0.0578	-0.0022	-0.0145	-0.0008	0.0440
$\ddot{\theta}$	0.0396	-0.0073	-0.1000	0.1483	-0.0754	-0.0101	0.1750	0.0006	-0.0518	-0.0228	0.0241
$\dot{z}_C$	-0.0066	-0.0014	0.0878	0.1940	-0.0108	0.0102	-0.0058	-0.0071	-0.2037	-0.0045	-0.0051
$\dot{\alpha}$	0.1876	-0.0231	0.0223	0.0115	-0.0170	-0.1968	-0.0066	-0.0047	-0.0207	0.0023	0.0198
$\dot{\theta}$	0.0536	0.0146	0.1360	-0.1163	0.0775	0.0002	0.1410	0.0050	-0.0952	0.0251	0.0142
$\dot{z}_C$	-0.0011	0.0229	-0.0619	-0.1524	-0.0371	-0.0327	-0.0093	0.0038	-0.1876	-0.003	-0.0194
$\alpha(selected)$	0.1017	0.0155	0.0198	-0.0214	0.0342	0.1202	-0.0467	<b>0.0904</b>	-0.0183	-0.0290	0.2539
$\theta(selected)$	0.0099	0.0154	-0.0792	-0.0391	0.2053	0.0347	-0.0688	<b>-0.0575</b>	-0.0035	0.0583	-0.0440
Sensation	0.0106	0.0146	0.0011	-0.0029	0.0111	0.0323	0.0558	<b>-0.7644</b>	0.1160	-0.1033	0.0009

Table 4.10: Mixing Matrix of the First ICA Model for Subject 2

Tables 4.10 and 4.11 show the mixing matrices  $\mathbf{A}$  of the two ICA models of subject 2. Using the same feature and input selection thresholds as before, the inputs selected for subject 2 are roll angle  $\alpha$  and pitch angle  $\theta$ . The motion variables influencing subject 2 is found to be different from those for subject 1. As before, three sets of selected previous motion data and the current motion data are grouped together to form the reduced input variable set. The total dimension of inputs is reduced from 40 to 12, which represents a 80% reduction in redundant data.

Figures 4.29 to 4.31 are generated from the sensation models of subject 2 trained from the inputs selected using ICA. The similarity values between the original human sensation output of subject 2 and the outputs of the three representative trained sensation models are shown in table 4.12.



	IC 1	IC 2	IC 3	IC 4	IC 5	IC 6	IC 7	IC 8	IC 9	IC 10	IC 11
Type	0.0144	0.0078	0.0083	-0.0014	0.0012	-0.4079	-0.0132	0.0727	-0.0716	0.0440	-0.0542
Length	0.0564	0.0688	0.0197	0.0184	0.0258	0.0002	-0.0611	0.0065	0.0205	-0.0130	0.5819
$\ddot{\alpha}$	0.0254	0.0821	0.2580	0.2537	-0.0149	0.0009	0.0575	-0.0167	-0.0022	0.0445	-0.0251
$\ddot{\theta}$	0.0999	0.1482	-0.0395	0.0103	-0.0529	0.0229	0.1746	0.0759	0.0005	0.0248	-0.0073
$\dot{z}_C$	-0.0875	0.1940	0.0066	-0.0102	-0.2039	0.0043	-0.0069	0.0099	-0.0071	-0.0052	-0.0014
$\dot{\alpha}$	-0.0223	0.0114	-0.1876	0.1967	-0.0209	-0.0022	-0.0067	0.0165	-0.0047	0.0206	-0.0231
$\dot{\theta}$	-0.1363	-0.1163	-0.0534	-0.0005	-0.0954	-0.0252	0.1409	-0.0772	0.0051	0.0141	0.0146
$z_C$	0.0620	-0.1526	0.0011	0.0327	-0.1876	0.0029	-0.0100	0.0362	0.0037	-0.0193	0.0229
$\alpha(\text{selected})$	-0.0199	-0.0214	-0.1014	-0.1211	-0.0181	0.0287	-0.0471	-0.0350	<b>0.0904</b>	0.2534	0.0154
$\theta(\text{selected})$	0.0793	-0.0391	-0.0100	-0.0350	-0.0021	-0.0585	-0.0676	-0.2055	<b>-0.0573</b>	-0.0448	0.0154
Sensation	-0.0013	-0.0027	-0.0106	-0.0323	0.1159	0.1035	0.0565	-0.0111	<b>-0.7643</b>	0.0010	0.0146

Table 4.11: Mixing Matrix of the Second ICA Model for Subject 2

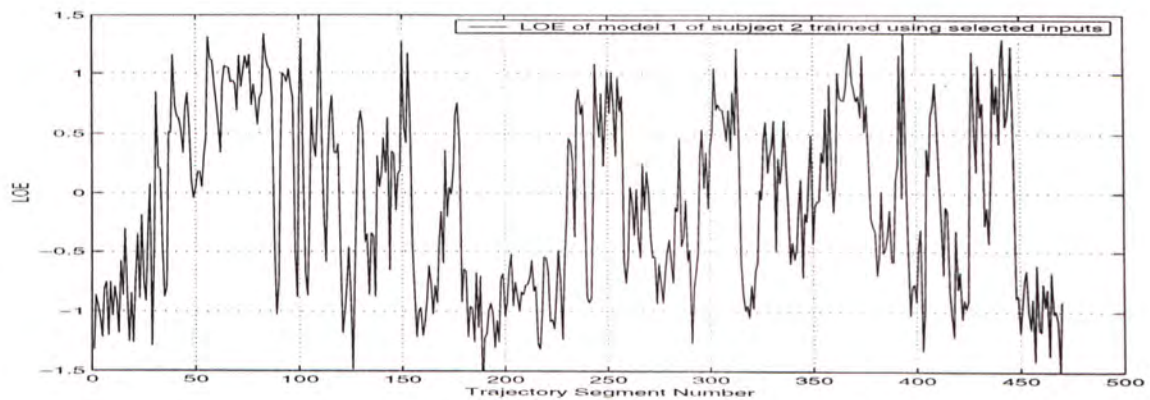


Figure 4.29: Sensation Model 1 of Subject 2, Input Selected by ICA

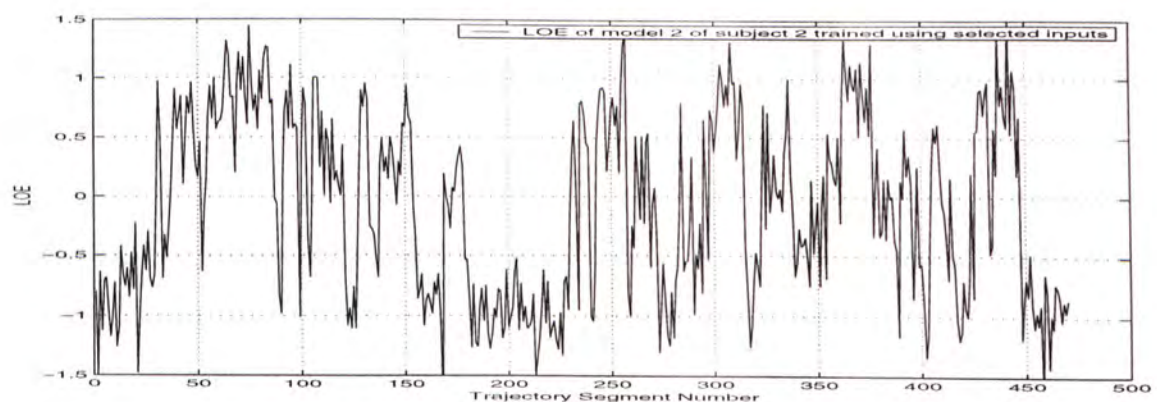


Figure 4.30: Sensation Model 2 of Subject 2, Input Selected by ICA

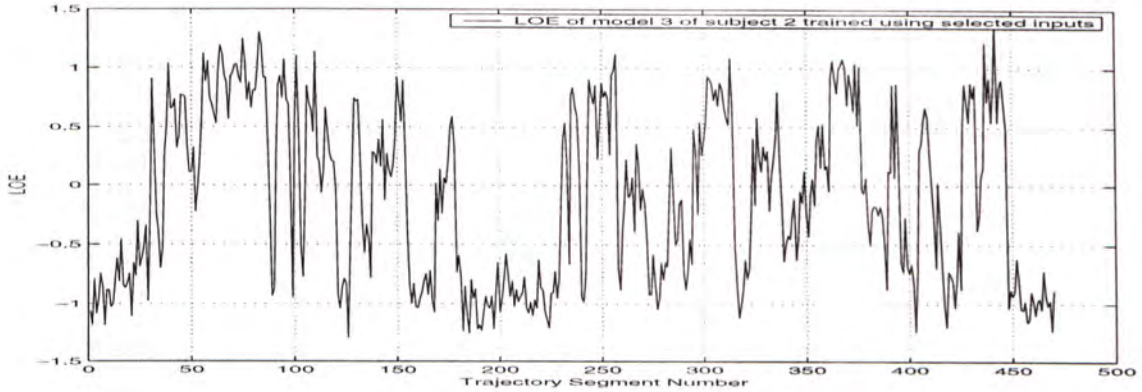


Figure 4.31: Sensation Model 3 of Subject 2, Input Selected by ICA

Model Number	Similarity
1	0.3321
2	0.3434
3	0.3328

Table 4.12: Similarity Measure Result for Models Trained Using ICA-Selected Inputs for Subject 2

### 4.6.6 Cross Verification of Selected Inputs

We verify the inputs selected for each of the two subjects by applying the inputs selected for one subject onto the other subject. Firstly, the inputs selected for subject 1 ( $\alpha, \theta, \dot{\theta}, \ddot{\theta}$ ) in the previous section are used for modeling the sensation of both subjects. Three models are trained for each subject and the similarities between the two subjects and the six trained sensation models are shown in table 4.13.

Secondly, the inputs selected for subject 2 ( $\alpha, \theta$ ) in the previous section are used for modeling the sensation of both subjects. Three models are trained for each subject and the similarities between the two subjects and the six trained sensation models are shown in table 4.14.



	Subject 1	Subject 1 Model 1	Subject 1 Model 2	Subject 1 Model 3	Subject 2	Subject 2 Model 1	Subject 2 Model 2	Subject 2 Model 3
Sub. 1	1	0.4786	0.4501	0.4589	0.1830	0.0094	0.0040	0.0179
Sub. 1 Model 1	0.4786	1	0.4639	0.4462	0.0189	0.0212	0.0179	0.0796
Sub. 1 Model 2	0.4501	0.4639	1	0.4269	0.0134	0.0170	0.0104	0.0526
Sub. 1 Model 3	0.4589	0.4462	0.4269	1	0.0165	0.0178	0.0103	0.1002
Sub. 2	0.1830	0.0189	0.0134	0.0165	1	0.0393	0.0712	0.1313
Sub. 2 Model 1	0.0094	0.0212	0.0170	0.0178	0.0393	1	0.1933	0.1542
Sub. 2 Model 2	0.0040	0.0179	0.0104	0.0103	0.0712	0.1933	1	0.1653
Sub. 2 Model 3	0.0179	0.0796	0.0526	0.1002	0.1313	0.1542	0.1653	1

Table 4.13: Model Similarity Measure Result, All Models Trained Using Inputs :  $\alpha, \theta, \dot{\theta}, \ddot{\theta}$ .

	Subject 1	Subject 1 Model 1	Subject 1 Model 2	Subject 1 Model 3	Subject 2	Subject 2 Model 1	Subject 2 Model 2	Subject 2 Model 3
Sub. 1	1	0.1909	0.1594	0.1847	0.1830	0.0816	0.0417	0.1244
Sub. 1 Model 1	0.1909	1	0.2042	0.2602	0.0462	0.0298	0.0714	0.0559
Sub. 1 Model 2	0.1594	0.2042	1	0.2651	0.0520	0.0489	0.1569	0.1056
Sub. 1 Model 3	0.1847	0.2602	0.2651	1	0.0448	0.1001	0.0458	0.1564
Sub. 2	0.1830	0.0462	0.0520	0.0448	1	0.3321	0.3434	0.3328
Sub. 2 Model 1	0.0816	0.0298	0.0489	0.1001	0.3321	1	0.3135	0.3012
Sub. 2 Model 2	0.0417	0.0714	0.1569	0.0458	0.3434	0.3135	1	0.3218
Sub. 2 Model 3	0.1244	0.0559	0.1056	0.1564	0.3328	0.3012	0.3218	1

Table 4.14: Model Similarity Measure Result, All Models Trained Using Inputs :  $\alpha, \theta$ .

Finally, the inputs selected for subject 1 ( $\alpha, \theta, \dot{\theta}, \ddot{\theta}$ ) are applied on subject 1 and the inputs selected for subject 2 ( $\alpha, \theta$ ) are applied on subject 2. Three models are trained for each subject and the similarities between the two subjects and the six trained sensation models are shown in table 4.15.

Based on the results in the tables, we can see that the similarities between the human data and the modeled data are best when the models are trained using the corresponding inputs selected in the previous section using ICA. If the models of a subject are trained using the inputs selected for another person, the performance of the models drop significantly, making them even worse than the case where the inputs are not reduced. When the correctly

selected inputs are applied for model training, not only the relative similarity between the human data and the modeled data is improved, but also the difference between models of different subjects is increased.

	Subject 1	Subject 1 Model 1	Subject 1 Model 2	Subject 1 Model 3	Subject 2	Subject 2 Model 1	Subject 2 Model 2	Subject 2 Model 3
Sub. 1	1	0.4786	0.4501	0.4589	0.1830	0.0816	0.0417	0.1244
Sub. 1 Model 1	0.4786	1	0.4639	0.4462	0.0189	0.0010	0.0023	0.0009
Sub. 1 Model 2	0.4501	0.4639	1	0.4269	0.0134	0.0008	0.0043	0.0036
Sub. 1 Model 3	0.4589	0.4462	0.4269	1	0.0165	0.0016	0.0006	0.0066
Sub. 2	0.1830	0.0189	0.0134	0.0165	1	0.3321	0.3434	0.3328
Sub. 2 Model 1	0.0816	0.0010	0.0008	0.0016	0.3321	1	0.3135	0.3012
Sub. 2 Model 2	0.0417	0.0023	0.0043	0.0006	0.3434	0.3135	1	0.3218
Sub. 2 Model 3	0.1244	0.0009	0.0036	0.0066	0.3328	0.3012	0.3218	1

Table 4.15: Model Similarity Measure Result, Models of Subject 1 Trained Using Inputs :  $\alpha, \theta, \hat{\theta}$ . Models of Subject 2 Trained Using Inputs :  $\alpha, \theta$ .

## 4.7 Summary on Input Reduction for Human Sensation Modeling

Input Processing	Ave. Similarity	% of Inputs Reduced
No Input Processing	0.354	0%
Feature Extraction Using PCA	0.0098	57.5%
ICA without Input Reduction	0.028	0%
Feature Extraction Using ICA	0.1186	60%
Input Selection Using ICA	0.443	60% (80% for sub.2)

Table 4.16: Summary of Results of Data Processing Methods on Subject 1



The summary of the results of the various input data reduction methods is shown on table 4.16. In terms of feature extraction techniques, ICA performs better than pure PCA. PCA searches for orthogonal directions of greatest variance in the data, whereas ICA component maps may not be orthogonal. In general, there is no reason to believe that the ICs forming the motion stimulus inputs to be spatially orthogonal to one another. Although PCA is often used for input reduction, this is not always useful. Because the variance of a signal is not necessarily related to the importance of the variable. The features retrieved may have no importance to the output. However, the performance of both methods are worse than the case where there is no processing on the inputs.

For ICA without input reduction, the result is particularly unsatisfactory for this application. The method retains the noise in the data and the outcomes suggest that transforming the environmental stimulus data linearly does not improve its relationship with human sensation, no matter the transformation is based on the variance criterion (PCA) or the independence criterion (ICA).

The input selection method based on ICA improves the modeling power of the system and reduced the number of inputs by 60% for the first subject and by 80% for the second subject. Using this methods, the motion factors which have high influence on human subjects in the virtual environment can be identified. In contrast to the use of PCA for feature extraction, the variables removed in the ICA approach are those which are independent of the output, which is different from removing those with low variance.

The proposed input selection method based on ICA is found to be able to give the best data reduction results compared to other processing methods presented. This method requires a relatively straight forward transformation and statistical test to be performed in order to achieve model-free input variable selection. By reducing the redundancy in the input data, the training process of the sensation model becomes more efficient. The results of similarity measure reveal that after the unrequired information is removed from the inputs, not only the key characteristics of the human sensation data can be retained, but also the modeling power of the system is actually improved. It is apparent that ICA provides a useful tool for reducing the stimulus input size and improving the performance of human sensation models in the virtual environments.

## Chapter 5

# Stimulus Modification Based on Human Sensation

In the previous chapter, motion attributes which have the highest influence on human sensation were selected by an input selection method based on ICA. In this chapter, we develop a trajectory modification scheme based on human sensation level. For reasons of safety and enjoyment, the trajectories of the VR system are to be modified such that the sensation experienced by the participants is not to exceed a specified level. The criteria for trajectory modification is based on the motion attributes selected to be important to the individuals as well as on the relationship between the magnitudes of the motion attributes and the sensation levels experienced by the individuals. Experiments are performed to change the trajectories of the motion platform in the motion-based movie system such that the sensation of the participants are adjusted not to surpass specified levels.

### 5.1 Need for Stimulus Modification

Improper use of full-body motion interfaces may cause problems to the users. One potential critical effect of full-body motion simulation exposure is postural disequilibrium, referred to as ataxia. Baltzley, et al. [1] reported that body unsteadiness and ataxia are the greatest immediate concern for safety because there have been reports of such posteffects lasting longer than 6 hours. Kolasinski [37] also found out that individuals who are less posturally stable will be more likely to experience simulator sickness or will experience more severe sickness; conversely, individuals who are more posturally stable will be less likely to experience simulator sickness or will experience less severe sickness. Although ataxia does not always result, this could be due to the motion simulation exposure time and the extent and complexity of



the motion generated.

Exposure to full-body motion, and many other physical and psychological stimuli in the VR, can result in short term changes in various physiological parameters, such as an increase in heart rate. The specific physiological effect of VR stimuli exposure include the following: cardiovascular, respiratory, motor processes, sensory processes, central nervous system and skeletal [20].

In our application of motion-based movie, the time duration is usually less than five minutes. The time period involved is relatively short compared to other full-body motion virtual reality applications, such as flight simulation for training. Therefore, in order to ensure the safety and enjoyment of the participants, we can reduce the degree of motion sickness and potential negative physiological responses experienced by the subjects by controlling the motion of the platform.

In recent robotics, a number of methods concerning the modification of manipulator trajectories have been proposed. Flash [16] uses a superposition scheme to handle the case where there is a sudden unexpected change in the target location. According to this strategy, a quintic trajectory leading from the first target to the final one is added vectorially to the initial one to yield the combined modified motion. Takayama [60] proposes using the concept of unit motion to synthesize and modify the trajectory of manipulators. A concept of unit motion is introduced as smooth primitive motions by employing normalized uniform B-spline functions. Complex motions are generated as superpositions of time-shifted and weighted unit motions. Approaches utilizing neural networks for trajectory modification are also proposed [51] [34].

The above mentioned methods involve the use of complex polynomial fitting and network models. They are too tedious and computationally intensive for our application. Here we propose a motion platform trajectory modification scheme based on human sensation.

## 5.2 Sensation Grades

In chapters 3 and 4, the level of human sensation is normalized to be within a continuous scale between 1 and -1. We now classify the recorded level of excitement into five different grades, based on table 5.1. Each sensation grade represents a range of human sensation readings.

Sensation Grade	Range of Excitement Level
5	$1 \geq LOE \geq 0.6$
4	$0.6 > LOE \geq 0.2$
3	$0.2 > LOE \geq -0.2$
2	$-0.2 > LOE \geq -0.6$
1	$-0.6 > LOE \geq -1$

Table 5.1: Sensation Grade and the Range of Level of Excitement Represented

We want to find out the relationship between the level of motion and the grades of sensation felt by the subjects. Based on the human sensation data presented in chapter 3, the absolute average values of the motion attributes for each of the five sensation grades are calculated for the two subjects. The results are shown in tables 5.2 and 5.3. The values of the standard deviation are shown in brackets.

Sensation Grade	Roll $ \alpha (deg)$	Pitch $ \theta (deg)$	Roll Rate $ \dot{\alpha} (degs^{-1})$	Pitch Rate $ \dot{\theta} (degs^{-1})$
5	8.54 (5.41)	6.72 (3.13)	10.92 (6.81)	6.67 (7.31)
4	7.30 (4.43)	5.63 (3.60)	9.71 (5.67)	6.09 (5.43)
3	5.44 (4.60)	4.44 (3.78)	7.46 (5.23)	6.00 (4.97)
2	4.38 (3.52)	4.19 (2.88)	6.37 (4.22)	4.18 (4.11)
1	0.87 (1.76)	0.66 (1.44)	0.83 (2.61)	0.53 (3.13)

Table 5.2: Average Values of Motion Attributes (and Standard Deviations) at Various Sensation Grades for Subject 1



Sensation Grade	Roll $ \alpha (deg)$	Pitch $ \theta (deg)$	Roll Rate $ \dot{\alpha} (degs^{-1})$	Pitch Rate $ \dot{\theta} (degs^{-1})$
5	9.53 (4.32)	5.11 (4.55)	11.05 (7.12)	7.56 (5.45)
4	6.32 (4.01)	4.73 (4.39)	10.04 (6.63)	6.48 (5.13)
3	5.95 (3.32)	4.51 (3.24)	9.61 (5.28)	5.94 (4.54)
2	5.47 (3.17)	3.59 (3.07)	8.02 (4.97)	4.32 (3.39)
1	2.79 (2.10)	1.94 (1.91)	3.52 (3.36)	1.89 (2.45)

Table 5.3: Average Values of Motion Attributes (and Standard Deviations) at Various Sensation Grades for Subject 2

### 5.3 Trajectory Modification Scheme

Now we propose a trajectory modification scheme based on the sensation of humans. The objective of the method is to modify the trajectory of the motion platform such that the sensation intensity of the participant on the platform is prevented from exceeding a certain level of excitement. The sensation grade specified can be determined by factors such as safety requirements, physical fitness of individuals and personal preferences. The procedures for trajectory modification are as follows :

1. Determine the sensation grade which the motion trajectories are to be modified to fit (grade 1 to grade 5).
2. Determine the degree(s) of freedom which trajectory modification is to be performed on. The DOF(s) can be chosen by an input selection method, such as the one discussed in the previous chapter.
3. For the motion trajectory of each degree of freedom, perform segmentation at all the zero crossing points.
4. For each trajectory segment, find the maximum magnitude (absolute value).
5. Define the maximum motion threshold for each segment as the average value plus one standard deviation of the motion attribute at the sensation grade determined in step 1 from tables like 5.2 and 5.3.

6. If the maximum magnitude of the segment is smaller than the maximum motion threshold for the specified sensation grade, leave the segment unchanged.
7. If the maximum magnitude of the segment is larger than the maximum motion threshold for the specified sensation grade, scale down the magnitude of the segment linearly such that the maximum magnitude of the segment is the same as the maximum motion threshold for the specified sensation grade.
8. If the velocity of the trajectory is also needed to be taken into consideration, the scale down ratio based on the position trajectory and that based on the velocity trajectory will be compared. The ratio which is larger will be adopted.

In terms of mathematics, let's denote the degrees of freedom of the platform by  $\delta$ .

$$\delta \in \{\alpha, \theta, z_C\} \quad (5.1)$$

$f_\delta(t)$  is the trajectory of any of the three degrees of freedom. We segment the trajectory at the position where it crosses the central position of the allowable workspace of the degree of freedom. The trajectory segments are denoted by  $f_{\delta i}(t)$ .

$$f_\delta(t) = \begin{cases} f_{\delta 1}(t), & 0 < t \leq t_1 \\ f_{\delta 2}(t), & t_1 < t \leq t_2 \\ \dots \\ f_{\delta n}(t), & t_{n-1} < t \leq t_n \end{cases} \quad (5.2)$$

where  $n$  is the total number of segments,  $t_n$  is the total length of the trajectory,  $i \in \{1, 2, \dots, n\}$ , and

$$f_\delta(t_i) = \begin{cases} 0deg, & \text{if } \delta = \{\alpha, \theta\} \\ 210mm, & \text{if } \delta = \{z_C\} \end{cases} \quad (5.3)$$

The derivatives of the trajectory is defined as :



$$\dot{f}_\delta(t) = \begin{cases} \dot{f}_{\delta 1}(t), & 0 < t \leq t_1 \\ \dot{f}_{\delta 2}(t), & t_1 < t \leq t_2 \\ \dots & \\ \dot{f}_{\delta n}(t), & t_{n-1} < t \leq t_n \end{cases} \quad (5.4)$$

Below, we only consider the motion trajectories for  $\alpha$  and  $\theta$ . For each subject, we define maximum allowable motion limits for the motion angles and angular velocities at each grade of sensation. The maximum motion limits  $\theta_{lg}$ ,  $\alpha_{lg}$ ,  $\dot{\theta}_{lg}$  and  $\dot{\alpha}_{lg}$  for the four motion attributes of subject  $l$  at sensation grade  $g$  are defined as the average motion attribute value at the particular sensation grade  $g$  plus one standard deviation (from tables 5.2 and 5.3). For example, the maximum allowable roll angle for subject 1 at sensation grade 2 is the average roll angle at sensation grade 2 of subject 1 plus its standard deviation, which is  $\alpha_{12} = 4.38 + 3.52 = 7.9^\circ$ . And the maximum allowable pitch rate for subject 2 at sensation grade 4 is the average pitch rate at sensation grade 4 of subject 2 plus its standard deviation, which is  $\theta_{24} = 6.48 + 5.13 = 11.61^\circ \text{s}^{-1}$ .

Based on the sensation grade specified, the original motion trajectory  $f_\delta(t)$  is modified into  $\bar{f}_\delta(t)$  by scaling the individual trajectory segments linearly by different factors  $e_i$ , where  $i \in \{1, 2, \dots, n\}$ .

$$\bar{f}_\delta(t) = \begin{cases} e_1 f_{\delta 1}(t), & 0 < t \leq t_1 \\ e_2 f_{\delta 2}(t), & t_1 < t \leq t_2 \\ \dots & \\ e_n f_{\delta n}(t), & t_{n-1} < t \leq t_n \end{cases} \quad (5.5)$$

Let's define the maximum amplitude of segment  $i$  of the  $\delta$  trajectory as  $\Gamma_{\delta i} = \max(|f_{\delta i}|)$  and the maximum amplitude of segment  $i$  of the  $\delta$  rate trajectory as  $\Upsilon_{\delta i} = \max(|\dot{f}_{\delta i}|)$ . The scaling ratio  $e_i$  of segment  $i$  can be found by the relationships between  $\Gamma_{\delta i}$ ,  $\Upsilon_{\delta i}$  and the limits of the sensation grades.

If we consider only the position trajectories  $\theta$  and  $\alpha$ , the scaling ratio is defined as follows.

$$e_i = \begin{cases} \frac{\delta_{lg}}{\Gamma_{\delta i}}, & \text{if } \Gamma_{\delta i} > \delta_{lg} \\ 1, & \text{if } \Gamma_{\delta i} \leq \delta_{lg} \end{cases} \quad (5.6)$$

If we consider both the position and angular rate trajectories  $\theta, \alpha, \dot{\theta}$  and  $\dot{\alpha}$ , the scaling ratio is as follows.

$$e_i = \begin{cases} \frac{\delta_{lg}}{\Gamma_{\delta i}}, & \text{if } (\Gamma_{\delta i} > \delta_{lg} \text{ and } \Upsilon_{\delta i} \leq \dot{\delta}_{lg}) \text{ or } (\Gamma_{\delta i} > \delta_{lg} \text{ and } \Upsilon_{\delta i} > \dot{\delta}_{lg} \text{ and } \frac{\delta_{lg}}{\Gamma_{\delta i}} \geq \frac{\dot{\delta}_{lg}}{\Upsilon_{\delta i}}) \\ \frac{\dot{\delta}_{lg}}{\Upsilon_{\delta i}}, & \text{if } (\Gamma_{\delta i} \leq \delta_{lg} \text{ and } \Upsilon_{\delta i} > \dot{\delta}_{lg}) \text{ or } (\Gamma_{\delta i} > \delta_{lg} \text{ and } \Upsilon_{\delta i} > \dot{\delta}_{lg} \text{ and } \frac{\delta_{lg}}{\Gamma_{\delta i}} < \frac{\dot{\delta}_{lg}}{\Upsilon_{\delta i}}) \\ 1, & \text{if } (\Gamma_{\delta i} \leq \delta_{lg} \text{ and } \Upsilon_{\delta i} \leq \dot{\delta}_{lg}) \text{ or else} \end{cases} \quad (5.7)$$

This trajectory modification scheme can be extended to include the acceleration trajectory in the determination of the scaling ratio. Because any linear scaling in the position trajectory segment will lead to the same ratio being applied to the corresponding velocity and acceleration trajectory segments. In that case, we need to find out the average acceleration for each sensation grade. The trajectories will then be modified such that the acceleration limit for the chosen sensation grade will also not be exceeded.

## 5.4 Experiments

In this section, we perform some experiments on trajectory modification. Based on the sensation of subjects 1 and 2, we modify the motion trajectories in figure 3.2. The trajectory modification scheme discussed in the previous section is applied on the original trajectories. From the results in chapter 4, we know that the sensation of subject 1 is mainly dependent on  $\theta, \alpha, \dot{\theta}$  and  $\ddot{\theta}$ , while the sensation of subject 2 is mainly dependent on  $\theta$  and  $\alpha$ . The inputs selected for the subjects determine the criteria used for trajectory segment scaling. For subject 1, equation (5.7) is used, and for subject 2, equation (5.6) is used. Two sets of motion trajectories are generated for each of the two subjects. The first set is the trajectories modified to fit for sensation grade 2 and the second set is fit for sensation grade 4. Figures 5.1 and 5.2 are modified trajectories fit for subject 1 at sensation grade 2. Figures 5.3 and 5.4 are modified trajectories fit for subject 1 at sensation grade 4. Figures 5.5 and 5.6 are modified trajectories fit for subject 2 at sensation grade 2. Figures 5.7 and 5.8 are modified trajectories fit for subject 2 at sensation grade 4. From the graphs, we can see that all the trajectory segments which exceed the motion limits of the corresponding sensation grades are scaled down.



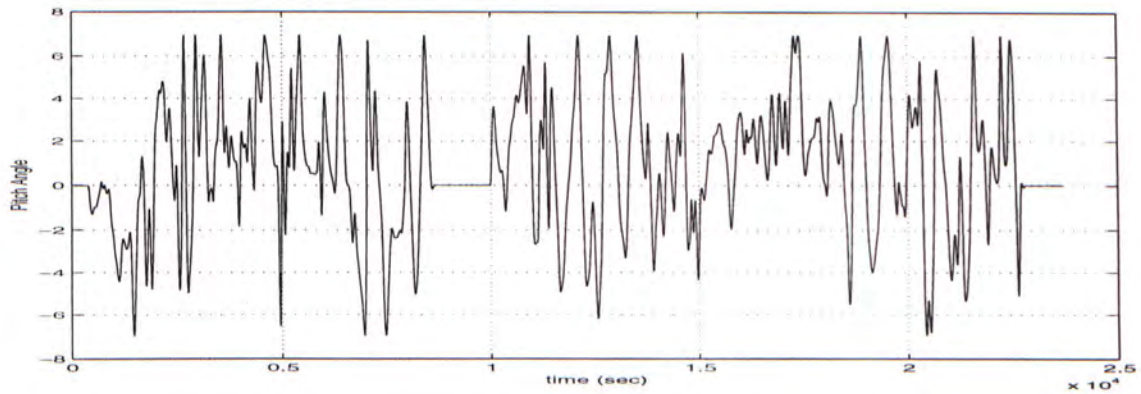


Figure 5.1: Modified Pitch Trajectory for Sensation Grade 2 of Subject 1

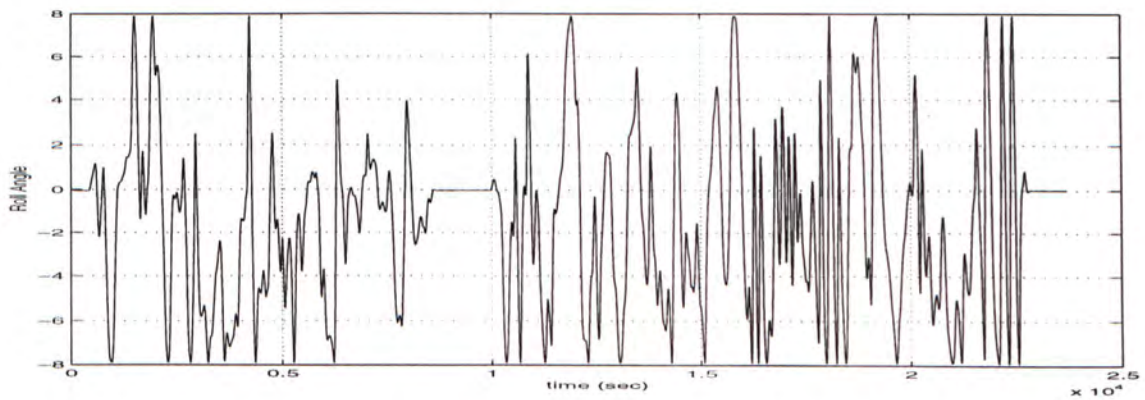


Figure 5.2: Modified Roll Trajectory for Sensation Grade 2 of Subject 1

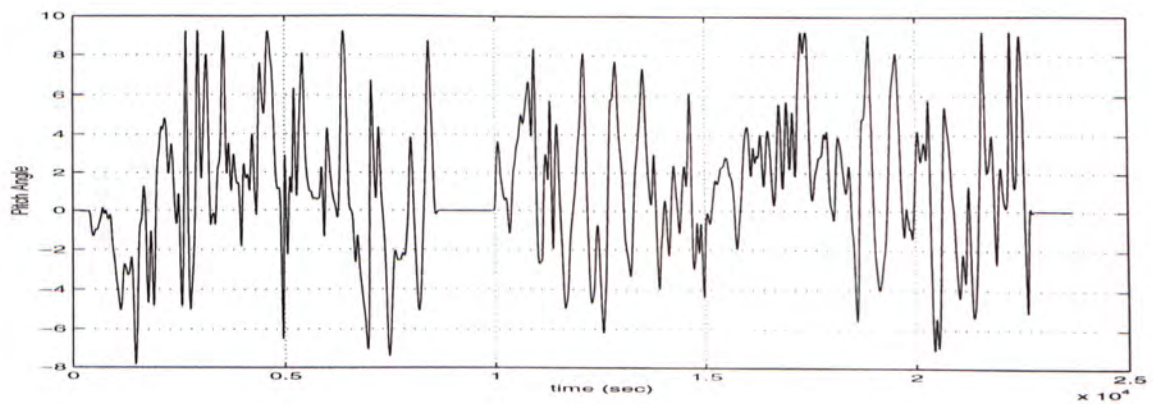


Figure 5.3: Modified Pitch Trajectory for Sensation Grade 4 of Subject 1

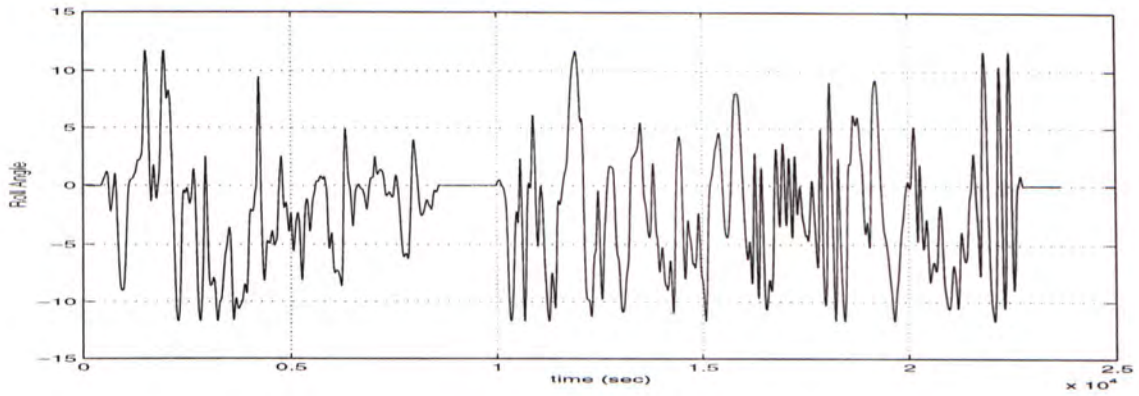


Figure 5.4: Modified Roll Trajectory for Sensation Grade 4 of Subject 1

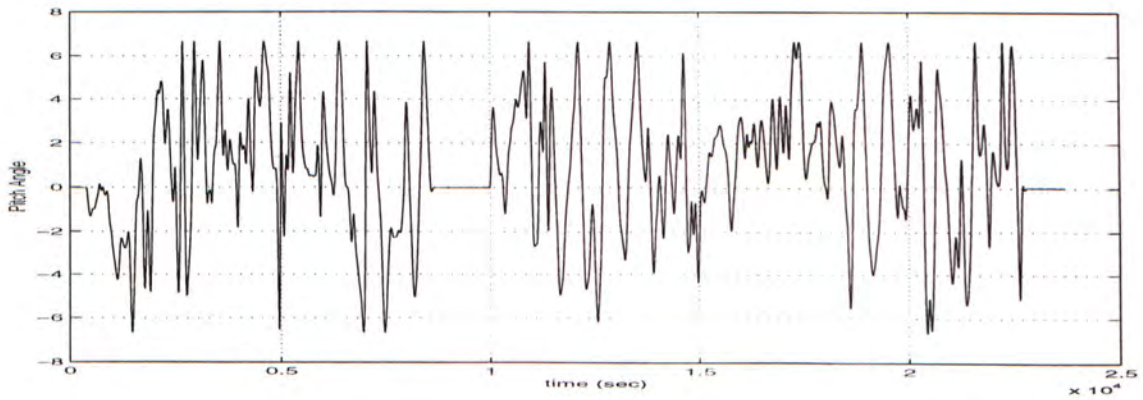


Figure 5.5: Modified Pitch Trajectory for Sensation Grade 2 of Subject 2

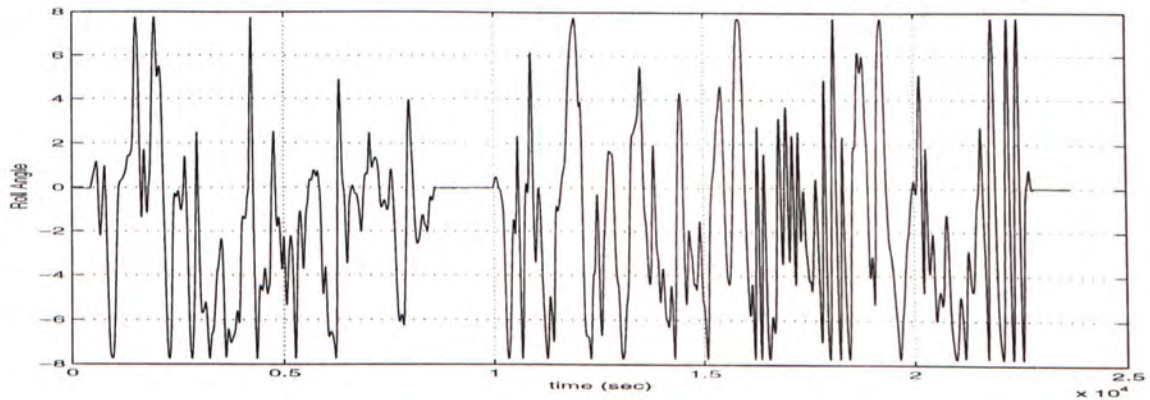


Figure 5.6: Modified Roll Trajectory for Sensation Grade 2 of Subject 2



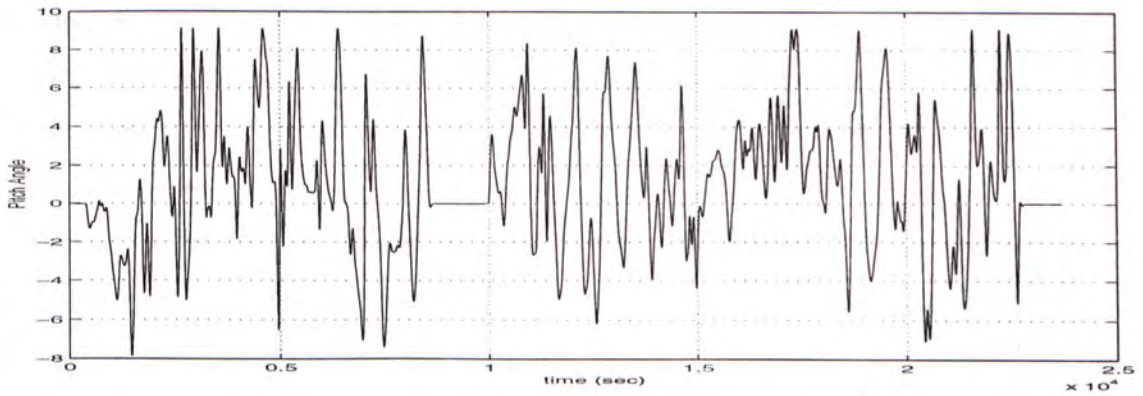


Figure 5.7: Modified Pitch Trajectory for Sensation Grade 4 of Subject 2

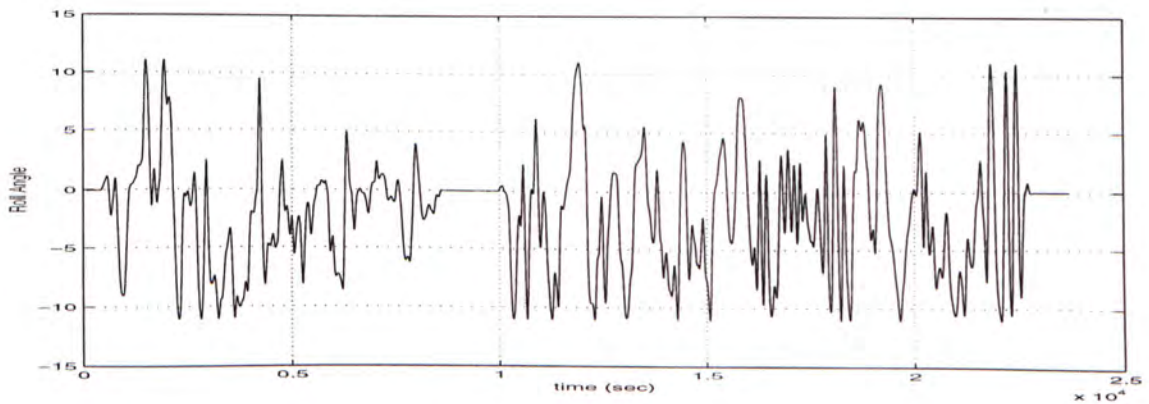


Figure 5.8: Modified Roll Trajectory for Sensation Grade 4 of Subject 2

The subjects are then asked to participate in the motion-based movie journeys in which the motion trajectories are modified to fit for different sensation grades. Each subject records the level of excitement experienced in the journeys of sensation grade 2 and 4. The sensation recorded are shown in figures 5.9 to 5.12.

After the modification of the motion trajectory, it is obvious that the sensation experienced by the participants is changed. The subjects have reflected an overall reduction in the level of excitement in the journey. As the specified sensation grade gets lower, the level of excitement experienced by the subjects becomes less distinguishable. The maximum level of sensation indicated is very close to the sensation grade specified in the modified trajectory. We can therefore conclude that our trajectory modification scheme has successfully caused the subjects to reflect a change in the sensation by adjusting the motion trajectory of the VR platform based on the level of excitement requested.

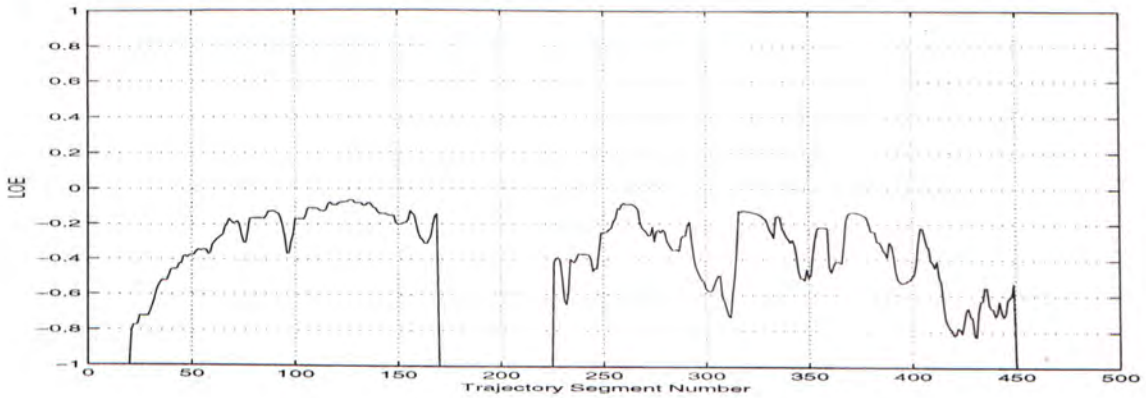


Figure 5.9: Sensation of Subject 1 on Motion Trajectory Modified to Sensation Grade 2



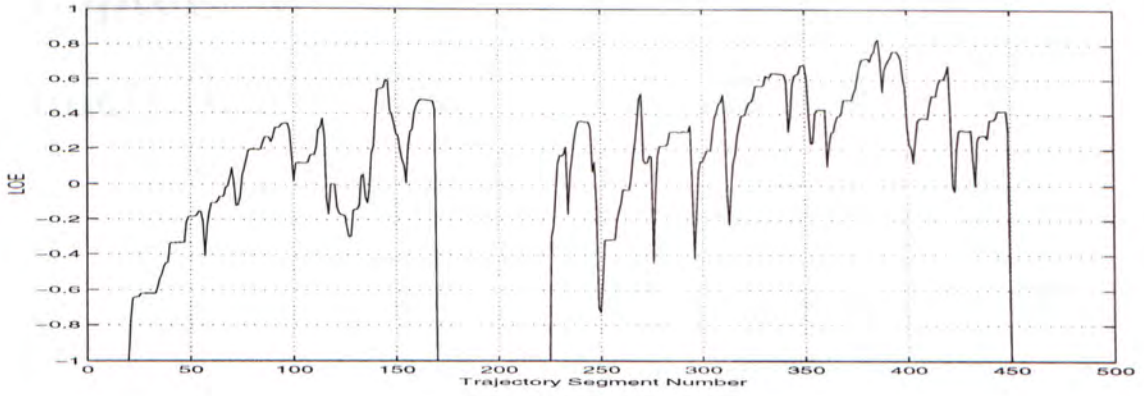


Figure 5.10: Sensation of Subject 1 on Motion Trajectory Modified to Sensation Grade 4

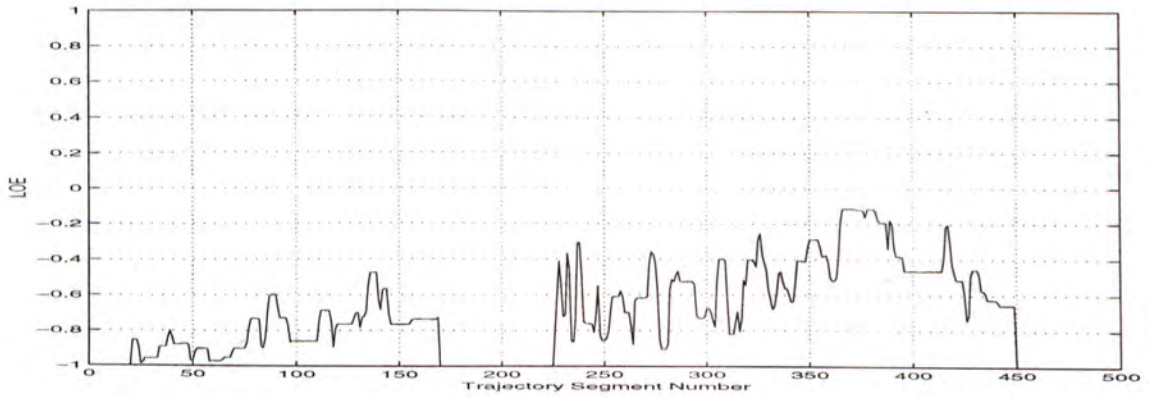


Figure 5.11: Sensation of Subject 2 on Motion Trajectory Modified to Sensation Grade 2

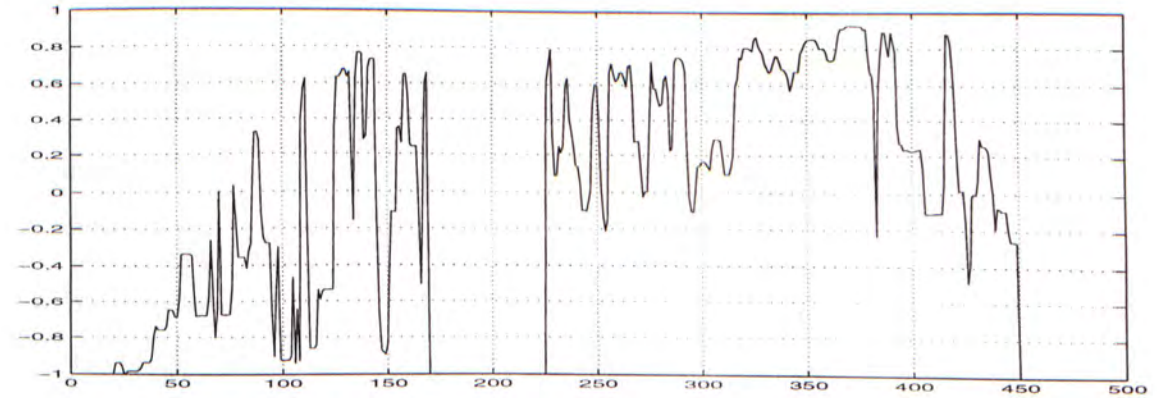


Figure 5.12: Sensation of Subject 2 on Motion Trajectory Modified to Sensation Grade 4

# Chapter 6

## Conclusion

### 6.1 Contributions

In this thesis, we have presented a framework for modeling human sensation in virtual environments. We summarize the original contributions of this work below.

- We proposed using a neural-network-based algorithm that combines flexible Cascade Neural Networks with Node-Decoupled Extended Kalman Filtering for modeling human sensation in virtual environments. As a sensation model validation tool, we proposed using a stochastic similarity measure based on Hidden Markov Models. The Cascade Neural Network models were shown to be capable of capturing the characteristics of human sensation. The relative similarity between the model-generated sensation and the actual human sensation were revealed by the HMM-based similarity measure.
- We proposed and developed a data selection method based on Independent Component Analysis. In the experiments, we demonstrated that the method not only was able to reduce the input data size for modeling, but it was also capable of selecting the inputs which were important to human sensation. The performance of this proposed input selection scheme was shown to be better than a number of other data reduction methods.
- We proposed and developed a motion trajectory modification algorithm for the application of ‘motion-based movie system’, based on human sensation. Using this method, we can adjust the stimuli presented to human subjects such that the sensation intensities of the subjects are prevented from exceeding certain specified levels. The effectiveness of the algorithm was demonstrated through human experimentation.



- We developed a full-body motion virtual reality system which is capable of recording human sensation. This has proven to be a valuable testing tool for the learning algorithms and statistical methods developed herein.

## 6.2 Future Work

This thesis provides the foundation for modeling and analyzing human sensations. There are a number of different directions in which this work can be extended and applied.

This thesis investigated one form of complicated stimulus, full-body motion. However, as we have outlined in chapter 2, human beings still have many other kinds of sense and sensation. It would be interesting and useful if other forms of sense and sensation involved in other applications are to be investigated.

Humans have the ability to adapt to the stimulus presented to them. That means the intensity of the stimulus has to increase gradually if the human is to maintain a certain level of sensation. However, different persons have different adaptability. If the relationship between human sensation and prolonged VR stimuli is to be established, the element of individual adaptability has to be incorporated into the sensation models.

Given a specific sensation requirement, it might be necessary to optimize a particular virtual reality system to that sensation measure. The unoptimized virtual reality system already gives an initial set of stimuli; optimization would refine the performance of the system with respect to the sensation characteristics of the sensation models.

Sensation models trained using human data can be transferred to virtual humans, agents and robots. It can create the necessary sense of realism to the actions and behaviors of the artificial life forms.

# Appendix A

## Platform Model

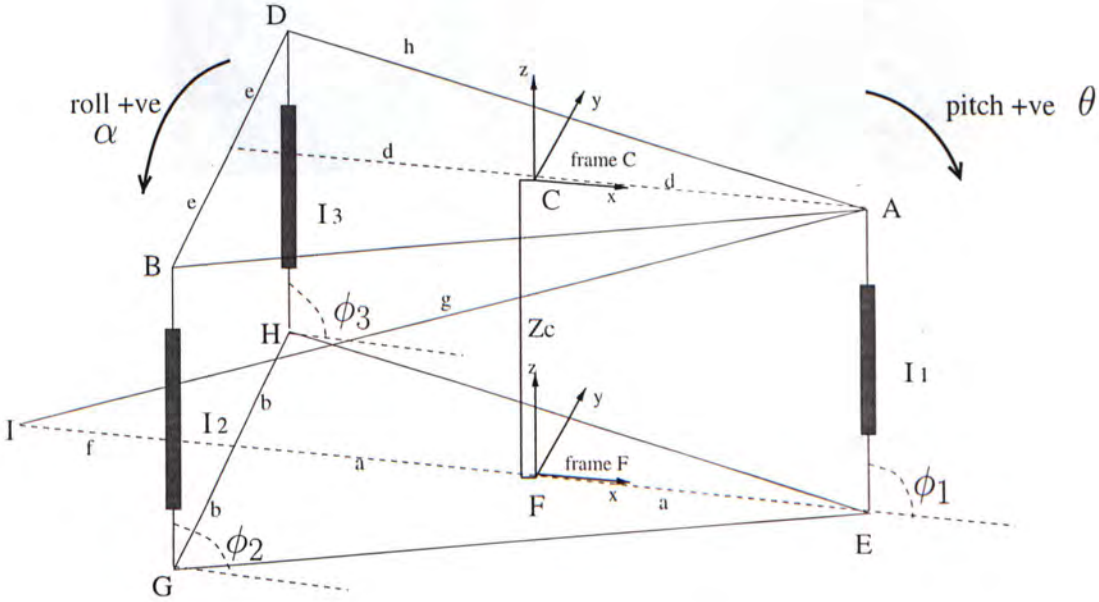


Figure A.1: Diagram of Motion Platform

Diagram A.1 shows a simplified model of the motion platform. The mechanism is composed of two flat plates and four links. There is one stationary platform  $EHG$  on the bottom and a moving platform  $ABD$  on the top. The moving platform is actuated by three prismatic joints,  $l_1, l_2$  and  $l_3$ . A rigid bar,  $AI$ , provides the necessary structural stability to the mechanism.

Two reference frames, frame  $C$  and frame  $F$ , are attached to the center of the moving plate and stationary plate, respectively. The platform has three degrees of freedom : roll, pitch and height. The roll angle of the platform is denoted by  $\alpha$ . The pitch angle of the platform is denoted by  $\theta$ . The height of the platform is the vertical position of frame  $C$





Figure A.2: Motion Platform

measured with respect to frame  $F$ , which is  $z_C$ . Roll angle  $\alpha$  is assumed to be positive when point  $B$  is lower than point  $D$ .  $\theta$  is assumed to be positive when the platform is pitched down.  $\phi_1, \phi_2$  and  $\phi_3$  are the angles between the horizontal plane and the three prismatic joints,  $l_1, l_2$  and  $l_3$ , respectively.

Let  $\vec{v}$  denotes the  $Z$ -axis of frame  $C$ . Roll angle  $\alpha$  is defined as the angle between  $\vec{v}$  and the  $Z - X$  plane of frame  $F$ . Pitch angle  $\theta$  is defined as the angle between  $Z$ -axis of frame  $F$  and  $\vec{v}$ 's projection on the  $Z - X$  plane of frame  $F$ .

The range of motion and the dimension of the platform model are shown in table A.1 and A.2, respectively.

DOF	Min. value	Max. value
Roll $\alpha$	-14 deg	+14 deg
Pitch $\theta$	-17 deg	+19 deg
Height $z_C$	75.15 cm	117.10 cm
$l_1, l_2, l_3$	76.0 cm	122.0 cm

Table A.1: Motion Range of Platform

parameter	value
a, d	60.27cm
b, e	50cm
f	39.63cm
g	177.42cm

Table A.2: Physical Dimension of Motion Platform

## A.1 Inverse Kinematics

The inverse kinematics of the mechanism is derived in this section and we start from the transformation between frame  $A$  and frame  $C$ .

$${}^F A = {}^F_C T {}^C A \quad (\text{A.1})$$

$${}^C A = \begin{bmatrix} d \\ 0 \\ 0 \end{bmatrix}, \quad {}^C B = \begin{bmatrix} -d \\ -e \\ 0 \end{bmatrix}, \quad {}^C D = \begin{bmatrix} -d \\ e \\ 0 \end{bmatrix} \quad (\text{A.2})$$

$${}^F E = \begin{bmatrix} a \\ 0 \\ 0 \end{bmatrix}, \quad {}^F G = \begin{bmatrix} -a \\ -b \\ 0 \end{bmatrix}, \quad {}^F H = \begin{bmatrix} -a \\ b \\ 0 \end{bmatrix} \quad (\text{A.3})$$

$${}^F_C T = \begin{bmatrix} n_1 & o_1 & p_1 & x_c \\ n_2 & o_2 & p_2 & y_c \\ n_3 & o_3 & p_3 & z_c \\ 0 & 0 & 0 & 1 \end{bmatrix} \quad (\text{A.4})$$

$$= \begin{bmatrix} \cos \theta & \sin \theta \sin \alpha & \sin \theta \cos \alpha & x_c \\ 0 & \cos \alpha & -\sin \alpha & 0 \\ -\sin \theta & \cos \theta \sin \alpha & \cos \theta \cos \alpha & z_c \end{bmatrix} \quad (\text{A.5})$$

To calculate the inverse kinematics involving  $l_1$ , we consider point A.



$${}^F A = {}_C^F T^C A = \begin{bmatrix} n_1 & o_1 & p_1 & x_c \\ n_2 & o_2 & p_2 & y_c \\ n_3 & o_3 & p_3 & z_c \\ 0 & 0 & 0 & 1 \end{bmatrix} \begin{bmatrix} d \\ 0 \\ 0 \\ 1 \end{bmatrix} \quad (\text{A.6})$$

$$= \begin{bmatrix} dn_1 + x_c \\ dn_2 + y_c \\ dn_3 + z_c \end{bmatrix} = \begin{bmatrix} d \cos \theta + x_c \\ 0 \\ -d \sin \theta + z_c \end{bmatrix} \quad (\text{A.7})$$

where  $\begin{bmatrix} n_1 \\ n_2 \\ n_3 \end{bmatrix}$  is the  $x$  axis of frame  $C$  represented in frame  $F$ .

For the length of the first prismatic joint :

$$l_1 = |{}^F E - {}^F A| \quad (\text{A.8})$$

$$l_1^2 = (dn_1 + x_c - a)^2 + (dn_2 + y_c)^2 + (dn_3 + z_c)^2 \quad (\text{A.9})$$

$$l_1^2 = (d \cos \theta + x_c - a)^2 + (-d \sin \theta + z_c)^2 \quad (\text{A.10})$$

To calculate the inverse kinematics involving  $l_2$ , we consider point B.

$${}^C B = \begin{bmatrix} -d \\ -e \\ 0 \end{bmatrix}$$

$${}^F B = {}_C^F T^C B = \begin{bmatrix} n_1 & o_1 & p_1 & x_c \\ n_2 & o_2 & p_2 & y_c \\ n_3 & o_3 & p_3 & z_c \\ 0 & 0 & 0 & 1 \end{bmatrix} \begin{bmatrix} -d \\ -e \\ 0 \\ 1 \end{bmatrix} \quad (\text{A.11})$$

$$= \begin{bmatrix} -dn_1 - eo_1 + x_c \\ -dn_2 - eo_2 + y_c \\ -dn_3 - eo_3 + z_c \end{bmatrix} \quad (\text{A.12})$$

For the length of the second prismatic joint :

$$l_2 = |{}^F B - {}^F G| \quad (\text{A.13})$$

$$l_2^2 = (-dn_1 - eo_1 + x_c + a)^2 + (-dn_2 - eo_2 + y_c + b)^2 + (-dn_3 - eo_3 + z_c)^2 \quad (\text{A.14})$$

$$l_2^2 = (-d \cos \theta - e \sin \theta \sin \alpha + x_c - a)^2 + (-e \cos \alpha + b)^2 + (d \sin \theta - e \cos \theta \sin \alpha + z_c)^2 \quad (\text{A.15})$$

To calculate the inverse kinematics involving  $l_3$ , we consider point D.

$${}^C D = \begin{bmatrix} -d \\ e \\ 0 \end{bmatrix}$$

$${}^F D = {}^F_C T {}^C D = \begin{bmatrix} n_1 & o_1 & p_1 & x_c \\ n_2 & o_2 & p_2 & y_c \\ n_3 & o_3 & p_3 & z_c \\ 0 & 0 & 0 & 1 \end{bmatrix} \begin{bmatrix} -d \\ e \\ 0 \\ 1 \end{bmatrix} \quad (\text{A.16})$$

$$= \begin{bmatrix} -dn_1 + eo_1 + x_c \\ -dn_2 + eo_2 + y_c \\ -dn_3 + eo_3 + z_c \end{bmatrix} \quad (\text{A.17})$$

For the length of the third prismatic joint :

$$l_3 = |{}^F D - {}^F H| \quad (\text{A.18})$$

$$l_3^2 = (-dn_1 + eo_1 + x_c + a)^2 + (-dn_2 + eo_2 + y_c - b)^2 + (-dn_3 + eo_3 + z_c)^2 \quad (\text{A.19})$$

$$l_3^2 = (-d \cos \theta + e \sin \theta \sin \alpha + x_c - a)^2 + (e \cos \alpha - b)^2 + (-d \sin \theta + e \cos \theta \sin \alpha + z_c)^2 \quad (\text{A.20})$$

The restraining bar  $AI$  :

$$g = |{}^F A - {}^F I| \quad (\text{A.21})$$

$${}^F I = \begin{bmatrix} -a - f \\ 0 \\ 0 \end{bmatrix}, \quad {}^F A = \begin{bmatrix} d \cos \theta + x_c \\ 0 \\ -d \sin \theta + z_c \end{bmatrix} \quad (\text{A.22})$$



$$g^2 = (d \cos \theta + x_c + a + f)^2 + (-d \sin \theta + z_c)^2 \quad (\text{A.23})$$

$$z_c = d \sin \theta \pm \quad (\text{A.24})$$

$$\sqrt{-(a+f)^2 + g^2 - 2(a+f)d \cos \theta - d^2 \cos^2 \theta - 2(a+f)x_c - 2d \cos \theta x_c - x_c^2}$$

$$x_c = -(a+f) - d \cos \theta \pm \sqrt{g^2 - d^2 \sin^2 \theta + 2d \sin \theta z_c - z_c^2} \quad (\text{A.25})$$

## A.2 Forward Kinematics

The forward kinematics of the mechanism is derived in this section. Given  $l_1$ , we can find the position of  $A$  with respect to frame  $F$ .

$A$  moves in a circle, centered at  $(a, 0, 0)$ , radius =  $l_1$ .

$$(x - a)^2 + z^2 = l_1^2 \quad (\text{A.26})$$

constraint bar  $AI$  moves in a circle, centered at  $(-a - f, 0, 0)$ , radius =  $g$ .

$$(x + a + f)^2 + z^2 = g^2 \quad (\text{A.27})$$

from the above two equations,

$$(x - a)^2 - l_1^2 = (x + a + f)^2 - g^2 \quad (\text{A.28})$$

$$l_1^2 = x(-4a - 2f) - f^2 - 2af + g^2 \quad (\text{A.29})$$

Let  $Q = g^2 - f^2 - 2af$  and  $R = -4a - 2f$ .

$$x_A = \frac{l_1^2 - Q}{R} \quad (\text{A.30})$$

$$z_A = \sqrt{l_1^2 - (x_A - a)^2} \quad (\text{A.31})$$

$$= \sqrt{l_1^2 - \left(-a + \frac{-Q + l_1^2}{R}\right)^2} \quad (\text{A.32})$$

$$y_A = 0 \quad (\text{A.33})$$

$$\phi_1 = \cos^{-1} \left( \frac{x_A - a}{l_1} \right) \quad (\text{A.34})$$

$$\dot{x}_A = \frac{2l_1\dot{l}_1}{R} \quad (\text{A.35})$$

$$\dot{z}_A = \frac{2l_1\dot{l}_1 - 4l_1(-a + \frac{-Q+l_1^2}{R})}{2\sqrt{l_1^2 - (-a + \frac{-Q+l_1^2}{R})^2}} \quad (\text{A.36})$$

Given  $l_3$  and position of  $A$ , we can find  $\phi_3$  and position of  $D$  with respect to frame  $F$ .

$D$  moves in a circle, centered at  $(-a, b, 0)$ , radius =  $l_3$ .

$$(x + a)^2 + z^2 = l_3^2 \quad (\text{A.37})$$

$$y = b \quad (\text{A.38})$$

Coordinates of point  $D$  :

$$x_D = \sqrt{l_3^2 - z_D^2} - a \quad (\text{A.39})$$

$$= l_3 \cos \phi_3 - a \quad (\text{A.40})$$

$$y_D = b$$

$$z_D = l_3 \sin \phi_3 \quad (\text{A.41})$$

The length of  $DA$  is  $h$ , if position of  $A$  is known, then

$$(x_A - x_D)^2 + (y_A - y_D)^2 + (z_A - z_D)^2 = h^2 \quad (\text{A.42})$$

$$(l_3 \cos \phi_3 - a - x_A)^2 + b^2 + (l_3 \sin \phi_3 - z_A)^2 = h^2 \quad (\text{A.43})$$

$$l_3^2 \cos^2 \phi_3 + x_A^2 + a^2 - 2l_3 \cos \phi_3 a - 2l_3 x_A \cos \phi_3 + 2a x_A + b^2 + \quad (\text{A.44})$$

$$l_3^2 \sin^2 \phi_3 + z_A^2 - 2l_3 z_A \sin \phi_3 = h^2$$

Let  $s_3 = \tan \frac{\phi_3}{2}$ ,  $\cos \phi_3 = \frac{1-s_3^2}{1+s_3^2}$ ,  $\sin \phi_3 = \frac{2s_3}{1+s_3^2}$

$$D = \begin{bmatrix} \frac{l_3(1-s_3^2)}{1+s_3^2} - a \\ b \\ \frac{2l_3 s_3}{1+s_3^2} \end{bmatrix} = \begin{bmatrix} x_D \\ y_D \\ z_D \end{bmatrix} \quad (\text{A.45})$$

$$\dot{z}_D = \frac{2s_3\dot{l}_3}{1+s_3^2} - \frac{4l_3 s_3^2 \dot{s}_3}{(1+s_3^2)^2} + \frac{2l_3 \dot{s}_3}{1+s_3^2} \quad (\text{A.46})$$

$$\dot{x}_D = \frac{(1-s_3^2)\dot{l}_3}{1+s_3^2} - \frac{2l_3 s_3(1-s_3^2)\dot{s}_3}{(1+s_3^2)^2} - \frac{2l_3 s_3 \dot{s}_3}{1+s_3^2} \quad (\text{A.47})$$



$$\begin{aligned}
s_3 &= (4 l_3 z_A + \sqrt{(16 l_3^2 z_A^2 - 4 (a^2 + b^2 - h^2 - 2 a l_3 + \\
& l_3^2 + 2 a x_A - 2 l_3 x_A + x_A^2 + z_A^2) \\
& (a^2 + b^2 - h^2 + 2 a l_3 + l_3^2 + \\
& 2 a x_A + 2 l_3 x_A + x_A^2 + z_A^2))})/ \\
& (2 (a^2 + b^2 - h^2 + 2 a l_3 + l_3^2 + 2 a x_A + 2 l_3 x_A + \\
& x_A^2 + z_A^2)) \\
\dot{s}_3 &= (-(4 l_3 \dot{z}_A + \sqrt{(16 l_3^2 z_A^2 - 4 (a^2 + b^2 - h^2 - \\
& 2 a l_3 + l_3^2 + 2 a x_A - 2 l_3 x_A + x_A^2 + z_A^2) \\
& (a^2 + b^2 - h^2 + 2 a l_3 + l_3^2 + 2 a x_A + 2 l_3 x_A + x_A^2 + z_A^2))}) \\
& (2 a \dot{l}_3 + 2 l_3 \dot{l}_3 + 2 x_A \dot{l}_3 + 2 a \dot{x}_A + 2 l_3 \dot{x}_A + 2 x_A \dot{x}_A + 2 z_A \dot{z}_A))/ \\
& (2 (a^2 + b^2 - h^2 + 2 a l_3 + l_3^2 + 2 a x_A + 2 l_3 x_A + x_A^2 + z_A^2)2) + \\
& (4 z_A \dot{l}_3 + 4 l_3 \dot{z}_A + (32 l_3 z_A^2 \dot{l}_3 + 32 l_3^2 z_A \dot{z}_A - 4 (a^2 + b^2 - h^2 + 2 a l_3 + \\
& l_3^2 + 2 a x_A + 2 l_3 x_A + x_A^2 + z_A^2) (-2 a \dot{l}_3 + 2 l_3 \dot{l}_3 - 2 x_A \dot{l}_3 + \\
& 2 a \dot{x}_A - 2 l_3 \dot{x}_A + 2 x_A \dot{x}_A + 2 z_A \dot{z}_A) - 4 (a^2 + b^2 - h^2 - 2 a l_3 + l_3^2 + \\
& 2 a x_A - 2 l_3 x_A + x_A^2 + z_A^2) (2 a \dot{l}_3 + 2 l_3 \dot{l}_3 + 2 x_A \dot{l}_3 + 2 a \dot{x}_A \\
& + 2 l_3 \dot{x}_A + 2 x_A \dot{x}_A + 2 z_A \dot{z}_A)))/(2 \sqrt{(16 l_3^2 z_A^2 - 4 (a^2 + b^2 - h^2 \\
& - 2 a l_3 + l_3^2 + 2 a x_A - 2 l_3 x_A + x_A^2 + z_A^2) (a^2 + b^2 - h^2 + 2 a l_3 + l_3^2 \\
& + 2 a x_A + 2 l_3 x_A + x_A^2 + z_A^2))})/(2 (a^2 + b^2 - h^2 + 2 a l_3 + l_3^2 \\
& + 2 a x_A + 2 l_3 x_A + x_A^2 + z_A^2)))
\end{aligned} \tag{A.48}$$

Given  $l_2$  and position of  $A$ , we can find  $\phi_2$  and position of  $B$  with respect to frame  $F$ .

$B$  moves in a circle, centered at  $(-a, -b, 0)$ , radius =  $l_2$ .

$$(x + a)^2 + z^2 = l_2^2 \tag{A.49}$$

$$y = -b \tag{A.50}$$

Coordinates of point  $B$  :

$$x_B = \sqrt{l_2^2 - z_B^2} - a \tag{A.51}$$

$$= l_2 \cos \phi_2 - a \quad (\text{A.52})$$

$$y_B = -b \quad (\text{A.53})$$

$$z_B = l_2 \sin \phi_2 \quad (\text{A.54})$$

The length of  $BA$  is  $h$ , if position of  $A$  is known, then

$$(x_B - x_A)^2 + (y_B - y_A)^2 + (z_B - z_A)^2 = h^2 \quad (\text{A.55})$$

$$(l_2 \cos \phi_2 - a - x_A)^2 + b^2 + (l_2 \sin \phi_2 - z_A)^2 = h^2 \quad (\text{A.56})$$

$$l_2^2 \cos^2 \phi_2 + x_A^2 + a^2 - 2l_2 a \cos \phi_2 - 2l_2 x_A \cos \phi_2 + 2a x_A + b^2 + \quad (\text{A.57})$$

$$l_2^2 \sin^2 \phi_2 + z_A^2 - 2l_2 z_A \sin \phi_2 = h^2$$

$$\text{Let } s_2 = \tan \frac{\phi_2}{2}, \quad \cos \phi_2 = \frac{1-s_2^2}{1+s_2^2}, \quad \sin \phi_2 = \frac{2s_2}{1+s_2^2}$$

$$B = \begin{bmatrix} \frac{l_2(1-s_2^2)}{1+s_2^2} \\ -b \\ \frac{2l_2 s_2}{1+s_2^2} \end{bmatrix} = \begin{bmatrix} x_B \\ y_B \\ z_B \end{bmatrix} \quad (\text{A.58})$$

$$\dot{z}_B = \frac{2s_2 \dot{l}_2}{1+s_2^2} - \frac{4l_2 s_2^2 \dot{s}_2}{(1+s_2^2)^2} + \frac{2l_2 \dot{s}_2}{1+s_2^2} \quad (\text{A.59})$$

$$\dot{x}_B = \frac{(1-s_2^2)\dot{l}_2}{1+s_2^2} - \frac{2l_2 s_2(1-s_2^2)\dot{s}_2}{(1+s_2^2)^2} - \frac{2l_2 s_2 \dot{s}_2}{1+s_2^2} \quad (\text{A.60})$$

$$\begin{aligned} s_2 &= (4l_2 z_A + \sqrt{(16l_2^2 z_A^2 - 4(a^2 + b^2 - h^2 - 2al_2 + l_2^2 + 2ax_A - 2l_2 x_A + x_A^2 + z_A^2))}) / \\ &\quad (a^2 + b^2 - h^2 + 2al_2 + l_2^2 + \\ &\quad 2ax_A + 2l_2 x_A + x_A^2 + z_A^2)) / \\ &\quad (2(a^2 + b^2 - h^2 + 2al_2 + l_2^2 + 2ax_A + 2l_2 x_A + \\ &\quad x_A^2 + z_A^2)) \\ \dot{s}_2 &= (-((4l_2 z_A + \sqrt{(16l_2^2 z_A^2 - 4(a^2 + b^2 - h^2 - 2al_2 + l_2^2 + 2ax_A - 2l_2 x_A + x_A^2 + z_A^2))}) / \\ &\quad (a^2 + b^2 - h^2 + 2al_2 + l_2^2 + 2ax_A + 2l_2 x_A + x_A^2 + z_A^2)) / \\ &\quad (2al_2 + 2l_2 \dot{l}_2 + 2x_A \dot{l}_2 + 2a \dot{x}_A + 2l_2 \dot{x}_A + 2x_A \dot{x}_A + 2z_A \dot{z}_A)) / \\ &\quad (2(a^2 + b^2 - h^2 + 2al_2 + l_2^2 + 2ax_A + 2l_2 x_A + x_A^2 + z_A^2)2) + \end{aligned} \quad (\text{A.61})$$



$$\begin{aligned}
& (4 z_A \dot{l}_2 + 4 l_2 \dot{z}_A + (32 l_2 z_A^2 \dot{l}_2 + 32 l_2^2 z_A \dot{z}_A - 4 (a^2 + b^2 - h^2 + 2 a l_2 + \\
& l_2^2 + 2 a x_A + 2 l_2 x_A + x_A^2 + z_A^2) (-2 a \dot{l}_2 + 2 l_2 \dot{l}_2 - 2 x_A \dot{l}_2 + \\
& 2 a \dot{x}_A - 2 l_2 \dot{x}_A + 2 x_A \dot{x}_A + 2 z_A \dot{z}_A) - 4 (a^2 + b^2 - h^2 - 2 a l_2 + l_2^2 + \\
& 2 a x_A - 2 l_2 x_A + x_A^2 + z_A^2) (2 a \dot{l}_2 + 2 l_2 \dot{l}_2 + 2 x_A \dot{l}_2 + 2 a \dot{x}_A \\
& + 2 l_2 \dot{x}_A + 2 x_A \dot{x}_A + 2 z_A \dot{z}_A)) / (2 \sqrt{(16 l_2^2 z_A^2 - 4 (a^2 + b^2 - h^2 \\
& - 2 a l_2 + l_2^2 + 2 a x_A - 2 l_2 x_A + x_A^2 + z_A^2) (a^2 + b^2 - h^2 + 2 a l_2 + l_2^2 \\
& + 2 a x_A + 2 l_2 x_A + x_A^2 + z_A^2))}) / (2 (a^2 + b^2 - h^2 + 2 a l_2 + l_2^2 \\
& + 2 a x_A + 2 l_2 x_A + x_A^2 + z_A^2)))
\end{aligned}$$

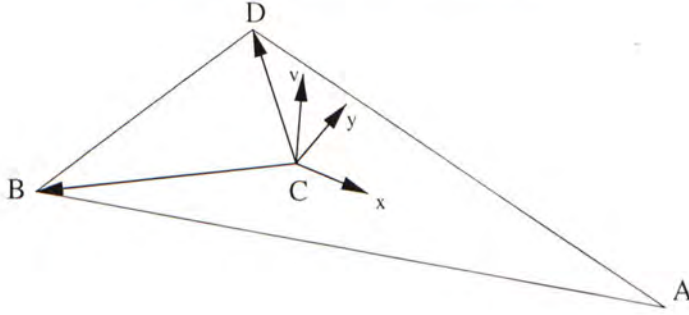


Figure 3 : Diagram of the Moving Plate

$\vec{v}$  is the vector perpendicular to the moving plate.

$$\text{let } \vec{v} = \vec{C\bar{D}} \times \vec{C\bar{B}} \quad (\text{A.62})$$

$$= v_x i + v_y j + v_z k \quad (\text{A.63})$$

$$\vec{C\bar{D}} = (x_D - x_C)i + (y_D - y_C)j + (z_D - z_C)k \quad (\text{A.64})$$

$$\vec{C\bar{B}} = (x_B - x_C)i + (y_B - y_C)j + (z_B - z_C)k \quad (\text{A.65})$$

$$\vec{v} = \begin{vmatrix} i & j & k \\ x_D - x_C & y_D - y_C & z_D - z_C \\ x_B - x_C & y_B - y_C & z_B - z_C \end{vmatrix} \quad (\text{A.66})$$

$$= i[(y_D - y_C)(z_B - z_C) - (z_D - z_C)(y_B - y_C)] \quad (\text{A.67})$$

$$+ j[(z_D - z_C)(x_B - x_C) - (x_D - x_C)(z_B - z_C)]$$

$$+ k[(x_D - x_C)(y_B - y_C) - (y_D - y_C)(x_B - x_C)]$$

where  $y_C = 0$ ,  $y_D = b$ ,  $y_B = -b$ .

To normalize  $\vec{v}$  :

$$\bar{v} = |\vec{v}| = \sqrt{v_x^2 + v_y^2 + v_z^2} \quad (\text{A.68})$$

The unit vectors are:  $\bar{v}_x = \frac{v_x}{|\vec{v}|}$ ,  $\bar{v}_y = \frac{v_y}{|\vec{v}|}$ ,  $\bar{v}_z = \frac{v_z}{|\vec{v}|}$

Given  $\vec{v}$ , we can find  $\theta, \alpha$  and  $z_C$ .

$$R = \begin{bmatrix} \cos \theta & \sin \theta \sin \alpha & \sin \theta \cos \alpha \\ 0 & \cos \alpha & -\sin \alpha \\ -\sin \theta & \cos \theta \cos \alpha & \cos \theta \cos \alpha \end{bmatrix} \quad (\text{A.69})$$

$$\bar{v} = R \begin{bmatrix} 0 \\ 0 \\ 1 \end{bmatrix} = \begin{bmatrix} \bar{v}_x \\ \bar{v}_y \\ \bar{v}_z \end{bmatrix} \quad (\text{A.70})$$

$$\bar{v}_x = \sin \theta \cos \alpha \quad (\text{A.71})$$

$$\bar{v}_y = -\sin \alpha \quad (\text{A.72})$$

$$\bar{v}_z = \cos \theta \cos \alpha \quad (\text{A.73})$$

$$\alpha = \sin^{-1}(-\bar{v}_y) \quad (\text{A.74})$$

$$\theta = \tan^{-1} \frac{\bar{v}_x}{\bar{v}_z} \quad (\text{A.75})$$

$$z_C = \frac{z_A + \frac{(z_B + z_D)}{2}}{2} \quad (\text{A.76})$$

$$\dot{\alpha} = \frac{\frac{\dot{v}_x}{\bar{v}_z} - \frac{\bar{v}_x \dot{v}_z}{\bar{v}_z^2}}{1 + \frac{\bar{v}_x^2}{\bar{v}_z^2}} \quad (\text{A.77})$$

$$\dot{\theta} = -\frac{\dot{v}_x}{\sqrt{1 - \bar{v}_x^2}} \quad (\text{A.78})$$

$$\dot{z}_C = \frac{1}{3}(\dot{z}_A + \dot{z}_B + \dot{z}_D) \quad (\text{A.79})$$



## A.3 Platform Dynamics

In Lagrangian formulation, the Generalized Coordinates of the system are  $l_1, l_2, l_3$ , and the Generalized Forces along the prismatic joints are  $F_1, F_2, F_3$ . The dynamics of the motion platform is:

$$KE = \frac{1}{2}M(\dot{x}_c^2 + \dot{y}_c^2 + \dot{z}_c^2) + \frac{1}{2}(I_{xx}\omega_x^2 + I_{yy}\omega_y^2 + I_{zz}\omega_z^2) \quad (\text{A.80})$$

$$= \frac{1}{2}M(\dot{x}_c^2 + \dot{z}_c^2) + \frac{1}{2}(I_{xx}\dot{\alpha}^2 + I_{yy}\dot{\theta}^2) \quad (\text{A.81})$$

$$PE = Mgz_c \quad (\text{A.82})$$

$$L = \frac{1}{2}M(\dot{x}_c^2 + \dot{z}_c^2) + \frac{1}{2}(I_{xx}\dot{\alpha}^2 + I_{yy}\dot{\theta}^2) - Mgz_c \quad (\text{A.83})$$

# Bibliography

- [1] D. Baltzley, et al., "The Time Course of Postflight Simulator Sickness Symptoms", *Aviation, Space, and Environmental Medicine*, 60(11), pp 1043-1048
- [2] H. Barlow, "Possible Principles Underlying the Transformation of Sensory Messages", *Sensory Communication*, Rosenblith, W.A (editor), MIT press, 1961
- [3] A. Bell and T. Sejnowski, "The Independent Components of Natural Scenes are Edge Filters", *Vision Research*, 37(23), pp 3327-3338
- [4] M. Bennett, et al., "An Investigation into Some of the Human Responses to Sinusoidal and Random Vibration in the Upright and Semi-reclined Seated Posture", *Report No. 78003*, Department of Mechanical Engineering, The Royal Military College of Science
- [5] S. Berretti, et al., "Sensation and Psychological Effects in Color Image Database", *Proc. International Conference on Image Processing*, Vol. 1, pp. 560-563, 1997
- [6] R. Blade, "VR Movie Rides: A Report from IAAPA", *The International Journal of Virtual Reality*, Vol. 2, NO. 4, pp 10-17, 1996
- [7] V. Bonnländer and A. Weigend, "Selecting Input Variables Using Mutual Information and Nonparametric Density Estimation", *Proc. of the 1994 International Symposium on Artificial Neural Networks (ISANN'94)*, pp 42-50, Taiwan, 1994
- [8] G. Box, G. Jenkins and G. Reinsel, *Time Series Analysis : Forecasting and Control*, 2nd ed., pp 408, Prentice Hall, 1994
- [9] G. Castellano and A. Fanelli, "Variable Selection Using Neural Network Models", *Neurocomputing*, 31, pp 1-13, 2000
- [10] P. Comon, "Independent Component Analysis: A New Concept?", *Signal Processing*, 36, pp 287-311, 1994



- [11] C. Corbridge, and M. J. Griffin, "Vibration and Comfort: Vertical and Lateral Motion in the Range 0.5-5.0Hz", *Ergonomics*, Vol 29, pp 249-272, 1986
- [12] *British Standard BS 6841*, London: British Standards Institution, 1987
- [13] S. Fahlman and C. Lebiere, "The Cascade-Correlation Learning Architecture", *Technical Report CMU-CS-90-100*, School of Computer Science, Carnegie Mellon University, 1990
- [14] S. Fahlman, et al., "The Cascade 2 Learning Architecture", *Technical Report CMU-CS-97-150*, School of Computer Science, Carnegie Mellon University, 1998
- [15] S. Fahlman, "An Empirical Study of Learning Speed in Back-Propagation Networks", *Technical Report CMU-CS-TR-88-162*, School of Computer Science, Carnegie Mellon University, 1988
- [16] T. Flash and T. Gat-Falik, "The Superposition Strategy for Arm Trajectory Modification in Robotic Manipulator", *IEEE Trans. on Systems, Man, and Cybernetics - Part B: Cybernetics*, Vol. 29, No. 1, Feb., 1999
- [17] X. Giannakopoulos, et al., "Experimental Comparison of Neural ICA Algorithms", *Proc. Int. Conf. on Artificial Neural Networks (ICANN'98)*, pp 651-656, Sweden, 1998
- [18] M. Gray, et al., "A Comparison of Visual Representation for Speechreading", *IEEE Pattern Analysis and Machine Intelligence*,
- [19] B. Griefahn, and P. Brode, "Comfort Contours: Inter-axis Equivalence", *Journal of sound and Vibration*, Vol 204, No. 1, pp 85-97, 1997
- [20] M. Griffin, *Handbook of Human Vibration*, Academic Press, 1990
- [21] M. Griffin, et al., "Vibration and Comfort : 1. Translational Seat Comfort", *Ergonomics*, 25, pp 602-630, 1982
- [22] M. Griffin and E. Whitham, "Individual Variability and Its Effects on Subjective and Biodynamic Response to Whole-Body Vibration", *Journal of Sound and Vibration*, 58, pp 239-250, 1978

- [23] M. Hamdi and G. Lachiver, "A Fuzzy Control System Based on the Human Sensation of Thermal Comfort", *Proc. IEEE International Conference on Computational Intelligence*, Vol. 1, pp. 487-492, 1998
- [24] S. Haykin, *Neural Networks: A Comprehensive Foundation*, Prentice Hall, 1999
- [25] A. Healey, et al., "Automobile Ride Quality Experiments Correlated to ISO-Weighted Criteria", *Proc. of Ride Quality Symposium*, Williamsburg, Virginia, pp. 581-600, Aug., 1975
- [26] X. Huang, et al., *Hidden Markov Models for Speech Recognition*, Edinburgh University Press, 1990
- [27] P. Hubber, "Projection Pursuit", *The Annals of Statistics*, 13(2), pp 435-475, 1985
- [28] A. Hyvarinen, "Fast and Robust Fixed-Point Algorithms for Independent Component Analysis", *IEEE Transactions on Neural Networks*, 10(3):626-634, 1999
- [29] A. Hyvarinen, "New Approximation of Differential Entropy for Independent Component Analysis and Projection Pursuit", *Advances in Neural Information Processing Systems*, Vol. 10, pp 273-279, MIT Press, 1998
- [30] *International Standard ISO 2631*, International Organization for Standardization, 1974
- [31] R. Jagielski, "An Application of Neural Network to Emulation of Aesthetic Judgments," *Proc. First New Zealand International Two-Stream Conference on Artificial Neural Networks and Expert Systems*, pp. 334-337, 1993
- [32] A. Jain and D. Zongker, "Feature Selection: Evaluation, Application, and Small Sample Performance", *IEEE Trans. on Pattern Analysis and Machine Intelligence*, Vol. 19, No. 2, Feb., 1997
- [33] I.T. Jolliffe, *Principal Component Analysis*, 1986, Springer-Verlag.
- [34] S. Jung and T. Hsia, "On Reference Trajectory Modification Approach for Cartesian Space Neural Network Control of Robot Manipulators", *Proc. of IEEE Int. Conf. on Robotics and Automation*, pp 575-580, 1995



- [35] C. Juttin and J. Herault, "Blind Separation of Sources, Part 1: An Adaptive Algorithm Based on Neuromimetic Architecture", *Signal Processing*, 24, pp. 1-10, 1991
- [36] R. Kalawsky, *The Science of Virtual Reality and Virtual Environments : a Technical, Scientific and Engineering Reference on Virtual Environments*, Addison-Wesley, 1993
- [37] E. Kolasinski, *Prediction of Simulator Sickness in a Virtual Environment*, Ph.D. thesis, University of Central Florida, 1996
- [38] A. Kundu, et al., "Transient Sonar Signal Classification Using Hidden Markov Models and Neural Nets", *IEEE Journal on Oceanic Engineering*, Vol. 19, No. 1, pp 88-99, 1994
- [39] D. Laming, *The Measurement of Sensation*, Oxford Science Publications, 1997
- [40] T. Lee, et al., "Combining Time-Delayed Decorrelation and ICA: Towards Solving the Cocktail Party Problem", *Proc. 1998 IEEE Int. Conf. of Acoustics, Speech and Signal Processing*, Vol.2, pp 1249 -1252, 1998
- [41] T. Lee, *Independent Component Analysis: Theory and Applications*, Kluwer Academic Publishers, 1998
- [42] Y. Linde, A. Buzo and R. Gray, "An Algorithm for Vector Quantizer Design", *IEEE Trans. Communication*, Vol COM-28, No. 1, pp 84-95, 1980
- [43] M. McKeowm, et al., "Analysis of fMRI by Blind Source Separation into Independent Spatial Components", *Human Brain Mapping*, 6, pp 1-31
- [44] E. Mira, "The Vestibular System", *Human and Machine Perception: Information Fusion*, Ed. V. Cantoni, et al., Plenum Press, New York, 1997
- [45] P. Narendra and K. Fukunaga, "A Branch and Bound Algorithm for Feature Subset Selection", *IEEE Trans. on Computers*, C-26(9), pp 917-922, Sep., 1977
- [46] K. Narendra and K. Parthasarathy, "Identification and Control of Dynamical Systems Using Neural Networks", *IEEE Trans. of Neural Networks*, Vol. 1, No. 1, pp 4-27, 1990
- [47] M. Nechyba and Y. Xu, "Cascade Neural Networks with Node-Decoupled Extended Kalman Filtering", *Proc. IEEE Int. Symp. on Computational Intelligence in Robotics and Automation*, Vol. 1, pp. 214-9, 1997

- [48] M. Nechyba and Y. Xu, "Learning and Transfer of Human Real-Time Control Strategies", *Journal of Computational Intelligence*, Vol. 1, No. 2, pp 137-154, 1997
- [49] M. Nechyba and Y. Xu, "Stochastic Similarity for Validating Human Control Strategy Models", *IEEE Transactions on Robotics and Automation*, Vol. 14, No. 3, June 1998, pp. 437-451
- [50] M. Nechyba, "Learning and Validation of Human Control Strategy", Ph.D. Thesis, Carnegie Mellon University, 1998
- [51] K. Ochiai, et al., "A New Trajectory Planning Method of Manipulators with Time Scaling Neural Network", *Proc. of 1993 Int. Joint Conf. on Neural Networks*, pp 665-668, 1993
- [52] K. Parsons and M. Griffin, "Vibration and Comfort : 2. Rotational Seat Vibration", *Ergonomics*, 25, pp 631-644, 1982
- [53] W. Press, et al., *Numerical Recipes in C: The Art of Scientific Computing*, 2nd ed., Cambridge University Press, 1992
- [54] G. Puskorius and L. Falkemp, "Decoupled Extended Kalman Filter Training of Feedforward Layered Networks", *Proc. Int. Joint Conf. on Neural Networks*, Vol. 3, No. 1, pp 122-130, 1992
- [55] L.R. Rabiner, "A Tutorial on Hidden Markov Models and Selected Applications in Speech Recognition", *Proc. of the IEEE*, Vol. 77, No. 2, Feb 1989, pp. 2688-2693
- [56] R. Rojas, *Neural Networks: A Systematic Introduction*, Springer, 1996
- [57] M. Rosenblum, et al., "Human Emotion Recognition from Motion Using a Radial Basis Function Network Architecture", *Proc. of the 1994 IEEE Workshop on Motion of Non-Rigid and Articulated Objects*, pp 43-49, 1994
- [58] G. Salvendy, *Handbook of Human Factors and Ergonomics*, John Wiley, 1997 Press
- [59] D. Shiliang, et al., "Analysis of the Human Vibration Response by Artificial Neural Network", *Journal of Tsinghua University (Sci & Tech)*, Vol. 36, No. 8, pp. 87-92, 1996



- [60] K. Takayama and H. Kano, "A New Approach to Synthesizing Free Motions of Robotic Manipulators Based on a Concept of Unit Motions", *IEEE Trans. on Systems, Man, and Cybernetics*, Vol. 25, No. 3, Mar., 1995
- [61] L. Turner, *International Encyclopedia of Psychology*, 1996, Salem Press
- [62] R. Vigario, "Extraction of Ocular Artifacts from EEG Using Independent Component Analysis", *Electroenceph. Clin. Neurophysiol.*, 103(3), pp 395-404, 1997
- [63] R. Warren and A. Wertheim, *Perception and Control of Self-Motion*, Erlbaum Assoc., 1990
- [64] J. Yang, et al., "Hidden Markov Model Approach to Skill Learning and its Applications to Telerobotics", *IEEE Trans. on Robotics and Automation*, Vol. 10, No. 5, pp. 621-631, 1994
- [65] J. Yang, et al., "Human Action Learning Via Hidden Markov Models", *IEEE Trans. on Systems, Man and Cybernetics - Part A: Systems and Humans*, Vol. 27, No. 1, pp 34-44, 1997
- [66] Y. Xu, W. Yu and K. Au, "Modeling Human Control Strategy in a Dynamically Stabilized Robot", *Proc. of the 1999 IEEE/RSJ Int. Conf. on Intelligent Robots and Systems*, Vol. 2, pp. 507-512, 1999





CUHK Libraries



003803827